nagra.

Arbeitsbericht NAB 21-18

Morphology of the Overdeepened Gebenstorf-Stilli Trough (Lower Aare Valley) from Seismic Surface Wave Investigations

September 2021

National Cooperative
for the Disposal of
Radioactive Waste

Hardstrasse 73
P.O. Box 280
5430 Wettingen
Switzerland
Tel. +41 56 437 11 11

www.nagra.ch

nagra.

Arbeitsbericht NAB 21-18

Morphology of the Overdeepened Gebenstorf-Stilli Trough (Lower Aare Valley) from Seismic Surface Wave Investigations

September 2021

KEYWORDS

Gebenstorf-Stilli Trough, overdeepening, Lower Aare Valley, surface waves, ambient vibration

National Cooperative
for the Disposal of
Radioactive Waste

Hardstrasse 73
P.O. Box 280
5430 Wettingen
Switzerland
Tel. +41 56 437 11 11

www.nagra.ch

Nagra Arbeitsberichte ("Working Reports") present the results of work in progress that have not necessarily been subject to a comprehensive review. They are intended to provide rapid dissemination of current information.

"Copyright © 2021 by Nagra, Wettingen (Switzerland) / All rights reserved.
All parts of this work are protected by copyright. Any utilisation outwith the remit of the copyright law is unlawful and liable to prosecution. This applies in particular to translations, storage and processing in electronic systems and programs, microfilms, reproductions, etc."

Table of Contents

Table of Contents I

List of Tables II

List of Figures III

List of Enclosures IV

Glossar of Terminology and Acronyms V

Abstract 1

1 Introduction 3
1.1 Project context and aims 3
1.2 Project and report contributors 3

2 Geological overview 5

3 Survey concepts 9
3.1 Investigation methodology 9
3.2 Conceptual design 9
3.3 Survey equipment 10
3.4 Pilot line: design and field parameters 14
3.5 Productive lines: design and field parameters 15

4 Field operations and data acquisition 17
4.1 Permit acquisition 17
4.2 Positioning of field measurements 17
4.3 Execution of field data acquisition 17
4.4 In-field quality control 18

5 Seismic data processing 19
5.1 Processing of ambient vibration data 19
5.2 Processing of active measurements 23
5.3 Processing of passive array data 26
5.4 Frequency-to-depth conversion 28

6 Geophysical Base Quaternary 33
6.1 Drilling information 33
6.2 Base Quaternary models 33

7 Geological interpretation and morphology of the Gebenstorf-Stilli Trough 37
7.1 Database and procedure 37
7.2 Products of this study 37

7.3 Description and discussion of results 38
7.3.1 Base Quaternary subcrop 38
7.3.2 Gebenstorf-Stilli Trough morphology 39
7.3.3 Cross-sections 39
7.3.4 Synthesis 40
7.4 Conclusion 41

8 Acknowledgements 43

9 References 45

List of Tables

Tab. 3-1: Technical specifications of the seismic sensor Gemini-2 and its A/D converter board 10
Tab. 3-2: Technical specifications of geophones and the Geode seismograph used for passive array data acquisition 12
Tab. 3-3: Field acquisition parameters of the pilot line executed in March 2019 14
Tab. 3-4: Field acquisition parameters of productive lines from October 2019 to March 2020 15
Tab. 5-1: Summary table with information on automatically and manually picked f_0 28
Tab. 5-2 Tabulated equivalent velocity $v_{s,E}$ [m/s] in overburden 31
Tab. 6-1: Base Quaternary (BQu) depth differences between borehole logs and the interpretation of seismic data 34
Tab. 7-1: Key dimensions of the Gebenstorf-Stilli Trough compared with other foreland overdeepenings in Switzerland 41

List of Figures

Fig. 2-1: Overview map of the Gebenstorf-Stilli Trough with the locations of the Nagra Quaternary boreholes and seismic cross-sections 6
Fig. 2-2: Schematic section along the Gebenstorf-Stilli Trough (see Fig. 2-1 for trace) 7
Fig. 3-1: Single station ambient vibration recording 11
Fig. 3-2: Sledgehammer and steel plate for active data acquisition on line 19QLAV-1 at point 138 12
Fig. 3-3: Setup of equipment for passive ESAC array measurement close to point 116 on line 19QLAV-1 13
Fig. 5-1: HVSR processing sequence for ambient vibration data 20
Fig. 5-2: Raw field data in time (top) and frequency (bottom) domain for PID 126 21
Fig. 5-3: Processed spectral data for PID 126 22
Fig. 5-4: Normalised HVSR curves along line 19QLAV-1 22
Fig. 5-5: Gridded HVSR section 19QLAV-1 23
Fig. 5-6: General processing sequence for active surface wave data 24
Fig. 5-7: HoliSurface® processing data and results for point 115 (left) 25
Fig. 5-8: Results of multi-objective inversion of PID 115 25
Fig. 5-9: Edited ESAC data and array layout close to the QGBR borehole location (array 215) 26
Fig. 5-10: Processing sequence of ESAC records 26
Fig. 5-11: Example result of ESAC processing from array 215 27
Fig. 5-12: HVSR curves of pilot line 19QLAV-1 and the picked f_0 peaks 29
Fig. 5-13: Equivalent shear wave velocity concept 30
Fig. 5-14: Converting fundamental frequency f_0 to bedrock depths for profile 19QLAV-1 30
Fig. 6-1: BQu model of example line 19QLAV-1 33

List of Enclosures

Encl. 2-1: Base Quaternary subcrop map of the study area

Encl. 4-1: Basemap with trough location, seismic lines and boreholes

Encl. 4-2: Basemap with trough location, seismic lines and velocity measurements

Encl. 5-1: Seismic surface wave line 19QLAV-6 HVSR section, velocities and depth section

Encl. 5-2: Seismic surface wave line 19QLAV-2 HVSR section, velocities and depth section

Encl. 5-3: Seismic surface wave line 19QLAV-4 HVSR section, velocities and depth section

Encl. 5-4 Seismic surface wave line 19QLAV-1 HVSR section, velocities and depth section

Encl. 5-5: Seismic surface wave line 19QLAV-8 HVSR section, velocities and depth section

Encl. 5-6: Seismic surface wave line 19QLAV-5 HVSR section, velocities and depth section

Encl. 5-7: Seismic surface wave lines 19QLAV-3 & 19QLAV-9 HVSR sections, velocities and depth section

Encl. 5-8: Seismic surface wave line 19QLAV-7 HVSR section, velocities and depth section

Encl. 7-1: Base Quaternary subcrop map with Top Malm overlay

Encl. 7-2: Seismic surface wave line 19QLAV-6 HVSR section, borehole data and interpretation

Encl. 7-3: Seismic surface wave line 19QLAV-2 HVSR section, borehole data and interpretation

Encl. 7-4: Seismic surface wave line 19QLAV-4 HVSR section, borehole data and interpretation

Encl. 7-5: Seismic surface wave line 19QLAV-1 HVSR section, borehole data and interpretation

Encl. 7-6: Seismic surface wave line 19QLAV-8 HVSR section, borehole data and interpretation

Encl. 7-7: Seismic surface wave line 19QLAV-5 HVSR section, borehole data and interpretation

Encl. 7-8: Seismic surface wave lines 19QLAV-3 & 19QLAV-9 HVSR sections, borehole data and interpretation

Encl. 7-9: Seismic surface wave line 19QLAV-7 HVSR section, borehole data and interpretation

Encl. 7-10: Seismic surface wave lines 19QLAV-1 to 19-QLAV-9 summary plot

Encl. 7-11: Seismic surface wave lines 19QLAV-1 to 19-QLAV-9 longitudinal section

Glossar of Terminology and Acronyms

Nagra	National Cooperative for the Disposal of Radioactive Waste; Swiss technical competence centre in the field of deep geological disposal radioactive waste
BQu	Base of Quaternary sediments
ESAC	Extended spatial autocorrelation (see Ohori et al. 2002 for further details)
f_0	Fundamental frequency of ground shaking at a specific site. This value is mainly determined by shear wave velocities in the subsurface and depth to bedrock
FVS	Full velocity spectrum inversion, an inversion approach without the need for (subjective) definition ("picking") of modal dispersion curves (see Dal Moro 2019 for further details)
HVSR	Horizontal-to-vertical spectral ratio of a long duration 3-component seismic record
HoliSurface®	Holistic surface wave analysis software application (patented methodology) for seismic exploration via joint analysis of active and passive data obtained through simple and efficient acquisition procedures fundamentally based on the smart exploitation of all the data that can be obtained through mindful use of a single 3-component geophone
MFA	Multiple frequency analysis (see Dziewonski et al. 1969 for further details)
PID	Point identifier number of passive and active single-receiver measurements
RPM	Rayleigh wave particle motion: site-specific function of particle motion, mainly depending on frequency of signal (Dal Moro et al. 2019 for further details).
SESAME	Site EffectS assessment using AMbient Excitations European research project sponsored by the European Commission; Project No. EVG1-CT-20000-00023 SESAME (see SESAME 2004 for further details)
SPAC	Spatial autocorrelation, methodology for deriving phase velocities from ambient array measurements (see Aki 1957 for more details)
V_GR	Group velocity (spectrum) of radial component of Rayleigh wave
V_GZ	Group velocity (spectrum) of vertical component of Rayleigh wave
v_s	Velocity of seismic shear waves
$v_{s,av}$	Average velocity model of a specific transect
$v_{s,E}$	Mean (or equivalent) shear wave velocity of overburden at a specific position

Abstract

The confluence area of the rivers Aare, Reuss and Limmat ("Wasserschloss") and the northwards adjacent Lower Aare Valley in central Northern Switzerland are a key region of Alpine Quaternary geology. Below the area lies the Gebenstorf-Stilli Trough, a ~ 10 km-long, N-S trending overdeepening with a depth ≥ 112[1] m below surface. In the light of the unique underlying bedrock geology, including Mesozoic strata, this trough is of paramount interest for investigating subglacial erosion processes and relative rock erodibilities. To reveal its morphology, we targeted it with a set of seismic cross-sections featuring analyses of seismic surface waves.

Our application of seismic surface wave methods included measurements of the ambient noise wavefield, computation of the horizontal-to-vertical spectral ratio (HVSR) and analyses of dominant frequencies. We focused our investigations on imaging the Base Quaternary-bedrock interface on eight 2D sections that cross the Gebenstorf-Stilli Trough. Using independent active and passive measurements, we found shear wave velocity contrasts to the underlying bedrock (consisting of Tertiary or Late Jurassic sediments) that validated our findings and supported depth conversion of the dominant frequencies recorded. The procedure resulted in 50 m spaced depth measurements that were connected to build continuous Base Quaternary horizon models along 2D cross-sections. The results were validated against available borehole logs.

A first geological interpretation integrated these 2D cross-sections with surface geology and borehole data. The combined profiles greatly improved our knowledge of the dimensions and morphology as well as the infill of the Gebenstorf-Stilli Trough. The dataset allowed distinction of two separate sub-basins separated by a ridge located at Lauffohr. We distinguished between the southern, ≥ 112[1] m deep Gebenstorf Basin and the northern, ≥ 76[1] m deep Stilli Basin, with marked differences in underlying geology and infill sedimentology. This report provides the basis for detailed studies interpreting the shape and sedimentary infill of the Gebenstorf-Stilli Trough with respect to the bedrock geological and paleoglaciological conditions.

[1] Depth confirmed in a borehole; the trough may be deeper at other locations.

1 Introduction

1.1 Project context and aims

In the context of the Sectoral Plan for Deep Geological Repositories (SGT), Nagra is currently investigating three siting regions in Northern Switzerland for potentially hosting repositories for radioactive waste. The field exploration project "Quartäruntersuchungen" (QAU) is dedicated to the characterisation of Quaternary deposits within and around these siting regions to further constrain scenarios of their long-term geological evolution. The investigations support the reconstruction of Quaternary landscape evolution.

In order to better constrain its morphology and depth, the distal half of the Gebenstorf-Stilli Trough (north of the Jura fold-and-thrust belt and near the Jura Ost siting region) was targeted with a set of eight seismic cross-sections. They were acquired from late 2018 to early 2020 using a combination of three surface wave approaches, with the primary goal of imaging the Base Quaternary, i.e. the base of the Gebenstorf-Stilli Trough.

This report summarises the planning, field acquisition and data processing. Data interpretation is split into two parts. First, a geophysical data interpretation defines the Base Quaternary at each measurement point. The subsequent geological interpretation puts the geophysical findings into geological context and results in final geological cross-sections.

1.2 Project and report contributors

On behalf of Nagra, the acquisition, processing and geophysical interpretation of the seismic profiles was carried out by L. Keller (roXplore gmbh). The geological interpretation of the profiles was carried out by L. Gegg (Uni Bern), with the support of M. Buechi (Uni Bern). The Nagra project management team (T. Spillmann, G. Deplazes) was responsible for project organisation and editing of this report. The editors acknowledge support from M. Ruff (Nagra Data Management) for preparing GIS figures.

The report contributions are as follows:

Authors Ch. 1:	T. Spillmann, G. Deplazes
Authors Ch. 2:	L. Gegg, G. Deplazes, L. Keller, T. Spillmann
Authors Ch. 3-6:	L. Keller, T. Spillmann
Authors Ch. 7:	L. Gegg, M. Buechi

2 Geological overview

The confluence area of the rivers Aare, Reuss and Limmat ("Wasserschloss") and the northwards adjacent Lower Aare Valley in central Northern Switzerland are a key region of Alpine Quaternary geology (e.g. Dick et al. 1996). It is largely covered by Quaternary sediments with thicknesses locally exceeding 200 m (Bitterli-Dreher et al. 2007). Over the last decades, several studies have compiled geophysical, outcrop, and especially drilling information to create maps or digital elevation models of the underlying bedrock surface (e.g. Wildi 1984, Haldimann et al. 1984, Graf 2009, Pietsch & Jordan 2014). These works revealed the existence of a ~ 10 km-long, N-S trending glacial trough (Gebenstorf-Stilli Trough) with a depth of ≥ 112 m below surface (Fig. 2-1). North of this trough, between Würenlingen and Döttingen, the Jurassic bedrock rises to an elevation of ~ 300 m a.s.l. (Wildi 1984, Haldimann et al. 1984, Pietsch & Jordan 2014). We therefore consider the lower-lying part of the Gebenstorf-Stilli Trough to be subglacially overdeepened (Cook & Swift 2012).

The Gebenstorf-Stilli Trough originates in the wide Birrfeld basin in the south (Nitsche et al. 2001) and cuts through the Jura fold-and-thrust belt as well as the south-eastern margin of the Tabular Jura that partly overlain by a wedge of Molasse deposits (Fig. 2-1, Encl. 2-1). The area is characterised by different degrees of tectonic overprinting (Bitterli-Dreher et al. 2007): the Jura fold-and-thrust belt is affected by a dense stack of thrusts as well as conjugate faults that are largely missing in the Tabular Jura (Graf et al. 2006). We suspect that the lithological and structural properties of the various units have a strong effect on their erodibility. Knowledge of relative subglacial erosion efficiencies in different bedrock lithologies is limited to a few specific case studies (e.g. Brook et al. 2004, Dühnforth et al. 2010, Krabbendam & Glasser 2011, see also Goudie 2016). Against this background, the morphology of the Gebenstorf-Stilli Trough is of paramount interest for drawing conclusions about erosional processes and relative erodibilities, as other foreland overdeepenings in Switzerland generally occur only in the Molasse Basin (Preusser et al. 2010).

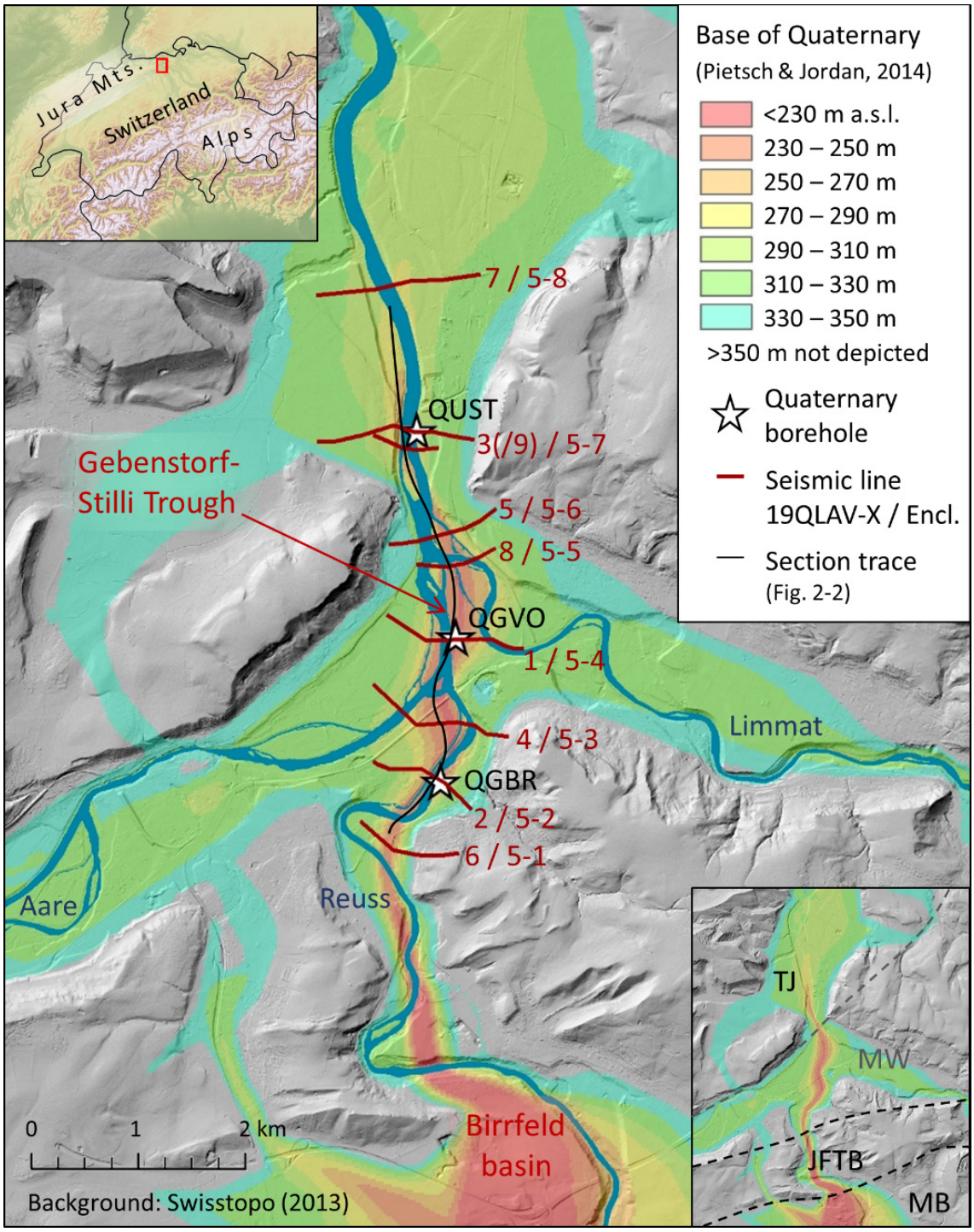


Fig. 2-1: Overview map of the Gebenstorf-Stilli Trough with the locations of the Nagra Quaternary boreholes and seismic cross-sections

The top left inset locates the study area (red rectangle) in the regional geological context. The lower right inset depicts the structural units in the vicinity of the Gebenstorf-Stilli Trough (TJ – Tabular Jura, MW – wedge of Molasse deposits overlying the south-eastern TJ, JFTB – Jura fold-and-thrust belt, MB – Molasse Basin; see also Encl. 2-1).

Previous models of the shape of the Gebenstorf-Stilli Trough rely on only a few boreholes that reached the base of the Quaternary so that the most recent bedrock model is largely based on "conceptual considerations" (Pietsch & Jordan 2014). Nagra drilled three scientific Quaternary boreholes along the Gebenstorf-Stilli Trough in 2018 (QBO Untersiggenthal / QUST, Gegg et al. 2019a; QBO Gebenstorf-Brüel / QGBR, Gegg et al. 2019b; QBO Gebenstorf-Vogelsang / QGVO, Gegg et al. 2019c; Fig. 2-1). These revealed a local discrepancy of ~ 40 m between the model of Pietsch & Jordan (2014) and the actual drilled bedrock depth (Fig. 2-2). Geological evidence, however, was insufficient to decide if this discrepancy was a feature of the trough base, or if the QGVO borehole missed the deepest point.

To fill this information gap, seismic measurements were performed along the 2D cross-sections shown in Fig. 2-1. The collection and processing of these data as well as their geological interpretation and the construction of a conclusive model of the Base Quaternary are the main objective of this report.

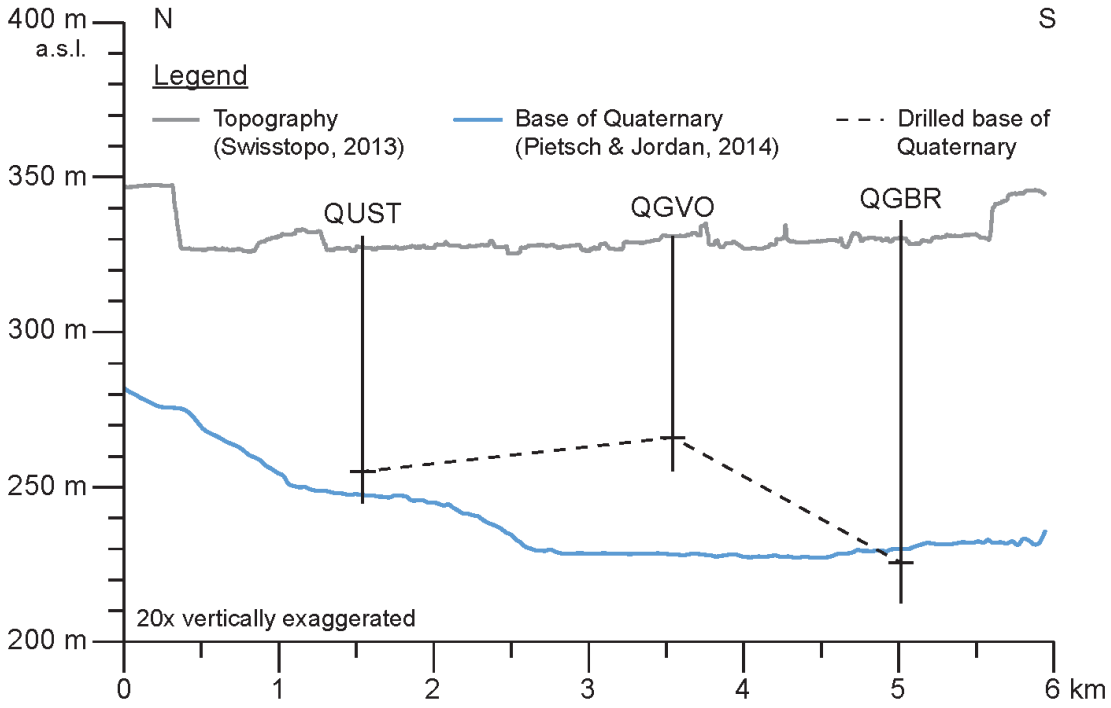


Fig. 2-2: Schematic section along the Gebenstorf-Stilli Trough (see Fig. 2-1 for trace)

Pietsch & Jordan (2014) model of the base of the Quaternary (in blue) compared with the drilled base of the Quaternary encountered in the QBO boreholes.

3 Survey concepts

3.1 Investigation methodology

Our application of surface wave methods, particularly measurements of the ambient noise wavefield, follows scientific concepts proposed by e.g. Aki (1957), Capon (1969), Nakamura (1989) and Ohori et al. (2002). We combined this with active measurements for group velocity analyses of surface waves, taking advantage of efficient data acquisition using single sensor and source points per point of investigation.

Our approach required acquisition of three different datasets:

1. Passive point measurements using 3-component (3C) sensors for determining the fundamental frequency f_0 at specific locations via spectral division of the vertical and horizontal components (HVSR – horizontal-to-vertical spectral ratio; Nakamura 1989, SESAME 2004).
2. Active measurements of Rayleigh waves from vertical sledgehammer blows were recorded on 3C sensors. Data analyses employed the multiple frequency analysis (MFA), the "HoliSurface®" (holistic surface wave analysis), a patented methodology (Dal Moro et al. 2016), or group velocity spectra inversions (Dziewonski et al. 1969) for determining the shallow (down to ~ 30 to 50 m depth) shear wave velocity v_s.
3. Passive L-shape array measurement of ambient wavefield (ESAC – extended spatial autocorrelation) to derive deeper (down to ~ 100 m) shear wave velocities v_s by inversion of the phase velocity spectra (Ohori et al. 2002).

Knowledge of the fundamental frequency f_0 (i.e. the peak frequency from the HVSR curve) and the average shear wave velocity in the upper layer $v_{s,E}$ (e.g. in the Quaternary) allows the estimation of the interface depth z to the underlying bedrock (Roesset 1970, Dobry et al. 1976):

$$z = v_{s,E}/(4f_0) \qquad \text{(Eq. 3-1)}$$

The following sections elaborate on the acquisition and processing of the three datasets.

3.2 Conceptual design

The geometry of the Gebenstorf-Stilli Trough is fairly well known from boreholes and geological evidence. Based on the Pietsch & Jordan (2014) Quaternary model and the location of the QBO boreholes, eight transects were defined for detailed field layout planning. The exact positioning of each measurement point considered the following criteria:

- transect proposal by Nagra
- existing Base Quaternary model
- borehole locations
- geological evidence and bedrock outcrops
- feasibility of seismic data acquisition in view of topographic constraints
- nominal point interval

The final layout of the seismic lines and measurement points was planned on a GIS system using the Base Quaternary model (Pietsch & Jordan 2014), topographic maps, orthophotos, and Street View provided by Google LLC.

3.3 Survey equipment

For the field measurements of passive (HVSR) and active (HoliSurface®) data, we used several low-frequency velocimeters (Model: Gemini 2Hz 3C LandGeophone, manufactured by PASI srl., IT-Torino). Tab. 3-1 shows the technical specifications of this instrument and Fig. 3-1 demonstrates the field setup. Parameter setup, quality control and recording were done using a standard computer running a Windows operating system and connection via USB port.

Tab. 3-1: Technical specifications of the seismic sensor Gemini-2 and its A/D converter board

Product name	**Gemini-2**
Natural resonance frequency	2 Hz ± 10 %
Sensitivity	200 V/m/sec ± 5 %
Internal resistance	5.8 kΩ ± 5 %
Damping	0.7 ± 5 %
Harmonic distortion	≤ 0.2 %
A/D converter	Real 24bit ΔΣ converter
S/N ratio	Max. 117 dB
Bandwidth	DC to 210 Hz
Distortion	0.0005 % @ 2 ms
Anti-alias filter	-3dB @ 75 % of Nyquist frequency



Fig. 3-1: Single station ambient vibration recording

Setup of the sensor in a small hole to protect it from wind. Generally, the sensor was also covered with a box.

The stock of velocimeters was used for rolling acquisition with active recording on a single instrument only. As a seismic source for active measurements, sledgehammer blows with 6 or 8 kg weight and with a 1.5-m-long handle were used (Fig. 3-2). A trigger-switch is mounted on the hammer handle and wire-connected to a computer to start acquisition accurately and punctually (< 1 ms delay).



Fig. 3-2: Sledgehammer and steel plate for active data acquisition on line 19QLAV-1 at point 138

For field measurement of the ESAC array data, we used low-frequency vertical geophones manufactured by Senshe, Xi'an (China) and a Geode seismograph system manufactured by Geometrics Inc, US-San Jose. Technical geophone specifications are given in Tab. 3-2. L-shaped geophone arrays were set up in the field for ambient noise recordings (Fig. 3-3).

Tab. 3-2: Technical specifications of geophones and the Geode seismograph used for passive array data acquisition

Geophone type	**Senshe SS-4.5N**
Natural resonance frequency	4.5 Hz ± 10 %
Sensitivity	28.8 V/m/sec ± 7.5 %
Internal resistance	375 Ω ± 7.5 %
Damping	0.6 ± 7.5 %
Harmonic distortion	≤ 0.2 %
Seismograph name	**Geode**
A/D converter	Real 24-bit ΔΣ converter
Bandwidth	1.75 Hz to 210 Hz
S/N ratio	Max. 110 dB
Distortion	0.0005 % @ 2 ms
Anti-alias filter	-3dB @ 83 % of Nyquist frequency



Fig. 3-3: Setup of equipment for passive ESAC array measurement close to point 116 on line 19QLAV-1

View to the corner point of the L-shaped array of 57 vertical geophones along the measuring tape. Close to the array, several additional HVSR measurements were performed to complement the dataset for inversion.

3.4 Pilot line: design and field parameters

In March 2019, a pilot line (19QLAV-1 in Fig. 2-1) was executed across the Nagra QGVO borehole close to the Reuss river in Gebenstorf-Vogelsang. The aims of the measurements were:

- feasibility testing of the methodological approach
- optimisation of field parameters, i.e. point interval and recording times

The field parameters for the pilot line (Tab. 3-3) were defined in order to collect sufficient data for evaluating bedrock depths between 20 and 100 m. The only varying parameter across the transect was the recording time, which was adapted according to the SESAME (2004) recommendations, considering the Base Quaternary model (Pietsch & Jordan 2014) and assuming an average shear wave velocity of 400 m/s.

Tab. 3-3: Field acquisition parameters of the pilot line executed in March 2019

Measurement	**Parameter**	**Value**
38 passive point measurements HVSR (Fig. 3-1)	Nominal point interval	40 m
	Receiver type	PASI Gemini 2 Hz LandGeophone 3C, continuously recording
	Recording time	10 min – 30 min, depending on transient noise level and expected depth to bedrock
	Sampling interval	5 msec
14 active point measurements HoliSurface® (Fig. 3-2)	Nominal point interval	120 m
	Source-receiver offset	40 m whenever feasible parallel to strike of Base Quaternary
	Receiver type	Triggered PASI Gemini 2Hz LandGeophone 3C
	Source type	Vertical sledgehammer 6 kg
	Vertical stacks/measurement	10 – 30 depending on transient noise level
	Recording time	3 sec
	Sampling interval	1 msec
4 passive array measurements ESAC (Fig. 3-3)	Nominal layout	L-shape, ~ 70 m × 140 m
	Receiver interval	3 m
	# of receivers	72 (nominal)
	Receiver type	Senshe SS-4.5N 4.5 Hz vertical velocimeter
	Recording time	20 – 30 min
	Sampling interval	4 msec

3.5 Productive lines: design and field parameters

The productive survey was carried out from October to December 2019 (few additional points were recorded in March 2020), with field parameters as shown in Tab. 3-4. As a conclusion from the pilot line, the passive measurement point distance was increased from 40 m (Tab. 3-3) to 50 m (Tab. 3-4) and that for active measurements from 120 m to 250 m.

Survey design recording times followed the recommendations from SESAME (2004), using the Base Quaternary model (Pietsch & Jordan 2014) and an estimated average shear wave velocity of 600 m/s for the Quaternary. The recommended recording time was multiplied by a factor of 2 to also collect sufficient data in noisy areas. After processing and interactive interpretation, it was decided to collect infill data along the lines 19QLAV-3 and 19QLAV-5 (see map in Fig. 2-1) to further constrain measurements of the bedrock topography along existing gaps due to the Aare river. Benefitting from low water levels in the river, additional data points were measured in March 2020.

Tab. 3-4: Field acquisition parameters of productive lines from October 2019 to March 2020

Measurement	**Parameter**	**Value**
198 passive point measurements HVSR	Nominal point interval	50 m
	Receiver type	PASI Gemini 2Hz LandGeophone 3C
	Recording time	10 min – 30 min, depending on transient noise level and expected depth to bedrock
	Sampling interval	5 msec
37 active point measurements HoliSurface®	Nominal point interval	250 m
	Source-receiver offset	40 m whenever feasible parallel to strike of Base Quaternary
	Receiver type	Triggered PASI Gemini 2Hz LandGeophone 3C
	Source type	Vertical sledgehammer 8 kg
	Vertical stacks/measurement	10 – 40 depending on transient noise level
	Recording time	3 sec
	Sampling interval	1 msec
6 passive array measurements ESAC	Nominal layout	L-shape, ~ 70 m × 140 m or L-shape, ~ 95 m × 190 m
	Receiver interval	3 m
	# of receivers	72 or 96 (nominal)
	Receiver type	Senshe SS-4.5N 4.5 Hz vertical velocimeter
	Recording time	30 – 45 min
	Sampling interval	4 msec

4 Field operations and data acquisition

4.1 Permit acquisition

Prior to any work on private ground, permits had to be obtained from landowners and tenants. Due to acquisition being early in the year (pilot line) and late in the year (productive lines), farming activities were low and many properties lay fallow. Access was generally permitted and only a few measurements had to be postponed for a few days until harvesting was completed.

4.2 Positioning of field measurements

The planned positions of measurements (pre-plot) were transferred into the field using maps. In the case of unforeseen obstacles, the positions were moved to locations that promised better data quality. Actual field coordinates were derived from orthophotos and maps with an accuracy of about 3 m (post-plot).

The source-receiver offset for active measurements and the geophone intervals for passive array measurements were surveyed with measuring tape.

Encl. 4-1 shows the post-plot survey layout for ambient vibration measurements superimposed on the Pietsch & Jordan (2014) Quaternary model. The numbering of the acquisition lines (1-8) reflects the priorities assigned by Nagra and guided the field acquisition sequence. Point identification numbers (PID) indicate the line number as first digit (hundreds) and increase from west to east, starting with 101 on line 19QLAV-1. In some situations, after the measurement points were defined, it was necessary to add more points between pre-defined positions. These identifiers are given a decimal number suffix, e.g. point 324.5 lies on line 19QLAV-3, between the 24th and 25th regular points from the west.

Encl. 4-2 features the same map as Encl. 4-1, but instead of boreholes the locations of ESAC arrays (red arches) and HoliSurface® measurements (green circles) are shown.

4.3 Execution of field data acquisition

Setting up the sensors firmly on the ground is essential for gathering good data. The uppermost soil with grass was removed prior to the careful planting and levelling of the sensors. Most positions could be recorded in the soil using spiked sensors. When the ground was hard, the sensor spikes were replaced by levelling screws.

In particular, strong wind and rain as well as monochromatic industrial vibrations (e.g. from power plants, heavy machinery) can hamper the reliability of ambient vibration data. Unfavourable weather conditions were avoided. In the case of light winds or the proximity of roads, the sensor was set up in a small hole or at least covered with a box to protect it (see Fig. 3-1). Structures such as buildings or large trees were avoided wherever possible.

A cement plant with a conveyor crossing the entire valley was located close to line 19QLAV-7 and vibrations from the conveyor affected the data significantly. While the eastern part of the line could be acquired during a shutdown of the conveyor, the increased noise level from the cement plant running 24/7 could not be avoided. This had a negative but unavoidable impact on results from this line.

4.4 In-field quality control

Individual shots for the active measurements were checked for data quality and then stacked in the field. Acceptance criteria were a good signal-to-noise ratio and the absence of transient signals that can occur due to traffic and footsteps.

Every second passive point acquisition was further analysed in the field by quick-look computation of the HVSR curve and the fundamental frequency f_0. Nevertheless, after in-depth analyses of data, it became obvious that about 15 % of the measurements would have to be repeated. After repetition, all the measurements fulfilled the SESAME (2004) criteria for a reliable HVSR curve.

5 Seismic data processing

The HVSR field data were analysed by roXplore gmbh using the winMASW 2019 software package (commercial software application running on Matlab®). roXplore gmbh subcontracted Eliosoft, IT-Cividale del Friuli for processing of the HoliSurface® active measurements and ESAC passive array measurements.

5.1 Processing of ambient vibration data

The analysis of HVSR data (i.e. determining the site-specific fundamental frequency f_0) followed the recommendations of SESAME (2004). In addition, several processing steps were added to improve the HVSR results:

- manual check of the reliability of single-component spectra
- manual removal of transient signals
- automatic removal of time windows with amplitudes higher than a pre-defined threshold
- automatic removal of HVSR time window outliers
- check of temporal persistence of spectra and spectral ratio
- check of azimuthal directivity of spectral ratio

For quality control, the SESAME (2004) criteria for a reliable HVSR curve and for a clear HVSR peak were computed and checked. When the QC control step failed for a particular measurement, data processing was repeated with adapted processing parameters. The acquisition of the field data was repeated if the QC criteria were not met.

Fig. 5-1 presents the general processing sequence. Fig. 5-2 shows an example of field data record (PID 126) in the time and frequency domain. Fig. 5-3 demonstrates the effect of spectral smoothing on the 3C data record and the final HVSR curve for the same PID as in Fig. 5-2 and highlights the fundamental frequency f_0.

Each PID was associated with its corresponding HVSR curve and plotted as a "trace-normalised" section (Fig. 5-4). Profile distances were derived as straight-line (Euclidian) distance from the first measurement point (i.e. from PID 101n in Fig. 5-4) to each PID. Consequently, the profiles are projected onto a straight line that connects the first and last PID. As an alternative data representation, Fig. 5-5 presents the HVSR as a gridded frequency map that visualises the spectral maximum f_0 as well as side maxima.

Encl. 5-1 to 5-8 present the processed data for all profiles in combination with shear wave velocity and bedrock topography profiles.

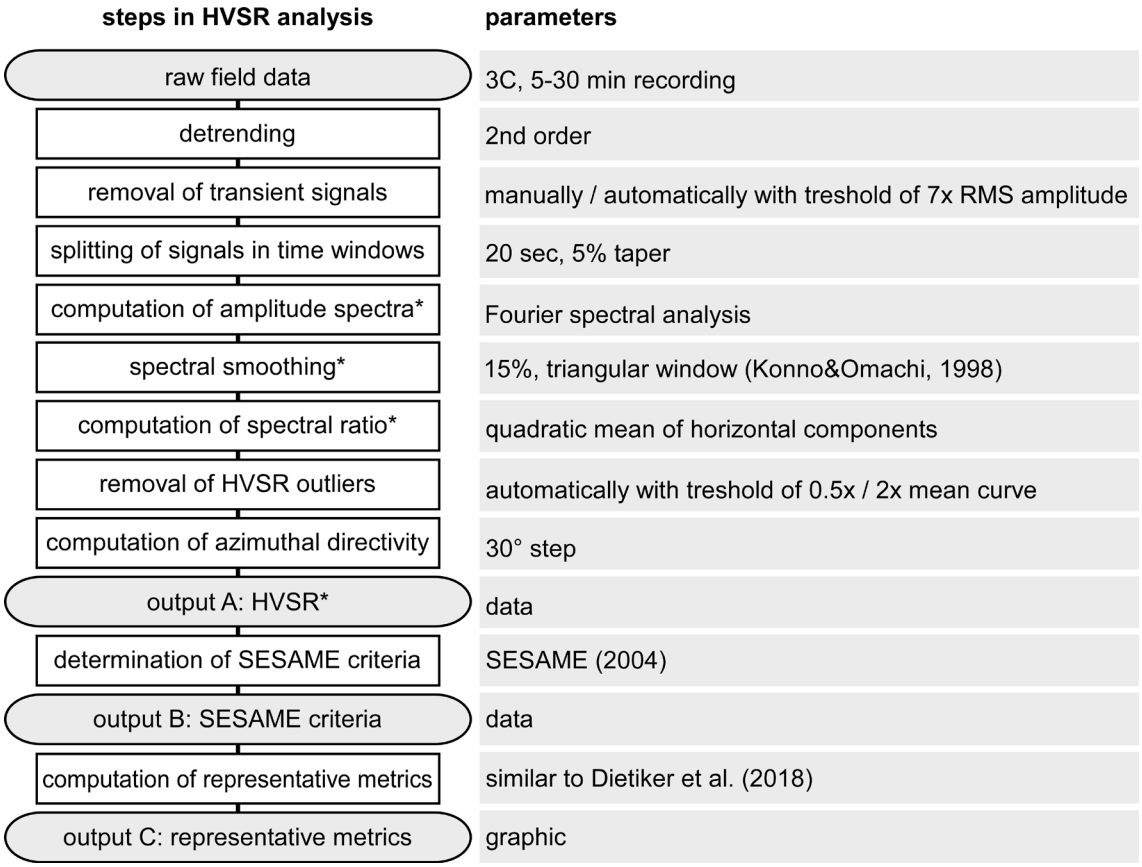


Fig. 5-1: HVSR processing sequence for ambient vibration data

* processing steps applied both to each time window and also to the whole time series.

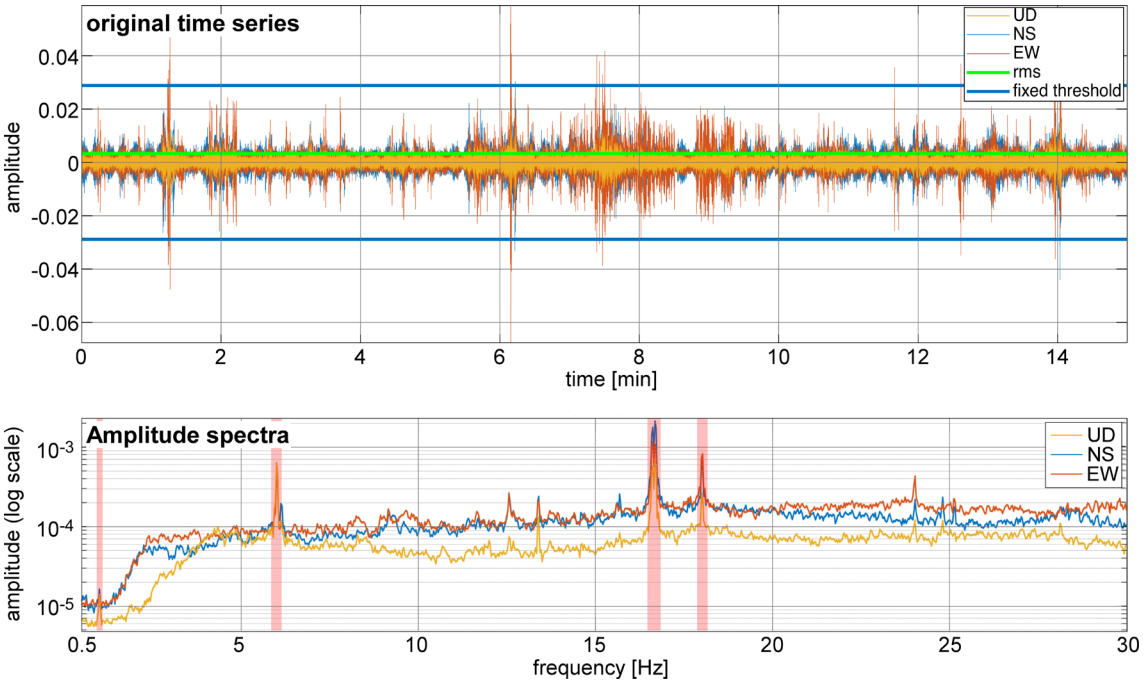


Fig. 5-2: Raw field data in time (top) and frequency (bottom) domain for PID 126

Top: detrended raw signal record of 15 min duration. The green line represents the RMS of the signal and the blue line denotes the threshold (here 7× RMS) of automatic transient removal.
Bottom: amplitude spectra of the three componeents; some spectral peaks induced by industrial monochromatic noise (e.g. @ 6.1 Hz, 6 Hz, 16.6 Hz and 18.0 Hz) are clearly displayed (red bars).

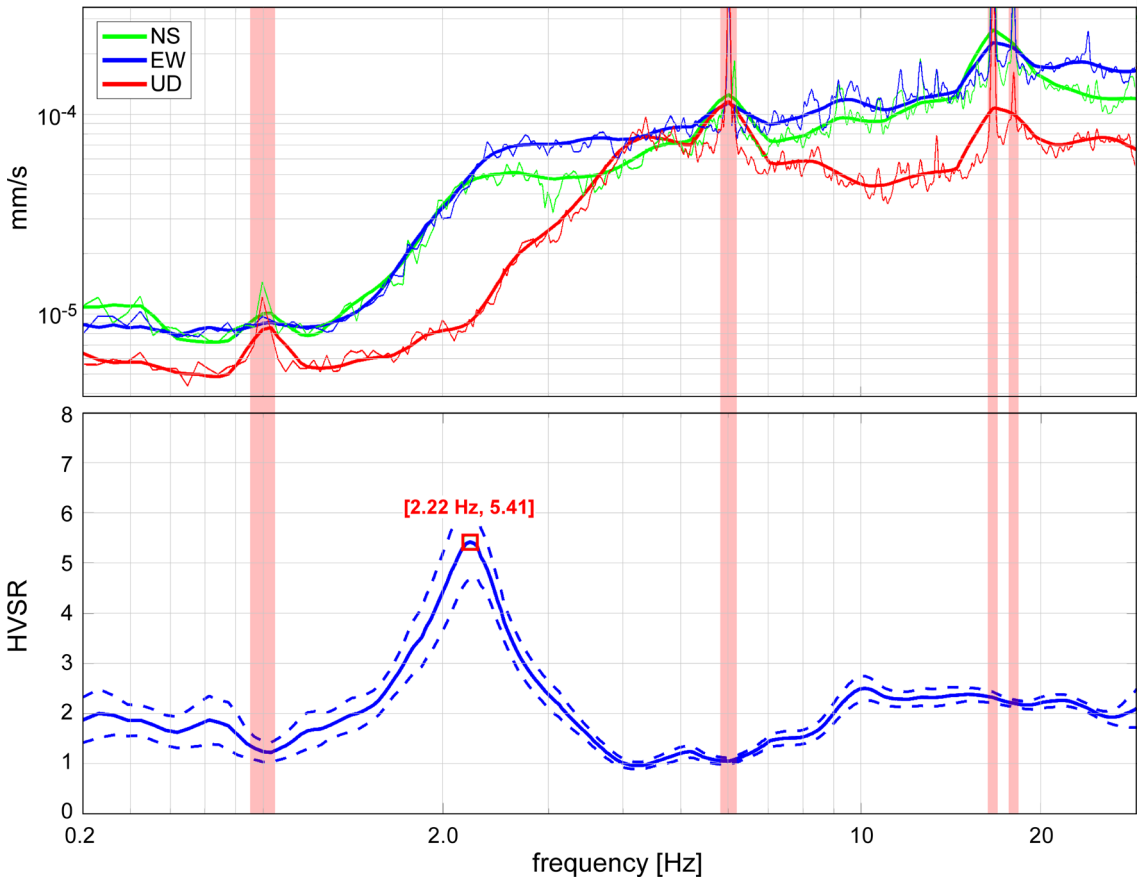


Fig. 5-3: Processed spectral data for PID 126

Top: Raw (thin line) and smoothed (thick line) spectra for north-south (NS), east-west (EW) and up-down (UD) components. Bottom: HVSR (thick blue) with +/- 1σ (dashed blue). Red square denotes automatically determined fundamental frequency f_0 with label for peak frequency and amplitude. Red bars mark industrially induced monofrequent noise.

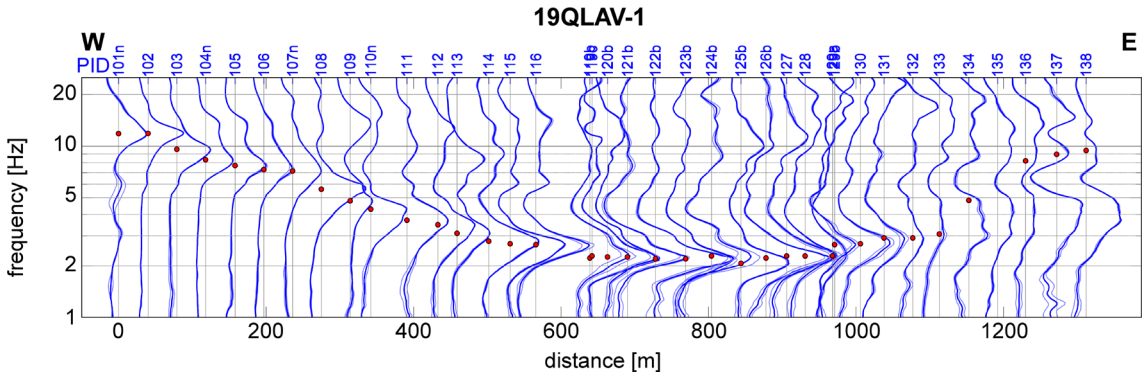


Fig. 5-4: Normalised HVSR curves along line 19QLAV-1

HVSR curves (bold blue) and +/-σ (thin blue). Red dots: interpreted fundamental frequency f_0. The HVSR curves are centred at the positions of the sensors (vertical grey lines).

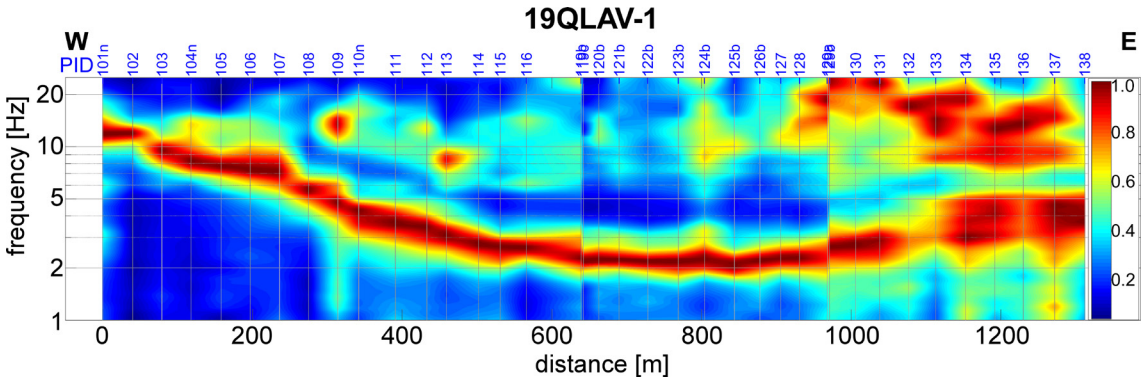


Fig. 5-5: Gridded HVSR section 19QLAV-1

Apparent discontinuities at PIDs 119 and 129 result from paired measurements with almost the same distance but lateral offsets due to river crossings.

5.2 Processing of active measurements

The analysis of active surface wave data aims to determine a vertical 1D shear wave velocity function (v_s) for the shallow underground at a particular point. The HoliSurface® methodology (e.g. Dal Moro et al. 2016, Dal Moro et al. 2019) according to the processing flow in Fig. 5-6 was applied. Pre-processing comprised the editing and vertical stacking of single shot data followed by the extraction of a data window to isolate the Rayleigh wave. This important step involved careful muting of the direct, refracted, body and coda wave components to minimise contamination of Rayleigh wave information. The pre-processed data were then used to compute three characteristic functions for input into the v_s model inversion:

- V_GZ: group velocity spectrum of vertical component applying the MFA algorithm (multiple frequency analysis; Dziewonski 1969)
- V_GR: group velocity spectrum of radial component applying the MFA algorithm
- RPM: Rayleigh wave Particle Motion characteristics from active measurements

A fourth input function was computed from the average of all passive (HVSR) measurements between HoliSurface® source and receiver positions.

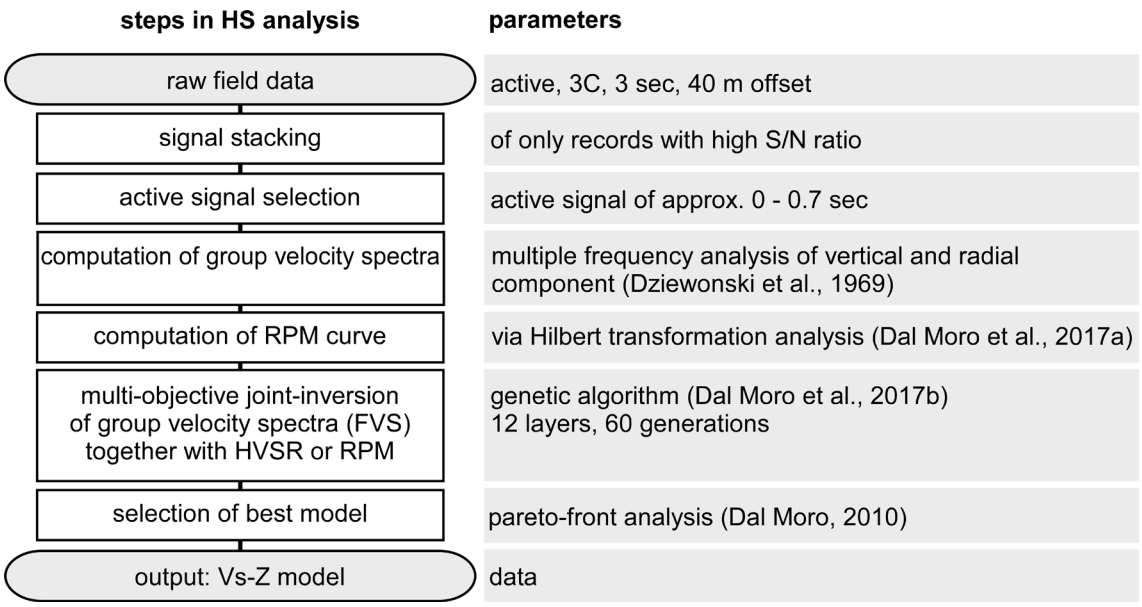


Fig. 5-6: General processing sequence for active surface wave data

This fourth input function helped to stabilise the velocity inversion at depth. Fig. 5-7 illustrates the pre-processing results for PID 115.

The subsequent inversion process featured adaptive weighting of three out of the four input functions. In particular, for data acquired above shallow bedrock, the RPM curve provided better inversion results than the HVSR curve and was therefore used instead of the latter.

A grid search variation was used to invert all input functions. The misfit between measured and modelled data was computed using thousands of virtually possible v_s models within a pre-defined but non-exclusive search space (green area in Fig. 5-8, left). Fig. 5-8, right, shows the misfit space for an inversion using V_GZ, V_GR and HVSR for PID 115. The misfit space was then scanned for the Pareto front models: these are best fitting v_s models in at least one characteristic (black circles in Fig. 5-8, right). The overall best-fitting v_s model results from the application of a global misfit minimisation scheme (minimum distance model in Fig. 5-8, see Dal Moro 2010 for methodological details). We used the overall best-fitting model for further analyses and depth conversions (see Section 5.3).

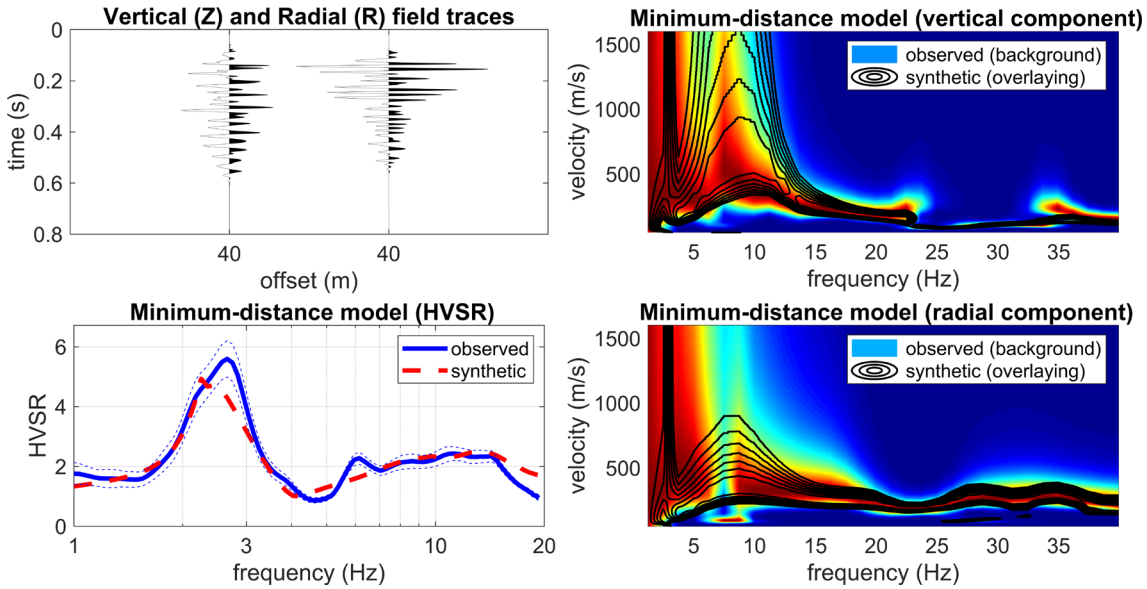


Fig. 5-7: HoliSurface® processing data and results for point 115 (left)

Top left: edited 2-component field data with vertical and radial time series;
Top right: group velocity spectrum of vertical component (in colours) with superimposed modelled group velocity spectrum in contours;
Bottom left: measured HVSR curve (blue) and modelled curve (red);
Bottom right: group velocity spectrum of radial component (in colours) with superimposed modelled group velocity spectrum in contours.

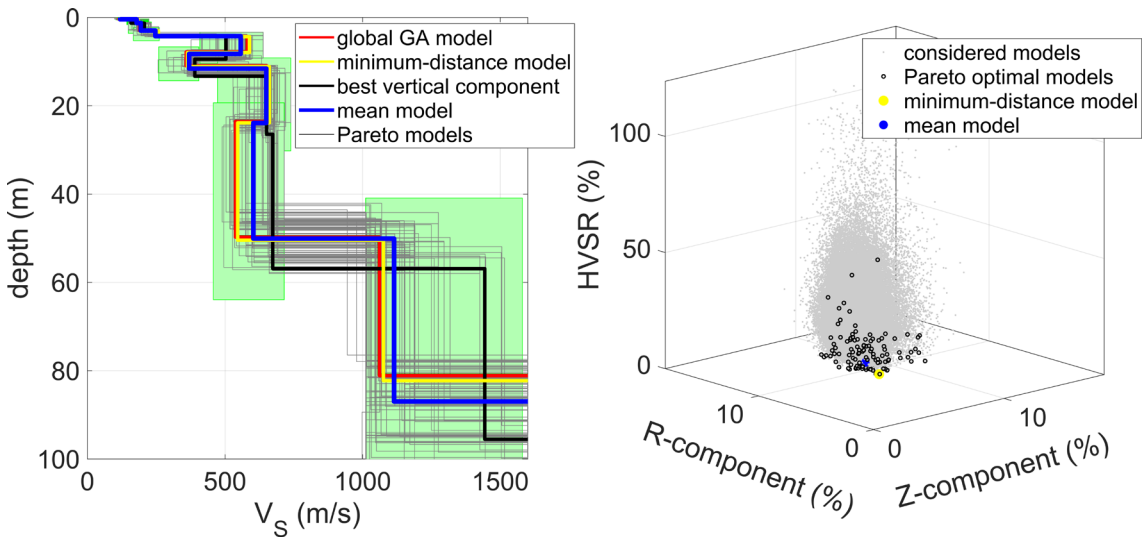


Fig. 5-8: Results of multi-objective inversion of PID 115

Left: shear wave velocity models. Green: model search space, grey: Pareto front models, yellow: minimum-distance model, blue: mean of all Pareto front models, red: global minimum model.
Right: 3D misfit plot shown in grey: all considered models, black: Pareto front models, yellow: minimum-distance model, and blue: mean Pareto front model.

5.3 Processing of passive array data

Ambient vibration data from L-shaped ESAC (extended spatial autocorrelation) arrays (Fig. 3-3) were analysed to determine shear velocities around the presumed trough centre. Fig. 5-9 shows the data recorded on an ESAC array layout that was realised on line 19QLAV-2. The processing scheme is outlined in Fig. 5-10 and follows Ohori et al. (2002). It resembles the classic SPAC (SPatial AutoCorrelation, Aki 1957) approach, but our approach required significantly less effort in the field.

We then inverted the phase velocity spectrum for the apparent dispersion following Tokimatsu et al. (1992). Fig. 5-11 shows the processed phase velocity spectrum overlain by the inverted dispersion model. The middle panel in Fig. 5-11 shows the averaged spectrum from the HVSR point measurements nearby, and the v_s profile resulting from the joint inversion of both datasets in the bottom panel.

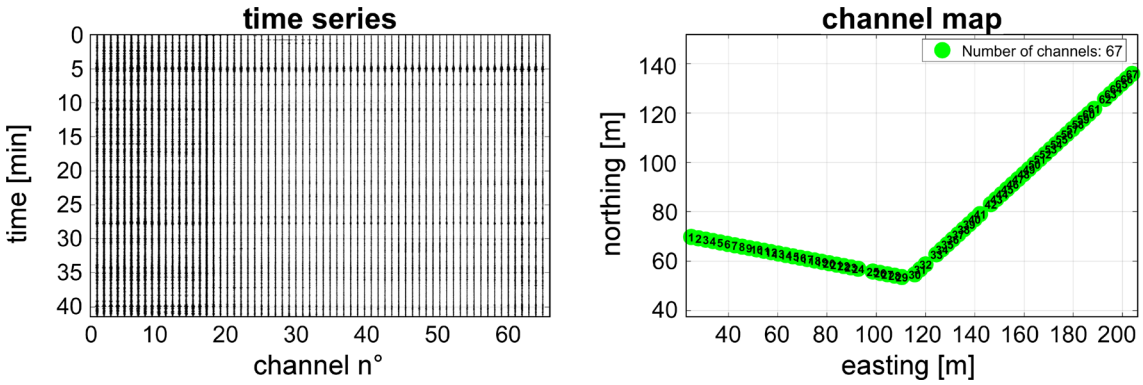


Fig. 5-9: Edited ESAC data and array layout close to the QGBR borehole location (array 215)

Left: seismic data of 45 min recordings after removal of noisy traces and transient signals. Right: ESAC array layout.

steps in ESAC analysis	parameters
raw field data	passive L-shaped array, 1C, 30 min, ~70 x 140 m, 72 chn
removal of bad data	eg. due to obstacles, bad coupling, etc. and transient signal
application of geometry	
computation of cross-spectra	for each pair of receivers (Capon, 1969)
compute phase velocity spectrum	fitting Bessel function to cross-spectra (see Aki 1957 and Ohori et al. (2002) for further details)
determination of apparent dispersion	non-modal approach (Tokimatsu et al., 1992)
inversion of apparent dispersion jointly with HVSR	trial and error with 12 layers
output: Vs-Z model	data and graphic

Fig. 5-10: Processing sequence of ESAC records

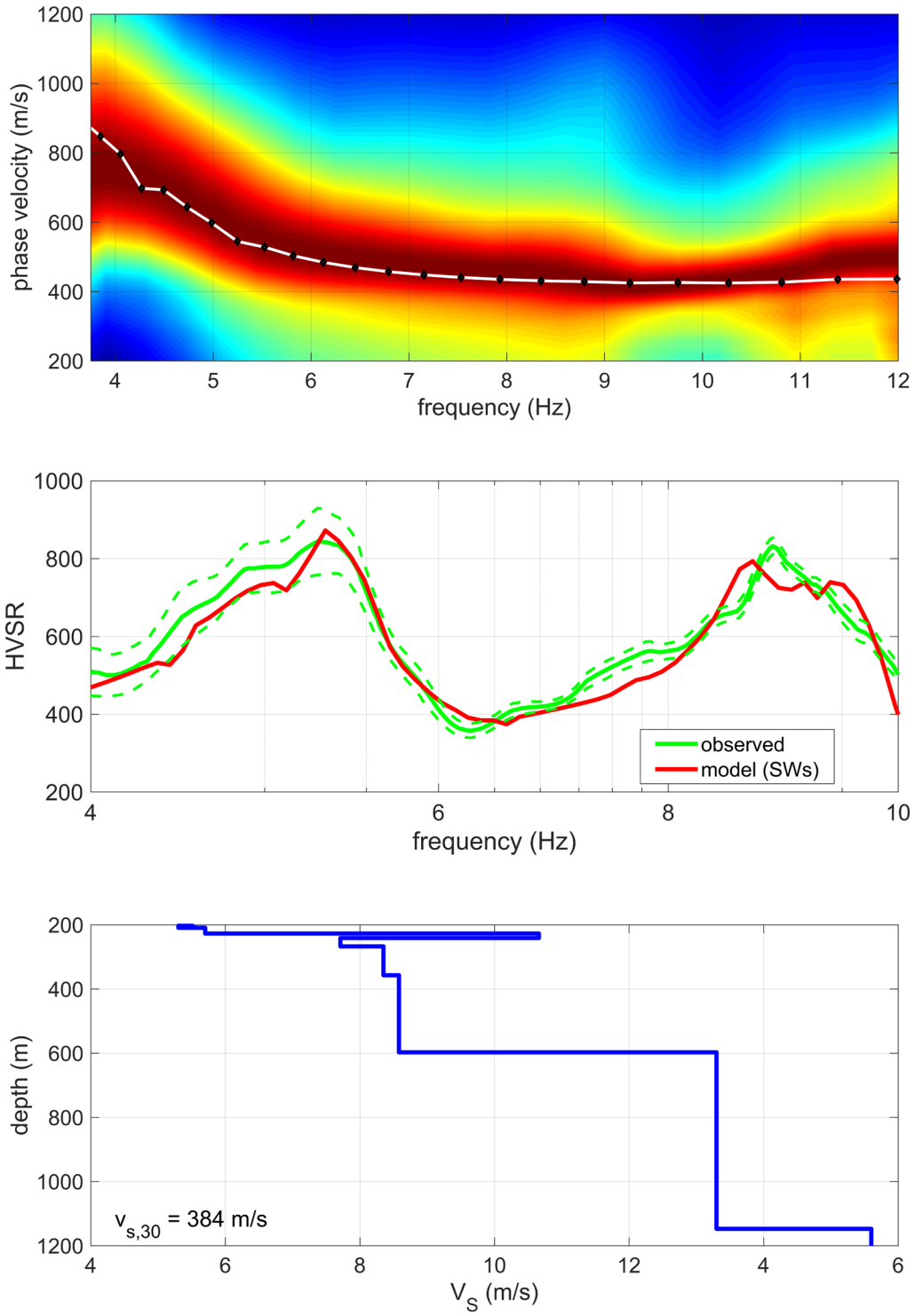


Fig. 5-11: Example result of ESAC processing from array 215

Top: phase velocity spectrum overlain by best-fitting dispersion curve (white).
Centre: observed (green) and modelled (red) HVSR. Observed HVSR is the average along the ESAC array (PID 215 and some additional measurements acquired along the branches of passive array).
Bottom: blocky shear wave velocity model inverted.

5.4 Frequency-to-depth conversion

Frequency-to-depth conversion consisted of three steps:

1. picking of the fundamental frequency f_0
2. determination of a representative 1D v_S model
3. conversion of f_0 to depth

In general, an automatic picking routing applied to HVSR curves gave reliable f_0 estimates. Each HVSR curve and its f_0 auto-pick were visually inspected for quality control and manually repicked if necessary. About 13 % of all picks were manually refined (Tab. 5-1), mainly because of the presence of secondary peaks or artificial noise.

Tab. 5-1: Summary table with information on automatically and manually picked f_0

Profile	**Total points**	**Automatic f_0**	**Manual f_0**	**Manual f_0** [in %]
19QLAV-6	23	18	5	22
19QLAV-2	24	18	6	25
19QLAV-4	33	31	2	6
19QLAV-1	38	32	6	16
19QLAV-8	18	16	2	11
19QLAV-5	23	22	1	4
19QLAV-3 / -9	51	43	8	40
19QLAV-7	30	28	2	7
Total	240	208	32	13

At several locations, the HVSR curves showed a secondary peak that was interpreted when geological evidence supported the existence of a second interface. Fig. 5-12 shows such an example on line 19QLAV-1. Prominent f_0 peaks at ~ 2 Hz characterise the trough's centre. We associate this response with the Quaternary – Malm interface that was encountered in the QGVO borehole. Towards the eastern side of the profile, the dominant frequency peak broadens and secondary maxima appear (distance 1'200 – 1'400 m in Fig. 5-12), likely caused by Molasse sediments between the Malm and Quaternary layers. We picked two HVSR maxima, one at about 3 Hz and one at about 5 – 10 Hz (Fig. 5-12), tentatively associated with Top and Bottom Tertiary. The general validity of using multiple HVSR maxima is further explored in Chapter 6.

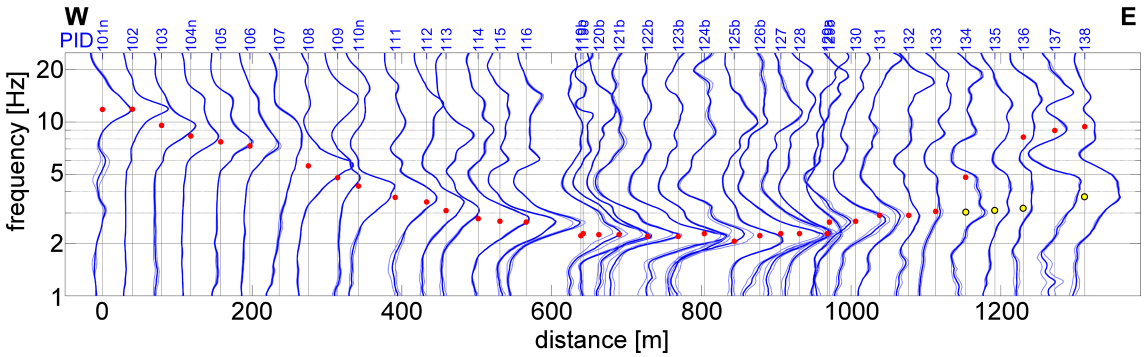


Fig. 5-12: HVSR curves of pilot line 19QLAV-1 and the picked f_0 peaks

In some areas, it was meaningful to interpret a second peak, in particular where a thin Tertiary layer overlaid Malm limestone. At these locations, two frequency values were stored (f_0 in red and f_1 in yellow).

Shear wave velocities were analysed separately for each of the profiles 19QLAV-1 to 19QLAV-7. It should be recalled that active HoliSurface® and passive ESAC measurements provide several shear wave velocity models along a transect (Sections 5.2 and 5.3). We computed average interval velocities $v_{s,av}$ by horizontally averaging the inverted v_s profiles as shown in Fig. 5-13.

Following Borcherdt (1994), a smoothed equivalent shear wave velocity function $v_{s,E}(z)$ was then computed down to depth z (Fig. 5-13) using

$$v_{s,E}(z) = \frac{z}{\sum \frac{h_i}{v_{si}}} \qquad \text{(Eq. 5-1)}$$

where z is depth, h_i the thickness of the ith layer and $v_{s,i}$ its average velocity.

It should be recalled that the conversion of the fundamental frequency f_0 to the Base Quaternary (bedrock) depth z required a velocity scalar (Eq. 3-1). Since $v_{s,E}(z)$ increased with depth, the application of a unique $v_{s,E}$, would overestimate velocities for positions with shallow Quaternary thickness (e.g. Fig. 5-13, light green example). To correct, we first estimated preliminary bedrock depths using the depth where v_s exceeds 1'100 m/s (Fig. 5-13) and averaged $v_s(z) < 1'100$ m/s. This step yielded PID-specific conversion velocities $v_{s,E}$ for application in Eq. 3-1.

Fig. 5-14 shows the depth conversion procedure for profile 19QLAV-1 and Tab. 5-2 summarises the velocity analyses for all profiles 19QLAV-1 to 19QLAV-8.

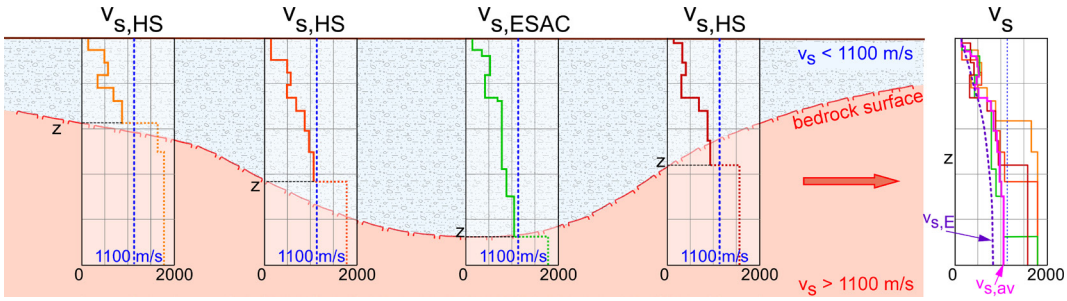


Fig. 5-13: Equivalent shear wave velocity concept

Left panel: four velocity functions along the profile. Solid lines indicate velocities in the unconsolidated overburden (< 1'100 m/s) and dashed lines in the bedrock (> 1'100 m/s). Right panel: $v_{s,av}$ is the average blocky velocity model and $v_{s,E}$ the equivalent shear wave velocity from surface to depth z.

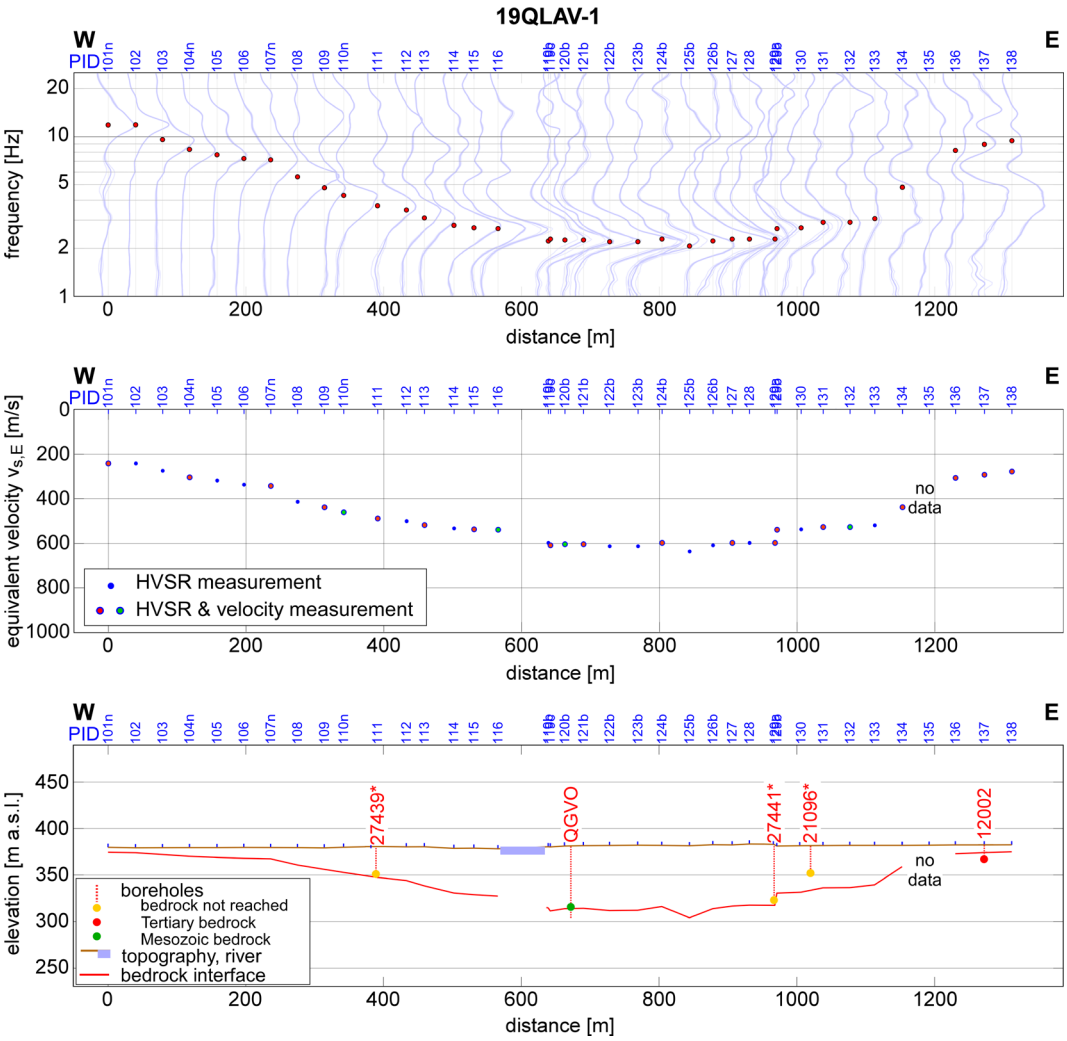


Fig. 5-14: Converting fundamental frequency f_0 to bedrock depths for profile 19QLAV-1

Top panel: HVSR curves with picks of fundamental frequency f_0 (red dots). Middle panel: equivalent shear wave velocity $v_{s,E}$ for velocity conversion. Bottom panel: Resulting Base Quaternary depth profile.

Tab. 5-2 Tabulated equivalent velocity $v_{s,E}$ [m/s] in overburden

Depth [m]	**19QLAV-6**	**19QLAV-2**	**19QLAV-4**	**19QLAV-1**	**19QLAV-8**	**19QLAV-5**	**19QLAV-3 / -9**	**19QLAV-7**
0 – 10	319	304	331	314	352	374	388	406
0 – 20	382	381	419	426	455	483	455	494
0 – 30	431	427	466	476	539	578	510	546
0 – 40	460	463	510	513	610	648	561	571
0 – 50	481	507	553	538	668	704	610	591
0 – 60	499	543	589	577	713	747	653	607
0 – 70	520	571	619	614	749	781	687	626
0 – 80	543	595	646	645	779	809	715	642
0 – 90	562	617	666	672	805	833	739	655
0 – 100	582	637	683		827	854	759	666
0 – 110	603	656	702		846	872	776	679
0 – 120	621	673	719		863	887	790	691

6 Geophysical Base Quaternary

6.1 Drilling information

The geophysical interpretation correlated the seismically derived Base Quaternary with borehole information. Boreholes located less than 200 m offset from a geophysical profile were considered and projected onto the profile. See Encl. 4-1 for a map showing the seismic measurements and borehole locations. Borehole positions were projected onto the seismic cross-section in a direction parallel to the strike of the Pietsch & Jordan (2014) Base Quaternary model.

6.2 Base Quaternary models

Base Quaternary models were constructed for each profile by linking the PID-based depth measurements (Section 5.3) with straight-line segments (see Fig. 6-1 for an example). Mostly across rivers, the distance between two measurements was larger than the nominal interval between two points. In the case of a gap exceeding 125 % of the nominal interval (50 m), the Base Quaternary model was interrupted (Fig. 6-1). Model interrupts also occurred when HVSR curves were not interpretable or no fundamental frequency could be picked. The geophysically derived Base Quaternary models were not tied to borehole information.

In some cases, secondary peaks in HVSR curves were recognised but not associated with Base Quaternary. Such secondary interfaces were not considered in the geophysical model (see Section 5.4).

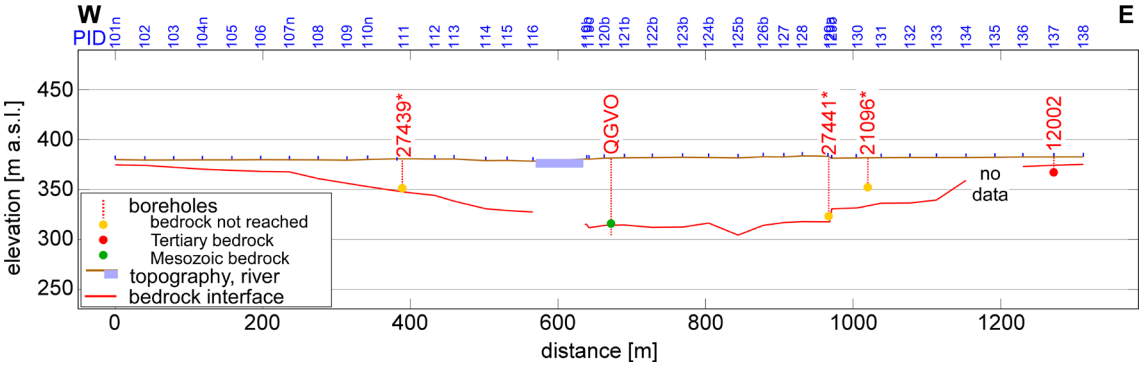


Fig. 6-1: BQu model of example line 19QLAV-1

The seismically derived bedrock model (Base Quaternary) is shown in red. Drilled bedrock depths are marked by red (Tertiary bedrock) and green (Mesozoic bedrock) dots. Yellow dots mark borehole end depths within the Quaternary.

Encl. 5-1 to 5-8 contain the processed data (HVSR curves with f_0 pick) conversion velocities and Base Quaternary depth model for each cross-section. Encl. 5-7 shows a joint section of 19QLAV-3 & 19QLAV-9. Section 19QLAV-9 was measured to fill a gap in 19QLAV-3, and the 19QLAV-9 measurement positions were therefore projected onto 19QLAV-3 along the contour lines of the existing bedrock model (Pietsch & Jordan 2014). Refer to Encl. 4-1 for a detailed map of the positions.

The depth models presented in Encl. 5-1– 5-8 result from depth conversion (Section 5.4) without well tie. Tab. 6-1 presents differences between Base Quaternary depths from borehole logs and results from our seismic data interpretation. Most differences range within +/- 10 m, which is reflected by the arithmetic mean for positive and negative differences at the bottom of Tab. 6-1. Such differences lay within the expected uncertainties of our method. The assessment of larger differences and construction of a best plausible Base Quaternary model was left to the geological interpretation (Chapter 7).

Tab. 6-1: Base Quaternary (BQu) depth differences between borehole logs and the interpretation of seismic data

Positive differences denote seismic measurements deeper than borehole information.

Encl.	**Cross-section**	**Borehole ID**	**Distance** [m]	**BQu** [m a.s.l.]		**Difference**	
				Seismic	**Borehole**	**Abs.** [m]	**Relative**
5-1 7-2	19QLAV-6	21078	170	325.9	316.0	9.9	74 %
5-1 7-2	19QLAV-6	29698	0	322.3	322.8	-0.5	3 %
5-1 7-2	19QLAV-6	27950	65	246.0	244.0 (?)	2.0	2 %
5-1 7-2	19QLAV-6	37104	0	373.3	377.0	-3.7	62 %
5-1 7-2	19QLAV-6	28284	0	393.3	377.0	16.3	82 %
5-1 7-2	19QLAV-6	33903	20	392.5	398.0	-5.5	231 %
5-2 7-3	19QLAV-2	29616	35	326.3	313.2	13.1	60 %
5-2 7-3	19QLAV-2	21114	0	326.5	311.8	14.7	78 %
5-2 7-3	19QLAV-2	21116	55	324.7	316.4	8.3	59 %
5-2 7-3	19QLAV-2	QGBR/34586	0	257.4	225.8	31.6	28 %
5-2 7-3	19QLAV-2	21090	90	301.9	323.5	-21.6	135 %
5-2 7-3	19QLAV-2	27920	55	335.1	349.0	-13.9	126 %
5-3 7-4	19QLAV-4	33878	40	311.3	315.2	-3.9	25 %
5-3 7-4	19QLAV-4	33876	85	307.1	312.7 (?)	-5.6	31 %

Tab. 6-1: Cont.

Encl.	Cross-section	Borehole ID	Distance [m]	BQu [m a.s.l.]		Difference	
				Seismic	Borehole	Abs. [m]	Relative
5-3 7-4	19QLAV-4	28225	20	369.1	362.0	7.1	44 %
5-4 7-5	19QLAV-1	QGVO/34587	30	264.1	266.1	-2.0	3 %
5-4 7-5	19QLAV-1	21102	0	324.0	317.7	6.3	43 %
5-5 7-6	19QLAV-8	35763	50	311.9	319.9	-8.0	21 %
5-6 7-7	19QLAV-5	28908	30	332.1	331.0	1.1	18 %
5-6 7-7	19QLAV-5	28907	70	331.2	326.0	5.2	44 %
5-6 7-7	19QLAV-5	37188	90	327.0	314.0	13.0	72 %
5-6 7-7	19QLAV-5	35594	30	345.4	338.6	6.8	34 %
5-6 7-7	19QLAV-5	29107	70	344.7	336.0	8.7	36 %
5-6 7-7	19QLAV-5	35764	25	345.4	342.5	2.9	15 %
5-7 7-8	19QLAV-3	29768	35	341.0	330.1	10.9	33 %
5-7 7-8	19QLAV-3	33872	160	326.6	310.7 (?)	15.9	30 %
5-7 7-8	19QLAV-3	29578	25	323.2	305.1 (?)	18.1	32 %
5-7 7-8	19QLAV-3	QUST/34599	0	276.0	255.2	20.8	27 %
5-7 7-8	19QLAV-3	4315	155	296.4	291.0	3.4	14 %
5-7 7-8	19QLAV-3	27437	140	321.6	312.2	9.4	43 %
5-8 7-9	19QLAV-7	17164	25	321.0	315.3	5.7	14 %
5-8 7-9	19QLAV-7	35687	175	320.4	324.0 (?)	3.6	14 %

Tab. 6-1: Cont.

Encl.	**Cross-section**	**Borehole ID**	**Distance** [m]	**BQu** [m a.s.l.]		**Difference**	
				Seismic	**Borehole**	**Abs.** [m]	**Relative**
5-8 7-9	19QLAV-7	29657	0	326.6	318.2 (?)	8.4	21 %
Average of positive/negative differences						+ 10.1 / - 7.2	

7 Geological interpretation and morphology of the Gebenstorf-Stilli Trough

7.1 Database and procedure

For the geological interpretation, the cross-sections 19QLAV-1 to -8 were complemented with surface geology, topography and borehole information. For the former two, we consulted the Geological Atlas of Switzerland 1:25.000 (map sheet Baden, Graf et al. 2006[2]) and the SwissALTI3D 2m DEM (Swisstopo 2013). The latter was compiled from the Nagra borehole database[3]. We took into consideration boreholes with a maximum distance of 200 m to the respective line. In the case of redundant boreholes (i.e. projecting at the same position along the line), priority was given to the deepest-reaching or, if total depths are similar, the borehole closest to the respective line. The corresponding drill logs were projected manually onto the cross-sections parallel to the isolines of the Gebenstorf-Stilli Trough from the Pietsch & Jordan (2014) model. The base of the Quaternary was then fitted to the boreholes and occasionally smoothed, while maintaining as closely as possible the trough shape as determined by the HVSR interpretation; the stratigraphy was added based on drill logs and surface geology.

In addition, we used the Nagra borehole database to construct a local-scale model of the plunging Tabular Jura surface (Encl. 7-1; indicated as "Top Malm model") where it is covered by Molasse deposits. This model was calculated in ESRI ArcGIS using the Topo-to-Raster function (3D Analyst toolbox, Raster Interpolation). We excluded the 2018 Quaternary boreholes as well as boreholes in the southernmost part of the 'Molasse wedge', i.e. south of 19QLAV-6, which record very irregular depths to Top Malm (see also Encl. 7-2). This is most likely due to either faults related to the Jura fold-and-thrust belt or to incorrect identification in previous boreholes and is thus not representative for the Top Malm surface.

7.2 Products of this study

Surface geology and borehole information were compiled to create a Base Quaternary subcrop map (Encl. 2-1). Encl. 7-2 to 7-9 show the individual cross-sections as listed. They are each subdivided into three panels: the upper plots the HVSR data and fundamental frequencies[4], while the middle reproduces the resulting surface seismic cross-section, which we complement with the respective borehole logs and – if applicable – the borehole-based Top Malm model. For comparison, we also plot the base of the Quaternary according to the model of Pietsch & Jordan (2014). On the lower panel the respective interpreted cross-section is plotted. Encl. 7-10 combines the individual profiles into one summary cross-section, and in Encl. 7-11 we provide a longitudinal section to visualise the trends in overdeepened trough morphology from north to south.

---

2 We noted that the island at Lauffohr (659'946.60, 261'471.70) is a limestone outcrop and not an alluvial bank as indicated by Graf et al. (2006).

3 These boreholes are referred to in the following by their ID according to the Nagra database.

4 Note: Encl. 5-1 to 5-8 project the individual HVSR measurements on a straight line connecting the first and last measurement point of each acquisition line. In contrast, Encl. 7-2 to 7-9 scale the HVSR profiles to the seismic line traces as plotted in the maps in these enclosures. This may result in differences in the total profile length and small (< 15 m) displacements of individual measurement positions.

7.3 Description and discussion of results

7.3.1 Base Quaternary subcrop

Encl. 2-1 provides a Base Quaternary subcrop map of the study area. For reference, Fig. 7-1 illustrates schematically the pre-Quaternary stratigraphic sequence as well as the dominant lithofacies. In the south of the study area, all stratigraphic units shown on Fig. 7-1 are exposed in the Jura fold-and-thrust belt, striking WSW-ENE and dipping moderately to steeply (up to 70°, Graf et al. 2006) southwards. A wedge of Molasse deposits follows northwards-adjacent and is ~ 1.5 km long at the position of the Gebenstorf-Stilli Trough. Beyond this Molasse wedge, with the boundary striking SW-NE, lies the Tabular Jura, in the study area generally represented by Upper Jurassic (Malm) rocks. Our borehole-based Top Malm model shows that the Tabular Jura plunges below the Molasse wedge, dipping 4-5° southeast (Encl. 7-1 and 7-11). It is in good qualitative agreement with the larger-scale models of e.g. Bitterli-Dreher et al. (2007: Fig. 15, 16) and Roth et al. (2010: App. 6.5), but our deepest points are below 200 m a.s.l. and are thus slightly deeper. The subglacial incision of the Gebenstorf-Stilli Trough is shown in Encl. 2-1 in the shape of a narrow corridor where geological boundaries are shifted southwards (i.e. in the dip direction).

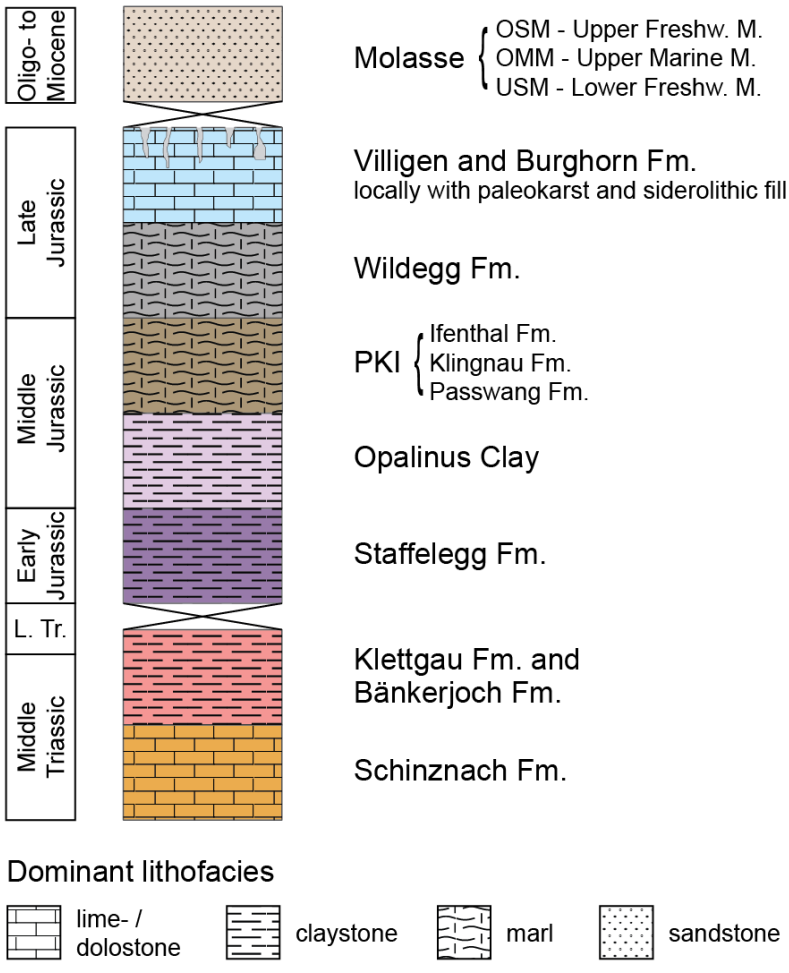


Fig. 7-1: Pre-Quaternary stratigraphy in the study area

After Bitterli-Dreher et al. (2007), Jordan & Deplazes (2019)

7.3.2 Gebenstorf-Stilli Trough morphology

The surface seismic approach employed has proven suitable for imaging the base of the Quaternary, i.e. the base of the Gebenstorf-Stilli Trough. However, the quality of the HVSR peaks, and thus the reliability of the respective depth conversions, varies between different measurement points. Major uncertainties affecting individual profiles are listed in Encl. 7-2 to 7-9. Where alternative interpretations of the trough shape are possible, these are plotted as dashed lines in the respective bottom panel (all except Encl. 7-4).

The average difference between the depth-converted HVSR interpretation closest to the drill sites and the actual drilled depth of the base of the Quaternary is ~ -7/+10 m (Tab. 6-1), with the maximum depth overestimation being +21.6 m (at borehole 21090 on 19QLAV-2) and the maximum depth underestimation being -31.6 m (at borehole QGBR/34586, also on 19QLAV-2). In conclusion, the applied surface seismic approach tends to image the Gebenstorf-Stilli Trough as being shallower than it is. However, it should be stressed that only some of the boreholes considered lie on the acquisition lines, while others are projected up to 170 m. Differences in elevation of the base of the Quaternary occurring over these projection distances may be significant and are included in the reported errors.

It should be noted that many of the boreholes considered have been drilled destructively, i.e. recovering cuttings instead of a complete core, which may result in uncertainties in the exact depths of geological units. Furthermore, small size and poor state of cuttings, crudely spaced sampling, or contamination with caving material may result in misinterpretation of entire units.

An example of an ambiguous log is from borehole 27950 on line 19QLAV-6 (Encl. 7-2). It records greenish-grey sand from 284 m a.s.l. up to its termination at 192 m a.s.l., with gravel and cobbles at 246-244 m a.s.l. We favour an explanation with glaciolacustrine sand from 284 to 246 m a.s.l, glacial gravel/diamicton marking the base of the Gebenstorf-Stilli Trough from 246 to 244 m a.s.l, and Molasse sand from 244 to194 m a.s.l, which is in good agreement with seismic data. However, from the archived log we can neither exclude that borehole 27950 recovered exclusively Quaternary deposits as it terminated in a narrow 'inner gorge' (Dürst Stucki et al. 2012; Jansen et al. 2014) within the Gebenstorf-Stilli Trough that is deeper than 194 m a.s.l. (but could not be seismically imaged), nor that the Trough is much shallower than this and the borehole log records sandy Molasse bedrock instead of glaciolacustrine sand.

7.3.3 Cross-sections

The interpreted cross-sections are provided in Encl. 7-2 to 7-9. The Enclosures include a brief description of the trough shape and infill as well as the main uncertainties affecting the respective cross-section. The distinction between V- and U-dominated trough shape follows Zimmer & Gabet (2018, V index). V indices (VI) of the GST range from 0.09 to 1.04. We classify VI < 0.25 as V-shaped, VI > 0.50 as U-shaped, and VI between 0.25 and 0.50 as intermediate (see Encl. 7-2 to 7-8). For some cross-sections, we offer an alternative interpretation of the trough morphology. This applies to locations where input data are inconclusive, poorly resolved or lacking. Encl. 7-10 displays the individual cross-sections in a combined plot, visualising trends in shape along the trough axis.

Bedrock nomenclature is based on Bitterli-Dreher et al. (2007) and complemented by Jordan & Deplazes (2019). Note particularly the gradual lithological transition between the Villigen Formation and the Wildegg Formation. The Quaternary stratigraphic nomenclature follows Graf & Burkhalter (2016). The nomenclature of the overdeepened trough infill below the Niederterrasse remains purely descriptive and is based exclusively on borehole logs. In the north

of the study area, the separation of coarse-grained trough infill and Niederterrasse is not based on a lithological boundary, but the base of the Niederterrasse is extrapolated from the south, where such a boundary exists (overlying fine-grained infill, see Encl. 7-11). Thin Holocene alluvial or colluvial deposits that cover large parts of the study area are not displayed separately, i.e. these deposits are included in the stratigraphic unit exposed at the surface.

7.3.4 Synthesis

The Gebenstorf-Stilli Trough cuts through the Jura fold-and-thrust belt in the shape of a narrow, buried V-valley (300 – 400 m wide at 300 m a.s.l.; Dürst Stucki & Schlunegger 2013, Pietsch & Jordan 2014, Gorhan & Griesser 1988). Upon exiting the Jura fold-and-thrust belt and entering Molasse deposits, the seismic data show the trough slowly widening until it reaches its maximum width (~ 800 m at 300 m a.s.l.) at line 19QLAV-1 (Encl. 7-5). This widening coincides with a transition to a more U-shaped profile and also a gradual shallowing of the trough from ~ 225 m to ~ 265 m a.s.l. that follows the trend of the Top Malm surface. The minimum trough depth (~ 295 m a.s.l.) is reached at line 19QLAV-8 (Encl. 7-6). From here on towards the north, the clear seismic image of the Gebenstorf-Stilli Trough deteriorates, but it is obvious from surface observations that it narrows again as it wedges through between the Bruggerberg in the west and Iberig/Iflue in the east, at the transition to the exposed Tabular Jura. This is accompanied by a deepening of the trough. It reaches a second local minimum of ~ 245 m a.s.l. at line 19QLAV-3/-9 (Encl. 7-8), from where it shallows towards its terminus. A steep eastern trough flank, well constrained by boreholes QUST and 4315 (Encl. 7-8), again suggests a more U-shaped cross-section in this part of the trough. In conclusion, we observe a trough section that appears to be composed of two separate 'nested sub-basins' (Patton et al. 2016). These are referred to in the following as the Gebenstorf Basin and Stilli Basin, separated by the Lauffohr Ridge (Encl. 7-11).

The analysed section of the Gebenstorf-Stilli Trough reaches its maximum depth in the Gebenstorf Basin, possibly near the site of QGBR (111.5 m of Quaternary and anthropogenic deposits), however the maximum depth in the Stilli Basin is not very well constrained. We also need to stress again that a potential narrow inner gorge (such as are known to occur in formerly glaciated regions; Dürst Stucki et al. 2012; Jansen et al. 2014) could likely not be imaged by the chosen methodology, and thus cannot be excluded. The maximum width of ~ 800 m at 300 m a.s.l. is reached at Vogelsang. Between lines 19QLAV-3/-9 and -7 (Encl. 7-8 and 7-9), the average adverse slope angle according to our interpretation is ~ 1.6°. A comparison of these values with other Swiss foreland overdeepenings is listed in Tab. 7-1: The Gebenstorf-Stilli Trough is slightly shallower and significantly narrower than average foreland overdeepenings, but it has a comparatively steep adverse slope (Magrani et al. 2020).

Tab. 7-1: Key dimensions of the Gebenstorf-Stilli Trough compared with other foreland overdeepenings in Switzerland

* Data from Magrani et al. (2020)

Maximum depth refers to present-day ground surface. The model of Magrani et al. (2020) uses a minimum sediment thickness or water column of 20 m to define overdeepening extent, thus maximum width is given 20 m below present-day ground surface.

	Max. depth [m]	**Max. width** [m]	**Adv. slope** [°]
Gebenstorf-Stilli Trough	≥ 112	920	1.6
Swiss foreland mean*	180	2024	1.0
Swiss foreland median*	115	1298	0.6

7.4 Conclusion

The Gebenstorf-Stilli Trough is a narrow, ~ 10 km long extension of the Birrfeld basin (Bitterli-Dreher et al. 2007, Graf 2009). The trough morphology was previously constrained by only a few boreholes, leaving considerable uncertainties about the position and elevation of its thalweg. Using diverse surface wave seismic methods, the missing information was acquired effectively. The course and morphology of the distal part of the Gebenstorf-Stilli Trough, north of the Jura fold-and-thrust belt, is imaged on eight seismic sections. We present a concise methodological summary, resulting depth sections and a first geological interpretation. This interpretation is currently being incorporated into an updated version of the Base Quaternary model of Northern Switzerland by Nagra (Loepfe et al. unpubl., version 15.07.2021).

The trough appears to be subdivided into two 'nested sub-basins' that are separated by a prominent ridge (see Encl. 7-11; Patton et al. 2016). Our study reveals that this morphology is controlled predominantly by the bedrock geology and resulting pre-glacial topography: the southern (proximal) Gebenstorf Basin is mostly incised into Molasse deposits, whereas the northern (distal) Stilli Basin is cut into predominantly calcareous marls of the Wildegg Formation. The stoss side of the separating ridge is formed by limestones at the top of the plunging Tabular Jura (Villigen Formation), which we consider an important mechanical boundary affecting subglacial incision (see e.g. Kühni & Pfiffner 2001, Fig. 13).

Bedrock geology might not be the only factor controlling the overdeepened trough shape; the paleoglaciological setting likely also played an important role. While the ice flow was laterally constrained above the Stilli Basin (by the Bruggerberg and Iberig/Iflue), we suspect it was significantly less constrained above the Molasse-hosted Gebenstorf Basin (Patton et al. 2016; Magrani et al. 2020). A further complication is added by the confluence situation of the "Wasserschloss", resulting in a localised increase in ice and meltwater flux where the individual drainages coalesce (Cook & Swift 2012).

These concepts are further discussed by Gegg et al. (2021), who additionally conclude that glacial erosion sensu stricto (i.e. quarrying and abrasion) was relatively inefficient in the Gebenstorf-Still trough. In contrast, basal water is considered as a significant or perhaps the main driver in past overdeepening erosion, in analogy to tunnel valleys (Dürst Stucki & Schlunegger 2013).

8 Acknowledgements

This study benefitted from previous work by Stefan Heuberger (Heuberger Geologie GmbH).

9 References

Aki, K. (1957): Space and time spectra of stationary stochastic waves, with special reference to microtremors: Bulletin of the Earthquake Research Institute, v. 35, p. 415-456.

Bitterli-Dreher, P., Graf, H.R., Naef, H., Diebold, P., Matousek, F., Burger, H. & Pauli-Gabi, T. (2007): Geologischer Atlas der Schweiz 1:25000. Blatt 1070 Baden. Erläuterungen, Geologischer Atlas der Schweiz 1:25000, 152 p.

Borcherdt, R.D. (1994): Estimates of site-dependent response spectra for design (methodology and justification): Earthquake spectra, v. 10, no. 4, p. 617-653.

Brook, M.S., Kirkbride, M.P. & Brock, B.W. (2004): Rock strength and development of glacial valley morphology in the Scottish Highlands and northwest Iceland: Geografiska Annaler: Series A, Physical Geography, v. 86, no. 3, p. 225-234.

Capon, J. (1969): High-resolution frequency-wavenumber spectrum analysis: Proceedings of the IEEE, v. 57, no. 8, p. 1408-1418.

Cook, S.J. & Swift, D.A. (2012): Subglacial basins: Their origin and importance in glacial systems and landscapes: Earth-Science Reviews, v. 115, no. 4, p. 332-372.

Dal Moro, G. (2010): Insights on surface wave dispersion and HVSR: Joint analysis via Pareto optimality: Journal of Applied Geophysics, v. 72, no. 2, p. 129-140.

Dal Moro, G. (2019): Surface wave analysis: improving the accuracy of the shear-wave velocity profile through the efficient joint acquisition and Full Velocity Spectrum (FVS) analysis of Rayleigh and Love waves: Exploration Geophysics, v. 50, no. 4, p. 408-419.

Dal Moro, G., Al-Arifi, N. & Moustafa, S.R. (2019): On the efficient acquisition and holistic analysis of Rayleigh waves: technical aspects and two comparative case studies: Soil Dynamics and Earthquake Engineering, v. 125, p. 105742.

Dal Moro, G., Keller, L., Al-Arifi, N. & Moustafa, S. (2016): Shear-wave velocity profiling according to three alternative approaches: a comparative case study: Journal of Applied Geophysics, v. 134, p. 112-124.

Dick, K., Graf, H., Müller, B., Hartmann, P. & Schlüchter, C. (1996): Das nordalpine Wasserschloss und seine eiszeitgeologische Umgebung: Eclogae Geologicae Helvetiae, v. 89, p. 635-645.

Dobry, R., Oweis, I. & Urzua, A. (1976): Simplified procedures for estimating the fundamental period of a soil profile: Bulletin of the Seismological Society of America, v. 66, no. 4, p. 1293-1321.

Dühnforth, M., Anderson, R.S., Ward, D. & Stock, G.M. (2010): Bedrock fracture control of glacial erosion processes and rates: Geology, v. 38, no. 5, p. 423-426.

Dürst Stucki, M. & Schlunegger, F. (2013): Identification of erosional mechanisms during past glaciations based on a bedrock surface model of the central European Alps: Earth and Planetary Science Letters, v. 384, p. 57-70.

Dürst Stucki, M., Schlunegger, F., Christener, F., Otto, J.-C. & Götz, J. (2012): Deepening of inner gorges through subglacial meltwater – An example from the UNESCO Entlebuch area, Switzerland: Geomorphology, v. 139, p. 506-517.

Dziewonski, A., Bloch, S. & Landisman, M. (1969): A technique for the analysis of transient seismic signals: Bulletin of the seismological Society of America, v. 59, no. 1, p. 427-444.

Gegg, L., Deplazes, G., Keller, L., Madritsch, H., Spillmann, T., Anselmetti, F.S. & Buechi, M.W. (2021): 3D morphology of a glacially overdeepened trough controlled by underlying bedrock geology. Geomorphology, DOI 10.1016/j.geomorph.2021.107950.

Gegg, L., Kuster, A.M., Amschwand, D., Huber, M., Deplazes, G., Madritsch, H. & Buechi, M.W. (2019a): Quaternary Borehole QBO Gebenstorf-Vogelsang (QGVO) Data Report. Nagra Arbeitsbericht NAB 19-03.

Gegg, L., Kuster, A.M., Deplazes, G., Madritsch, H. & Buechi, M.W. (2019b): Quaternary Borehole QBO Gebenstorf-Brüel (QGBR) Data Report. Nagra Arbeitsbericht NAB 19-02.

Gegg, L., Kuster, A.M., Schmid, D., Lemke, K., Deplazes, G., Madritsch, H. & Buechi, M.W. (2019c): Quaternary Borehole QBO Untersiggenthal (QUST) Data Report. Nagra Arbeitsbericht NAB 19-01.

Gorhan, H. & Griesser, J. (1988): Geothermische prospektion im Raum Schinznach Bad-Baden: Beiträge zur Geologie der Schweiz. Geotechnische Serie, no. 76.

Goudie, A.S. (2016): Quantification of rock control in geomorphology: Earth-Science Reviews, v. 159, p. 374-387.

Graf, H.R. (2009): Stratigraphie von Mittel-und Spätpleistozän in der Nordschweiz, Beiträge zur Geologischen Karte der Schweiz, 198 p.

Graf, H.R. & Burkhalter, R. (2016): Quaternary deposits: concept for a stratigraphic classification and nomenclature – an example from northern Switzerland: Swiss Journal of Geosciences, v. 109, no. 2, p. 137-147.

Graf, H.R., Bitterli-Dreher, P., Burger, H., Bitterli, T., Diebold, P. & Naef, H. (2006): Geologischer Atlas der Schweiz 1:25'000, Blatt 1070 Baden: Bundesamt für Landestopografie swisstopo, Wabern, Switzerland.

Haldimann, P., Naef, H. & Schmassmann, H. (1984): Fluviatile Erosions- und Akkumulationsformen als Indizien jungpleistozäner und holozäner Bewegungen in der Nordschweiz und angrenzenden Gebieten: Nagra Technischer Bericht NTB 84-16.

Jansen, J.D., Codilean, A.T., Stroeven, A.P., Fabel, D., Hättestrand, C., Kleman, J., Harbor, J.M., Heyman, J., Kubik, P.W. & Xu, S. (2014): Inner gorges cut by subglacial meltwater during Fennoscandian ice sheet decay: Nature communications, v. 5, no. 1, p. 1-7.

Jordan, P. & Deplazes, G. (2019): Lithostratigraphy of Consolidated Rocks expected in the Jura Ost, Nördlich Lägern and Zürich Nordost Regions. Nagra Arbeitsbericht NAB 19-14.

Krabbendam, M. & Glasser, N.F. (2011): Glacial erosion and bedrock properties in NW Scotland: abrasion and plucking, hardness and joint spacing: Geomorphology, v. 130, no. 3-4, p. 374-383.

Kühni, A. & Pfiffner, O.-A. (2001): The relief of the Swiss Alps and adjacent areas and its relation to lithology and structure: topographic analysis from a 250-m DEM: Geomorphology, v. 41, no. 4, p. 285-307.

Magrani, F., Valla, P.G., Gribenski, N. & Serra, E. (2020): Glacial overdeepenings in the Swiss Alps and foreland: Spatial distribution and morphometrics. Quaternary Science Reviews 243.

Nakamura, Y. (1989): A method for dynamic characteristics estimation of subsurface using microtremor on the ground surface: Railway Technical Research Institute, Quarterly Reports, v. 30, no. 1, p. 25-33.

Nitsche, F., Monin, G., Marillier, F., Graf, H. & Ansorge, J. (2001): Reflection seismic study of Cenozoic sediments in an overdeepened valley of northern Switzerland: the Birrfeld area: Eclogae Geologicae Helvetiae, v. 94, no. 3, p. 363-371.

Ohori, M., Nobata, A. & Wakamatsu, K. (2002): A comparison of ESAC and FK methods of estimating phase velocity using arbitrarily shaped microtremor arrays: Bulletin of the Seismological Society of America, v. 92, no. 6, p. 2323-2332.

Patton, H., Swift, D., Clark, C., Livingstone, S.J. & Cook, S.J. (2016): Distribution and characteristics of overdeepenings beneath the Greenland and Antarctic ice sheets: Implications for overdeepening origin and evolution: Quaternary Science Reviews, v. 148, p. 128-145.

Pietsch, J. & Jordan, P. (2014): Digitales Höhenmodell Basis Quartär der Nordschweiz - Version 2014 und ausgewählte Auswertungen. Nagra Arbeitsbericht NAB 14-02.

Preusser, F., Reitner, JM. & Schlüchter, C. (2010): Distribution, geometry, age and origin of overdeepened valleys and basins in the Alps and their foreland: Swiss Journal of Geosciences, v. 103, no. 3, p. 407-426.

Roesset, J. (1970): Fundamentals of soil amplification: Massachusetts Inst. of Tech., Cambridge.

Roth, P., Naef, H. & Schnellmann, M. (2010): Kompilation und Interpretation der Reflexionsseismik im Tafeljura und Molassebecken der Zentral- und Nordostschweiz: Nagra Arbeitsbericht NAB 10-39.

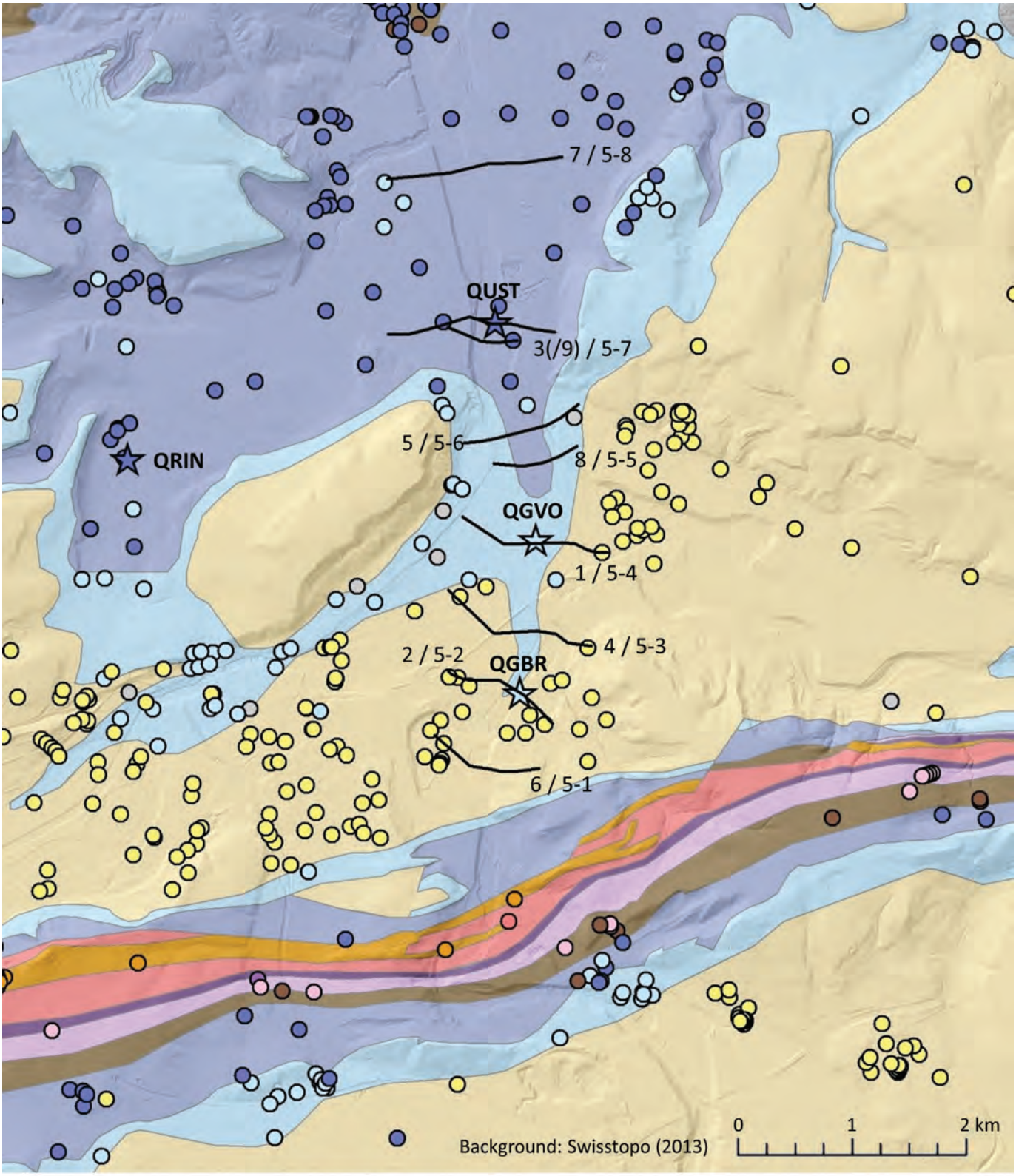
SESAME European Research Project (2004): Guidelines for the implementation of the H/V spectral ratio technique on ambient vibrations measurements, processing and interpretation: European Commission.

Swisstopo (2013): swissALTI3D, Federal Office of Topography swisstopo Wabern, Switzerland.

Tokimatsu, K., Tamura, S. & Kojima, H. (1992): Effects of multiple modes on Rayleigh wave dispersion characteristics: Journal of geotechnical engineering, v. 118, no. 10, p. 1529-1543.

Wildi, W. (1984): Isohypsenkarte der quartären Felstäler in der Nord-und Ostschweiz, mit kurzen Erläuterungen: Eclogae Geologicae Helvetiae, v. 77, no. 3, p. 541-551.

Zimmer, P.D. & Gabet, E.J. (2018): Assessing glacial modification of bedrock valleys using a novel approach: Geomorphology, v. 318, p. 336-347.



○ Borehole (Nagra borehole database) ☆ Nagra Quaternary borehole — Seismic line (19QLAV-X / Encl.)

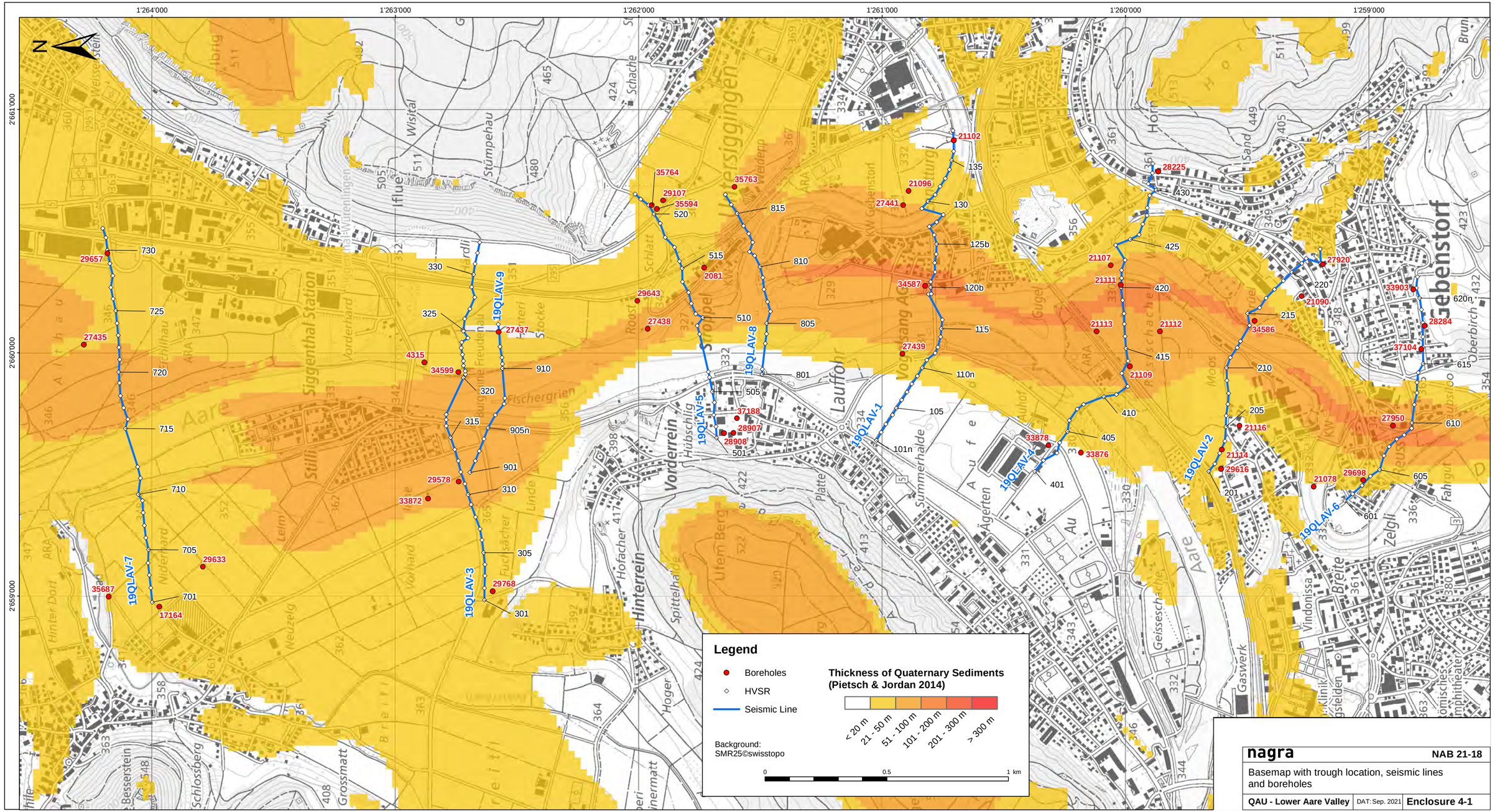
Boreholes: bedrock geology below base of Quaternary

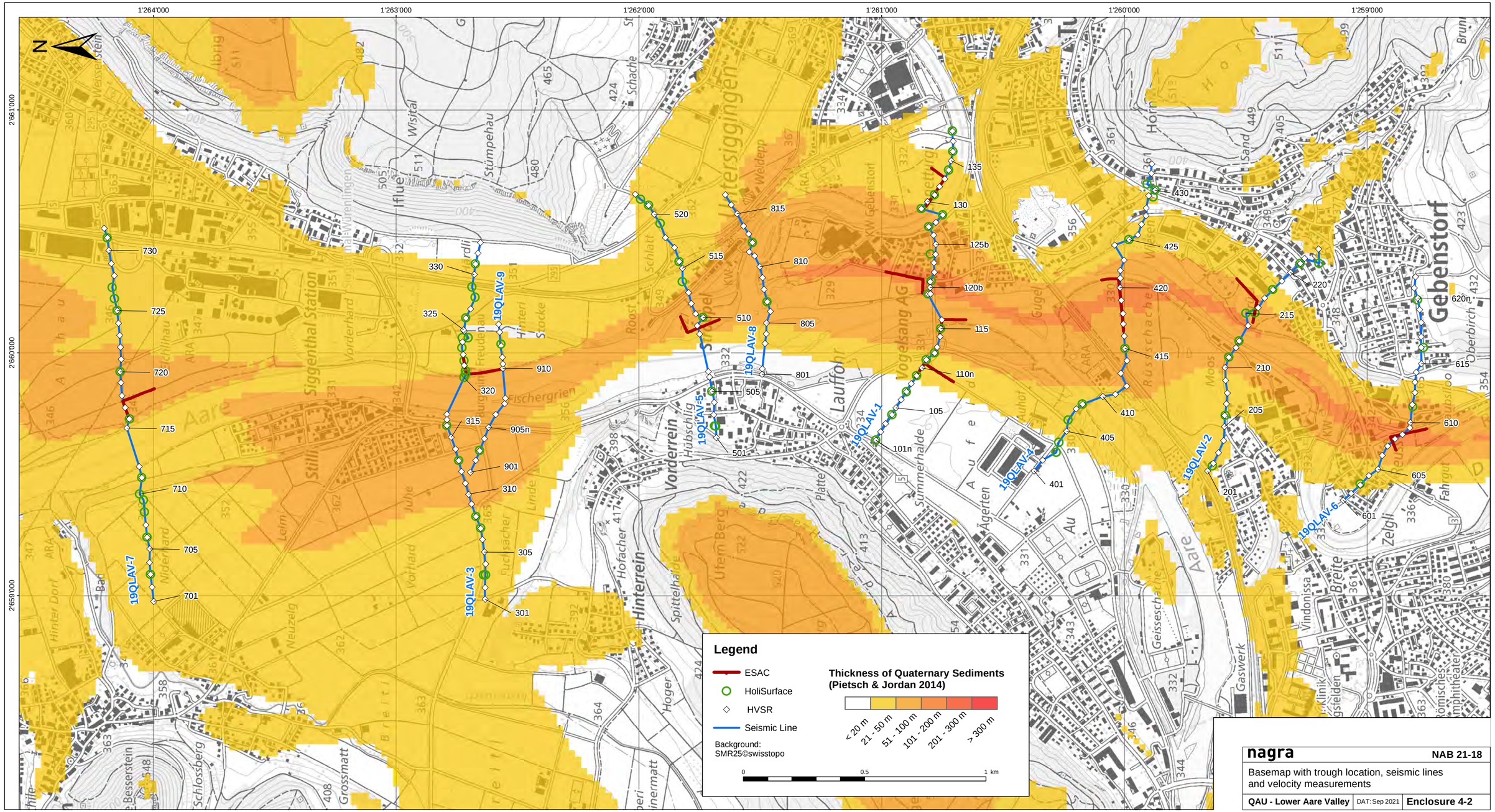
- Molasse, undifferentiated
- Siderolithic
- Villigen/Burghorn Fm.
- Wildegg Fm.
- PKI
- Opalinus Clay
- Staffelegg Fm.
- Klettgau/Bänkerjoch Fm.
- Schinznach Fm.

Base Quaternary subcrop stratigraphy (combining information from boreholes and Graf *et al.*, 2006)

- Molasse, undifferentiated
- Villigen/Burghorn Fm.
- Wildegg Fm.
- PKI
- Opalinus Clay
- Staffelegg Fm.
- Klettgau/Bänkerjoch Fm.
- Schinznach Fm.

nagra	NAB 21-18	
Base Quaternary subcrop map of the study area		
Lower Aare Valley	DAT.: Sep. 2021	**Enclosure 2-1**


1'264'000
1'263'000
1'262'000
1'261'000
1'260'000
1'259'000
2'661'000
2'660'000
2'659'000
N
19QLAV-1
19QLAV-2
19QLAV-3
19QLAV-4
19QLAV-5
19QLAV-6
19QLAV-7
19QLAV-8
19QLAV-9
730
725
720
715
710
705
701
330
325
320
315
310
305
301
910
905n
901
815
810
805
801
520
515
510
505
501
135
130
125b
120b
115
110n
105
101n
430
425
420
415
410
405
401
220
215
210
205
201
620n
615
610
605
601
Legend
Boreholes
HVSR
Seismic Line
Thickness of Quaternary Sediments (Pietsch & Jordan 2014)
< 20 m
21 - 50 m
51 - 100 m
101 - 200 m
201 - 300 m
> 300 m
Background:
SMR25©swisstopo
0
0.5
1 km
nagra
NAB 21-18
Basemap with trough location, seismic lines and boreholes
QAU - Lower Aare Valley
DAT: Sep. 2021
Enclosure 4-1

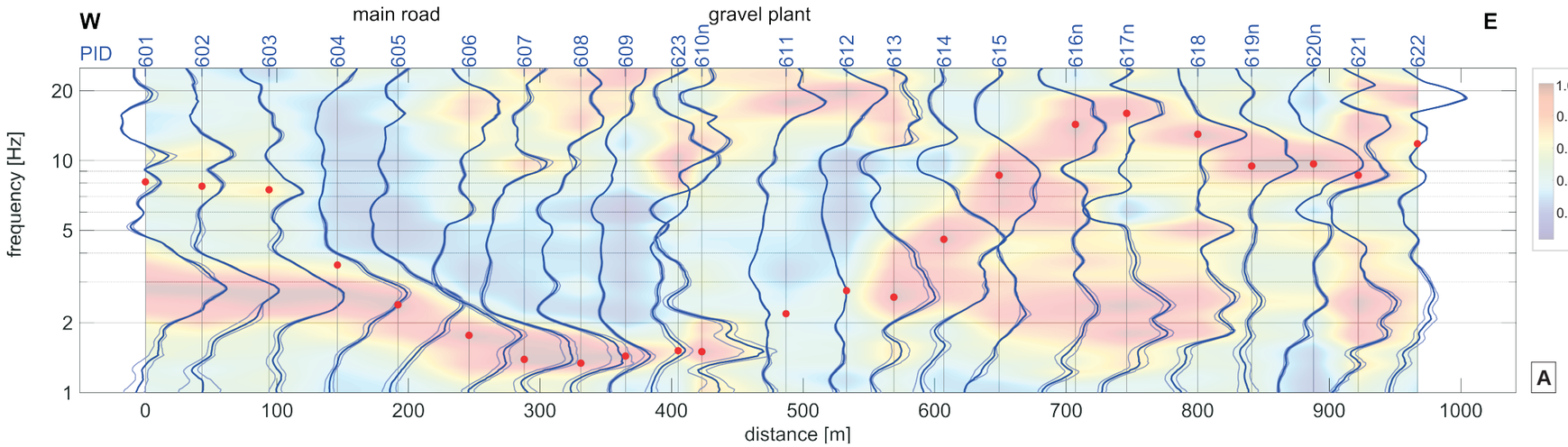


nagra NAB 21-18

Basemap with trough location, seismic lines and velocity measurements

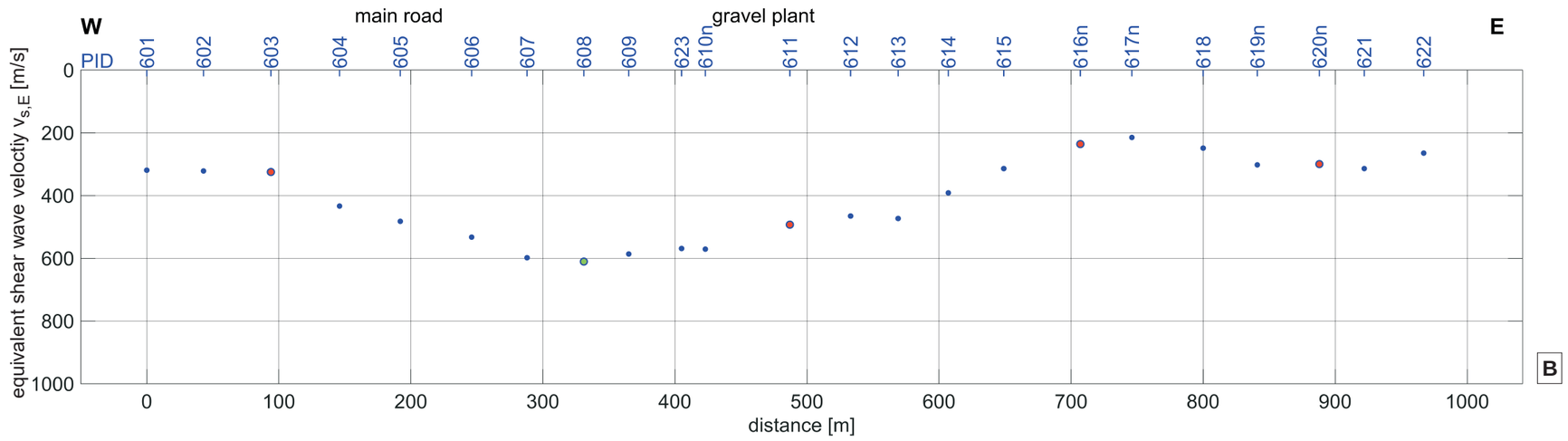
QAU - Lower Aare Valley | DAT: Sep 2021 | Enclosure 4-2

Seismic line 19QLAV-6



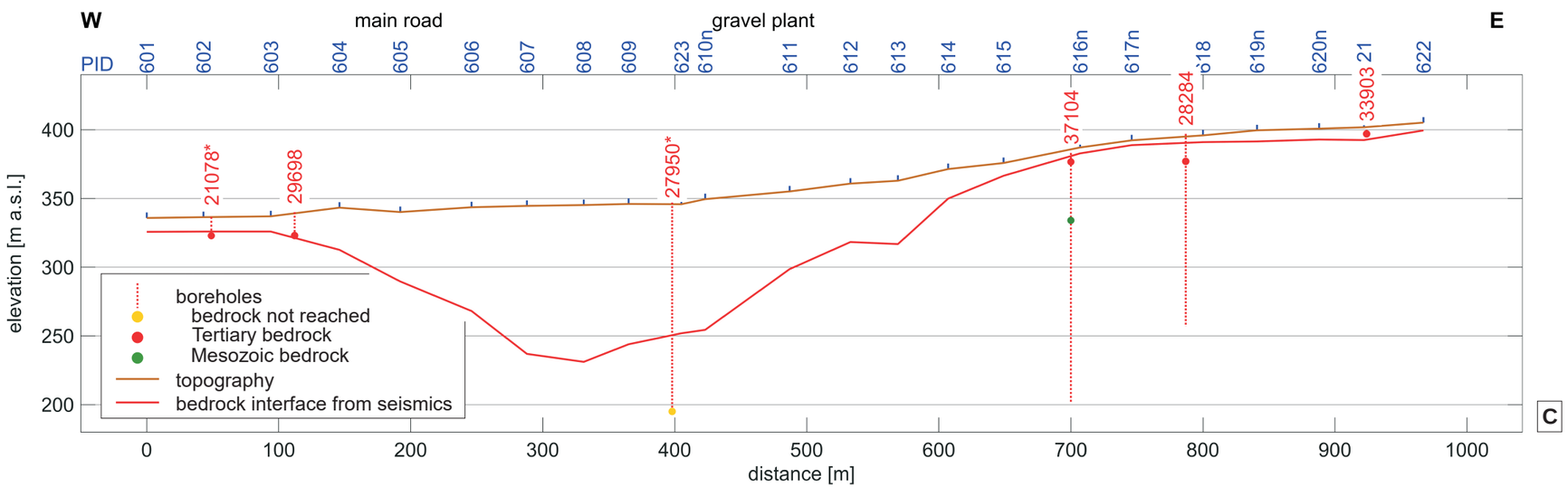
A: Raw HVSR section

The HVSR curves (thick blue lines) ± (thin blue lines) are drawn with amplitude of 1 at position of measurement along the transect.
Red dots represent peak frequencies interpreted as Base Quaternary.
Background colours denote normalised HVSR amplitudes.



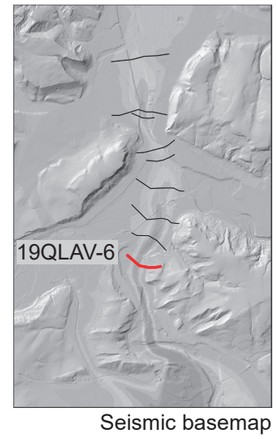
B: Equivalent shear wave velocities $v_{s,E}$

Equivalent shear wave velocity value of overburden $v_{s,E}$ used to convert fundamental frequency f_0 into depth of bedrock. The velocities are derived from active point (red) or passive array (green) measurements performed at several positions along the seismic line.



C: Bedrock topography in depth

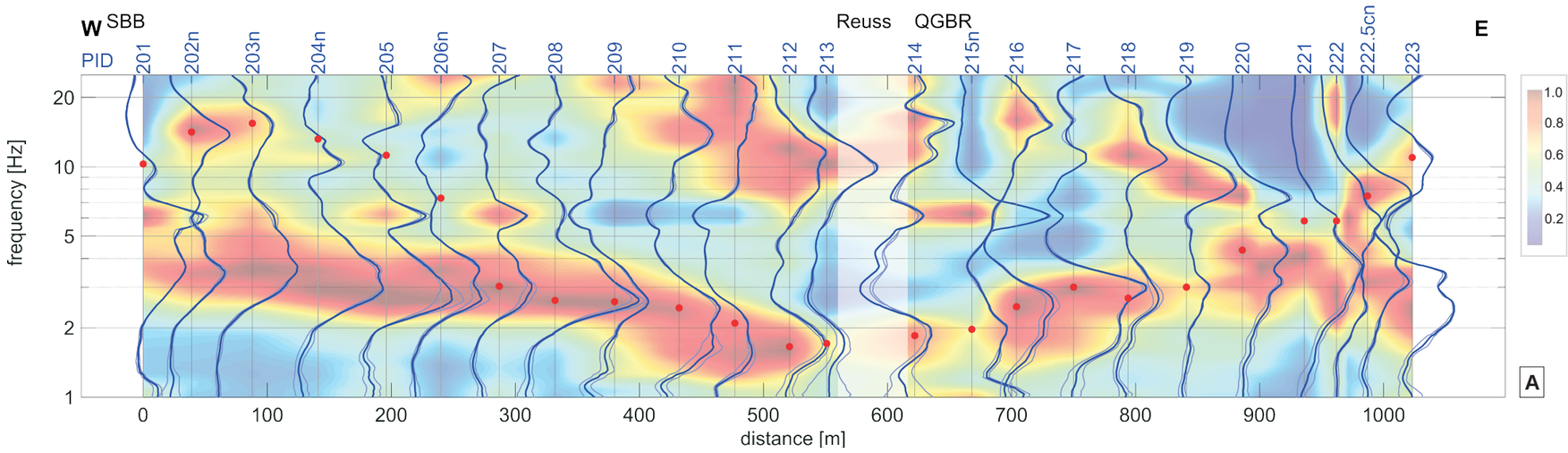
Most boreholes reached Tertiary bedrock, marked with red dots. Borehole 27950* did not reach bedrock (yellow mark) at a depth significantly below the seismically inferred bedrock interface (red).
Boreholes marked with * have a lateral offset of >50 m from the line.
The projection was applied ~parallel to strike of bedrock surface from BQu model (Jordan & Pietsch 2014)



Seismic basemap

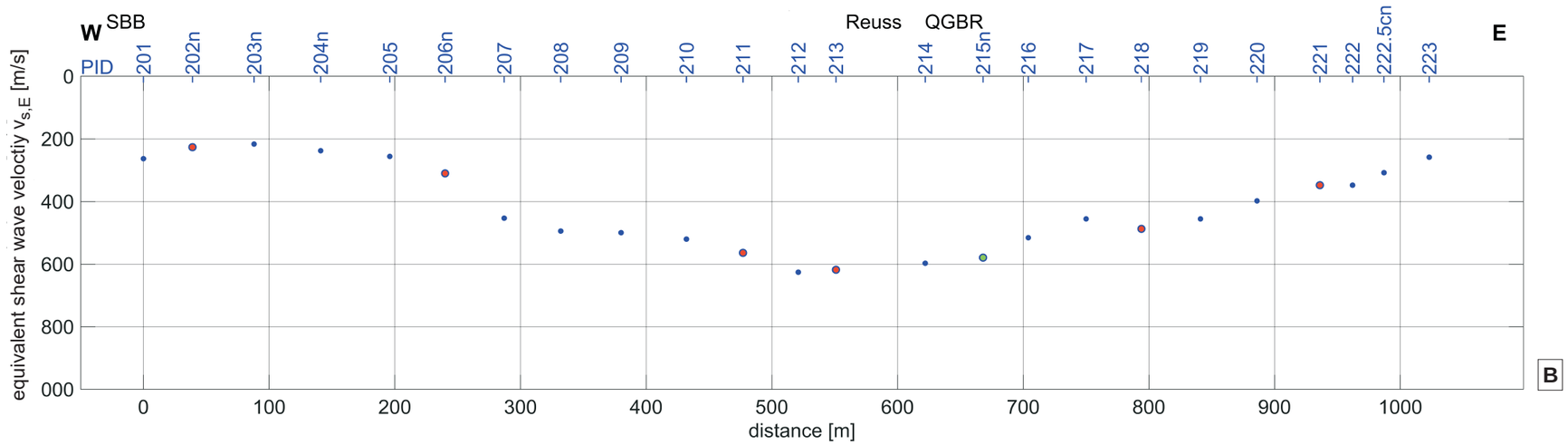
nagra	NAB 21-18
Seismic surface wave line 19QLAV-6 HVSR section, velocities and depth section	
Lower Aare Valley	DAT.: Sep. 2021 — **Enclosure 5-1**

Seismic line 19QLAV-2



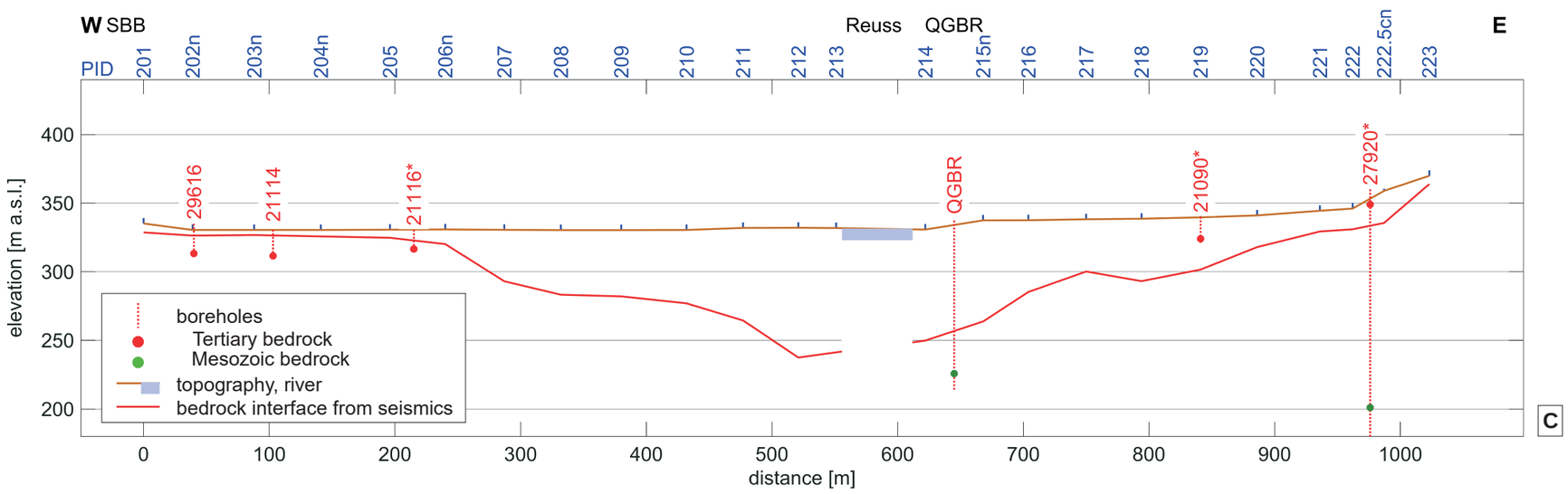
A: Raw HVSR section

The HVSR curves (thick blue lines) ± (thin blue lines) are drawn with amplitude of 1 at position of measurement along the transect.
Red dots represent peak frequencies interpreted as Base Quaternary.
Background colours denote normalised HVSR amplitudes.



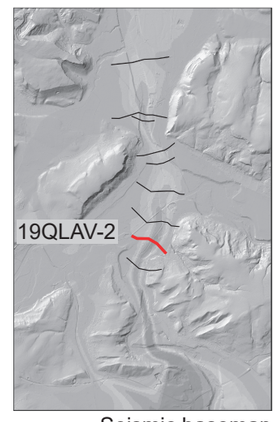
B: Equivalent shear wave velocities $v_{s,E}$

Equivalent shear wave velocity value of overburden $v_{s,E}$ used to convert fundamental frequency f_0 into depth of bedrock. The velocities are derived from active point (red) or passive array (green) measurements performed at several positions along the seismic line.



C: Bedrock topography in depth

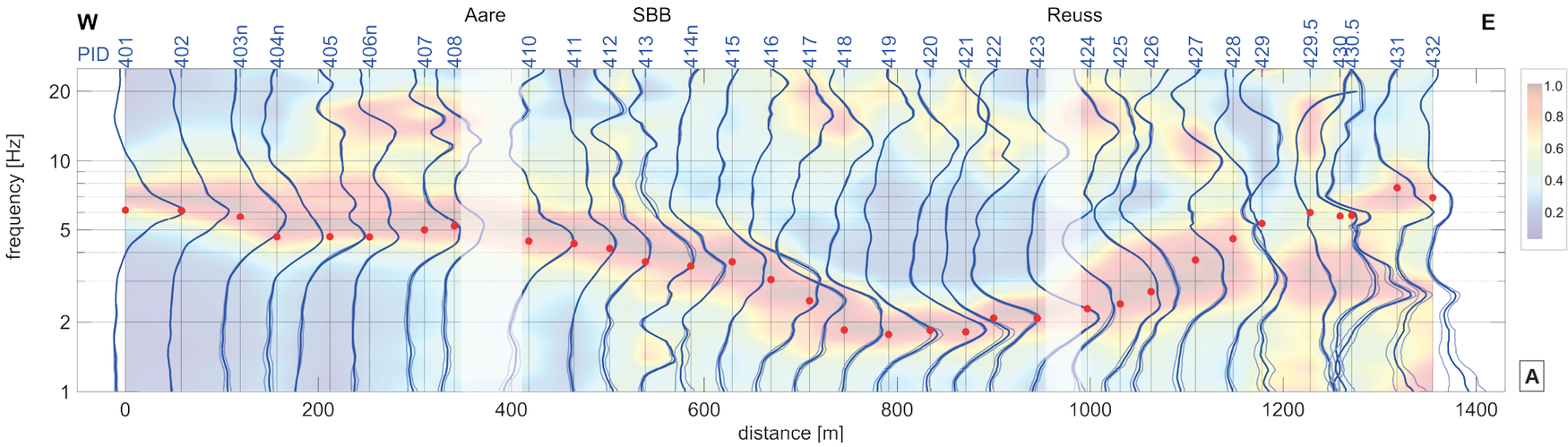
All boreholes reached bedrock, marked with green and red dots, respectively.
Boreholes marked with * have a lateral offset of >50 m from the line.
The projection was applied ~parallel to strike of bedrock surface from BQu model (Jordan & Pietsch 2014).



Seismic basemap

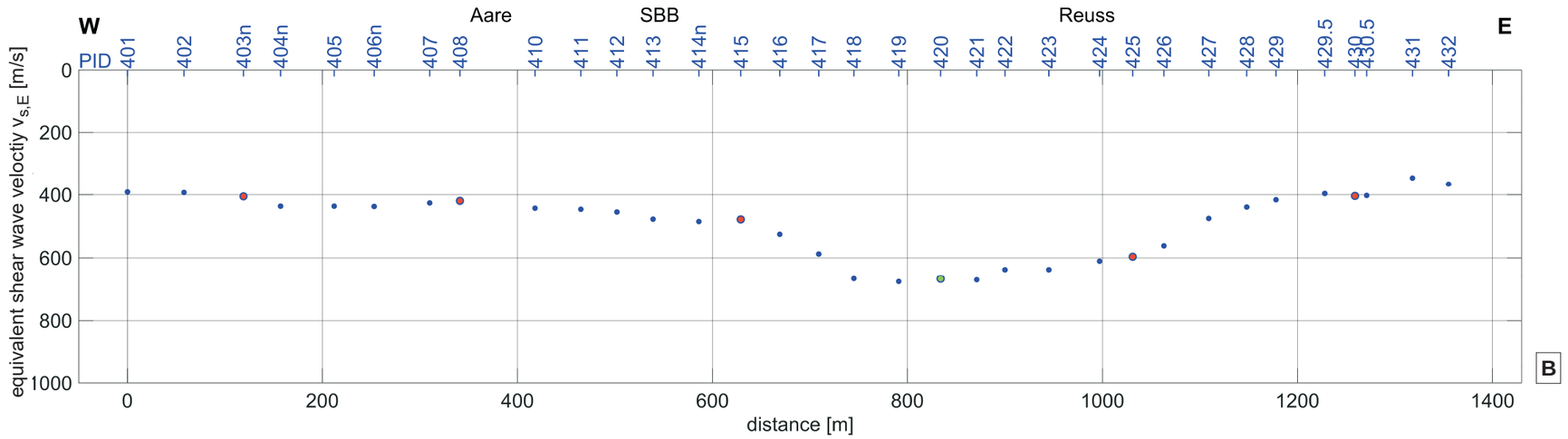
nagra	NAB 21-18
Seismic surface wave line 19QLAV-2 HVSR section, velocities and depth section	
Lower Aare Valley	DAT.: Sep. 2021 **Enclosure 5-2**

Seismic line 19QLAV-4



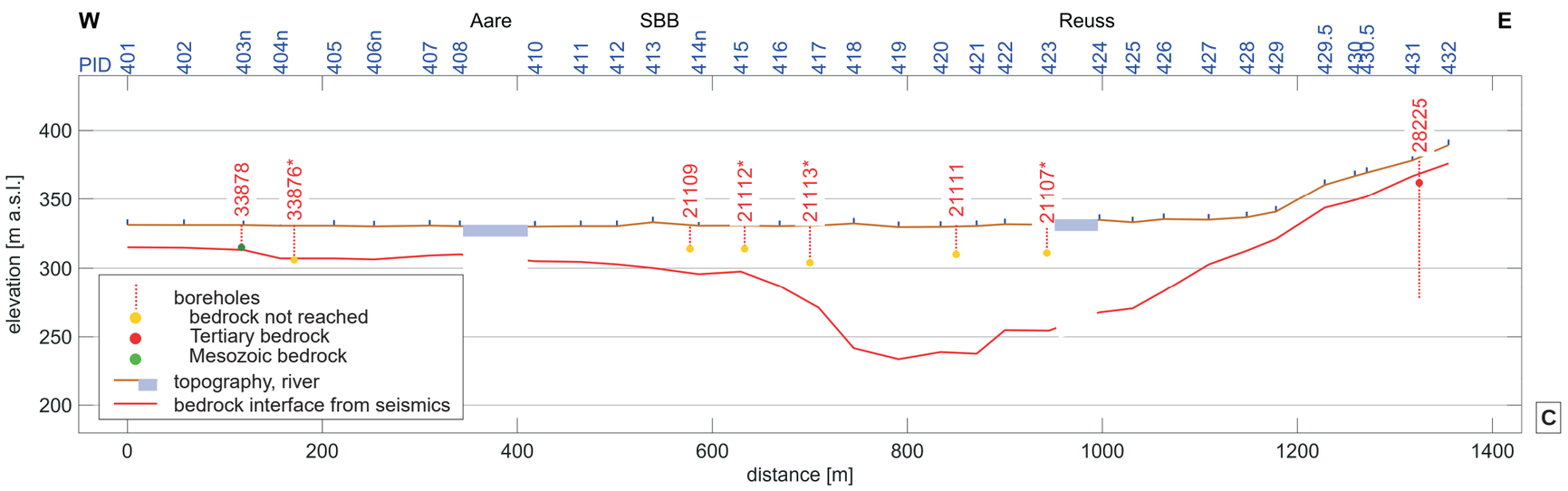
A: Raw HVSR section

The HVSR curves (thick blue lines) ± (thin blue lines) are drawn with amplitude of 1 at position of measurement along the transect.
Red dots represent peak frequencies interpreted as Base Quaternary.
Background colours denote normalised HVSR amplitudes.
PID429 - PID432: HVSR curves around expected peak frequencies of Quaternary-Molasse interface are highly contaminated by industrial noise.



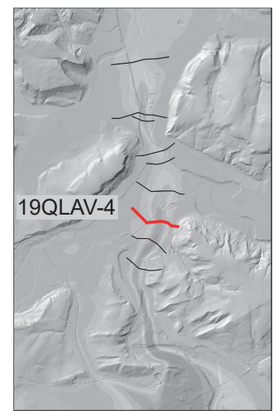
B: Equivalent shear wave velocities $v_{s,E}$

Equivalent shear wave velocity value of overburden $v_{s,E}$ used to convert fundamental frequency f_0 into depth of bedrock. The velocities are derived from active point (red) or passive array (green) measurements performed at several positions along the seismic line.



C: Bedrock topography in depth

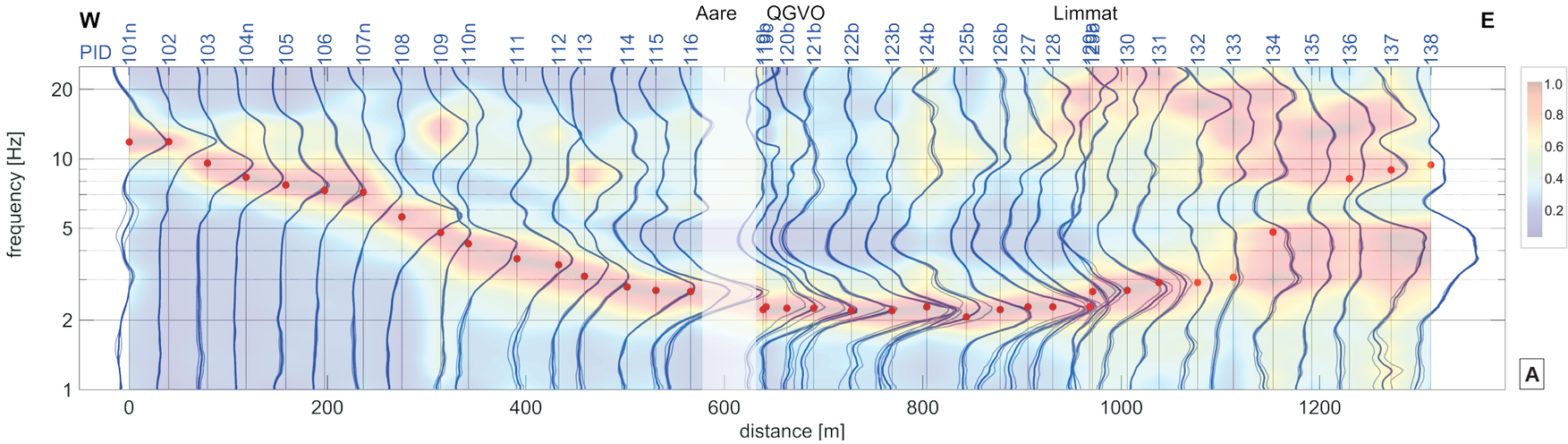
Boreholes 22878 (green dot) and 28225 (red dot) reached bedrock.
Yellow marked borehole depths did not reach bedrock.
Boreholes marked with * have a lateral offset of >50 m from the line and are projected ~parallel to strike of bedrock surface from BQu model (Jordan & Pietsch 2014).



Seismic basemap

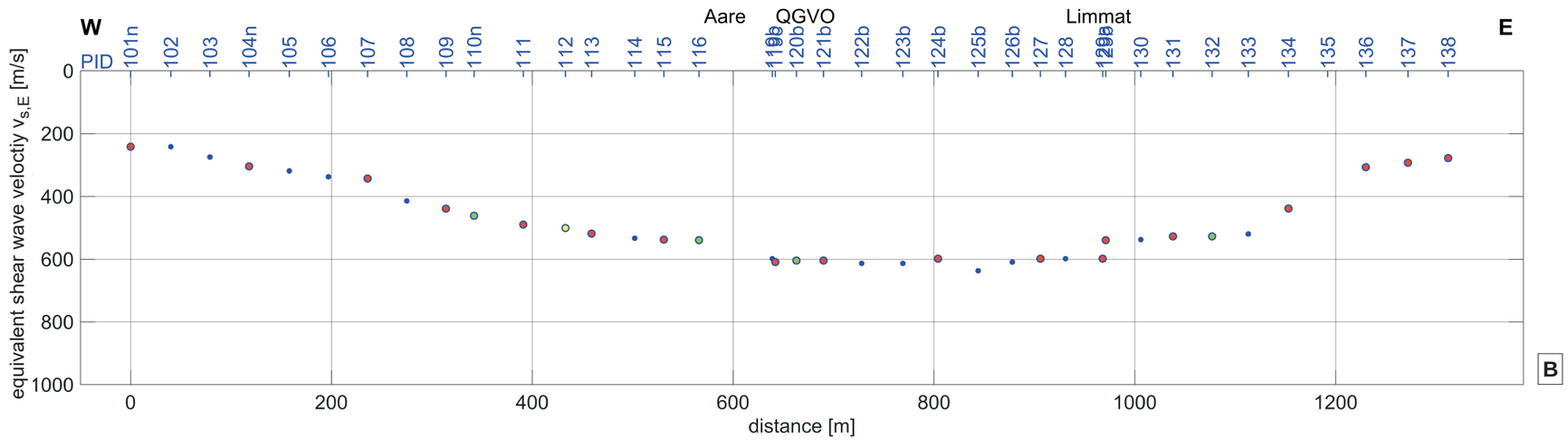
nagra	NAB 21-18	
Seismic surface wave line 19QLAV-4 HVSR section, velocities and depth section		
Lower Aare Valley	DAT.: Sep. 2021	**Enclosure 5-3**

Seismic line 19QLAV-1



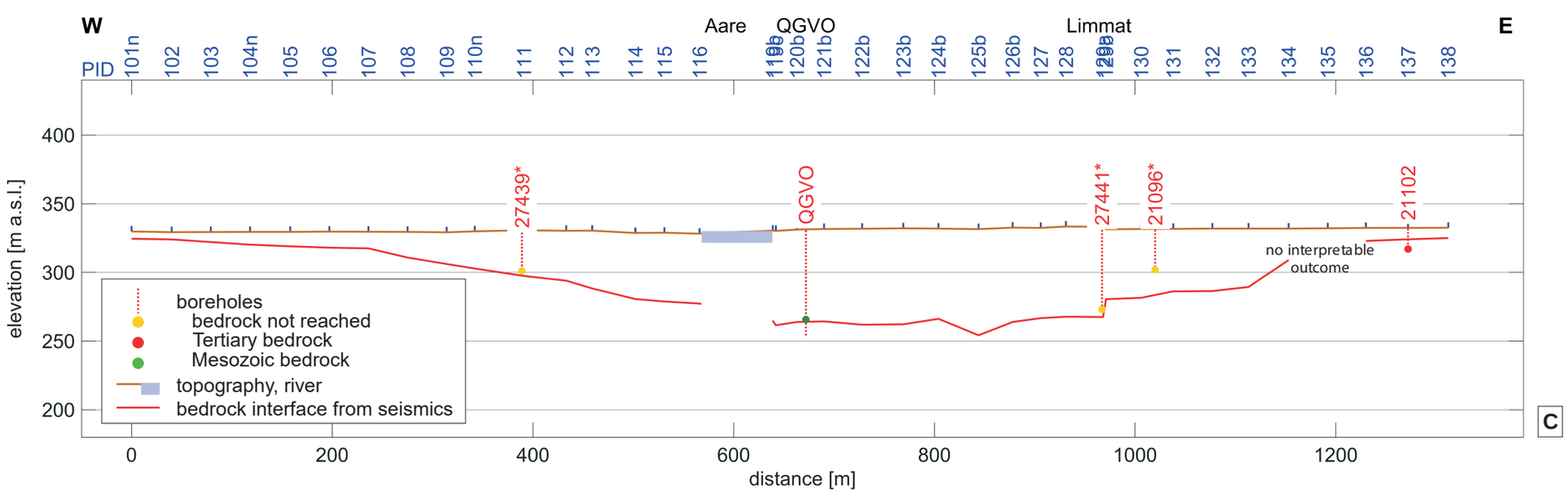
A: Raw HVSR section

The HVSR curves (thick blue lines) ± (thin blue lines) are drawn with amplitude of 1 at position of measurement along the transect.
Red dots represent peak frequencies interpreted as Base Quaternary.
Background: Colours denote normalised HVSR amplitudes.
PID135 @ 1192m: HVSR curve is not used for BQu interpretation.



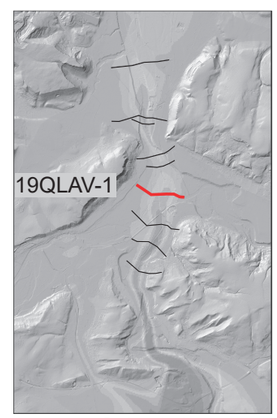
B: Equivalent shear wave velocities $v_{s,E}$

Equivalent shear wave velocity value of overburden $v_{s,E}$ used to convert fundamental frequency f_0 into depth of bedrock. The velocities are derived from active point (red) or passive array (green) measurements performed at several positions along the seismic line.



C: Bedrock topography in depth

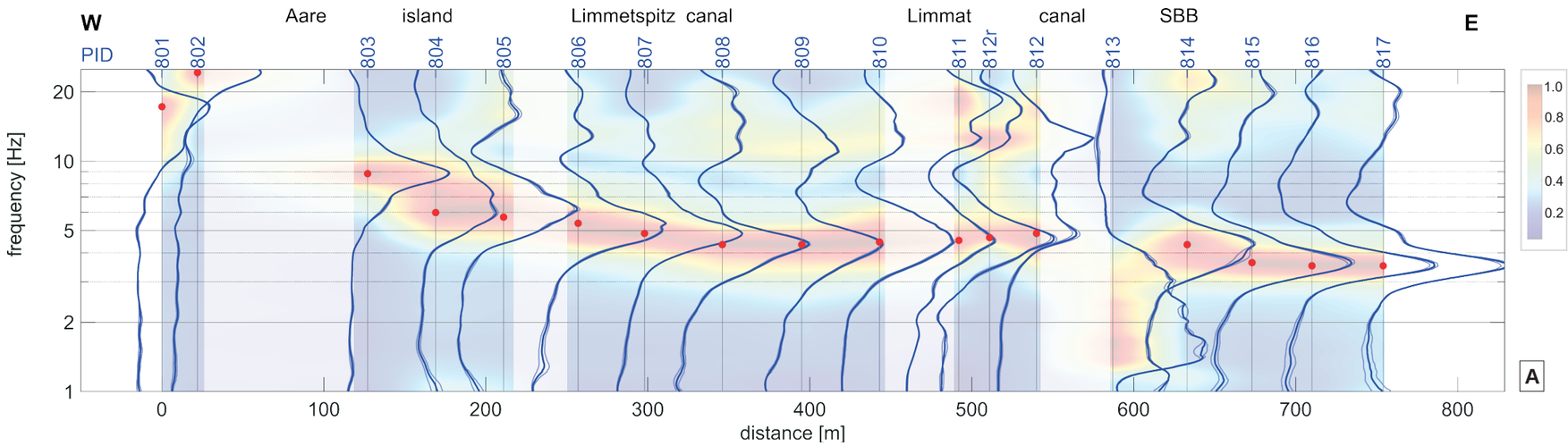
Boreholes QGVO (green dot) and 21102 (red dot) reach bedrock and confirm the seismcally inferred bedrock. Yellow marked borehole depths did not reach bedrock.
Boreholes marked with * have a lateral offset of >50 m from line and are projected ~parallel to the strike of the bedrock surface from BQu model (Jordan & Pietsch 2014).
The borehole information is consistent with the seismic measurements.



Seismic basemap

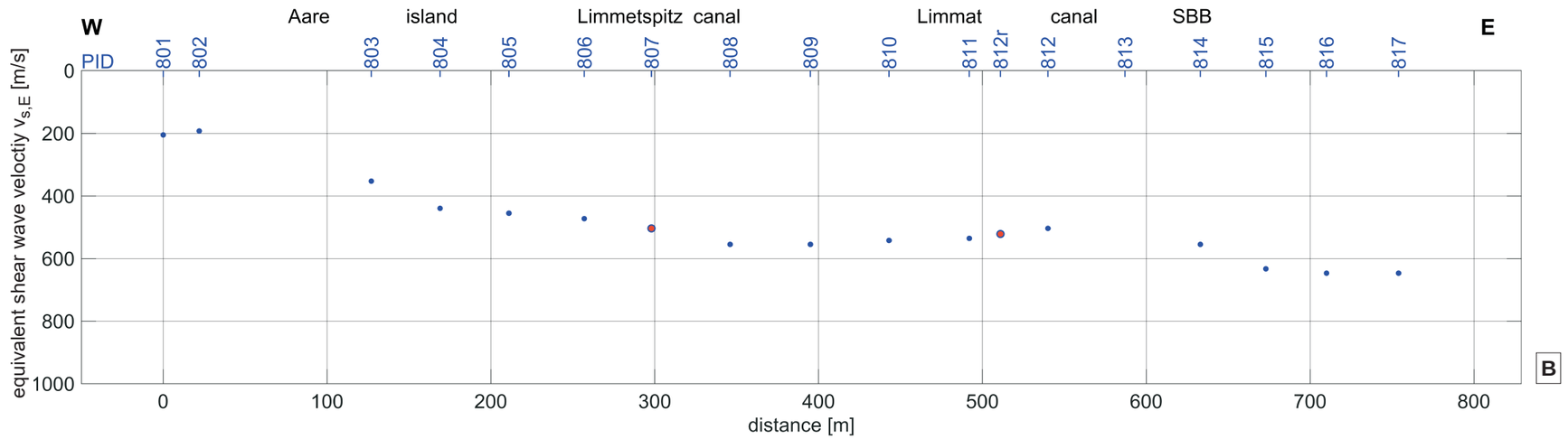
nagra	NAB 21-18
Seismic surface wave line 19QLAV-6 (pilot line) HVSR section, velocities and depth section	
Lower Aare Valley	DAT.: Sep. 2021 **Enclosure 5-4**

Seismic line 19QLAV-8



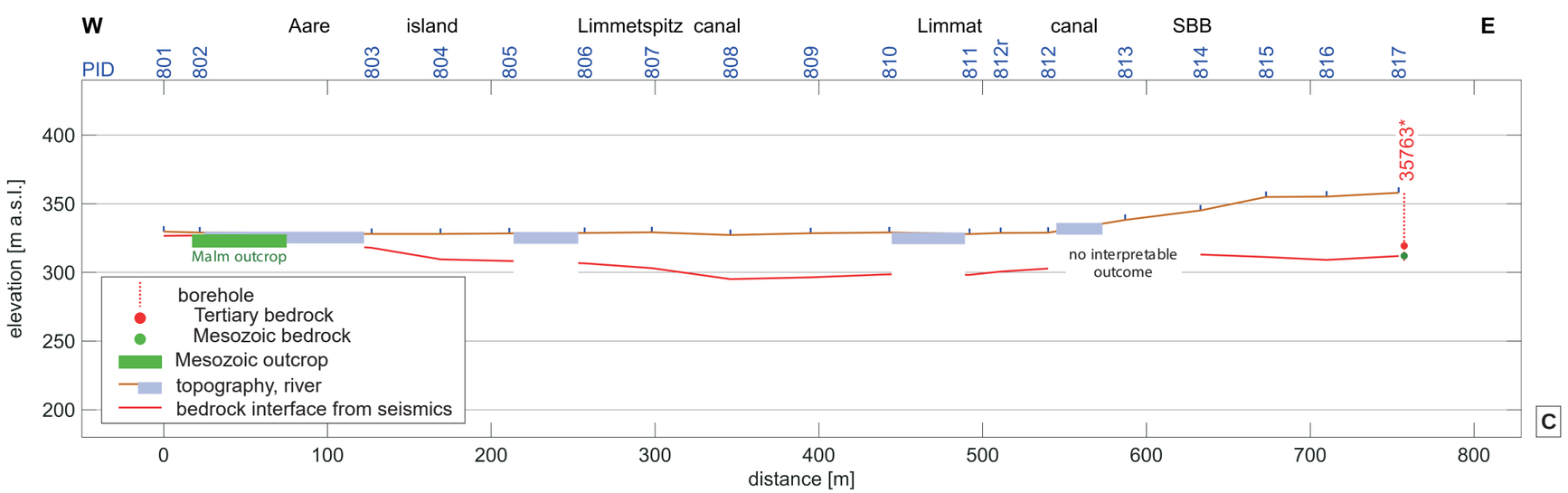
A: Raw HVSR section

The HVSR curves (thick blue lines) ± (thin blue lines) are drawn with amplitude of 1 at position of measurement along the transect.
Red dots represent peak frequencies interpreted as Base Quaternary.
Background colours denote normalised HVSR amplitudes.
PID802 @ 22 m: well imaged HVSR curve with clear peak @ 24.2 Hz.
PID813 @ 587 m: very noisy and cannot be interpreted.



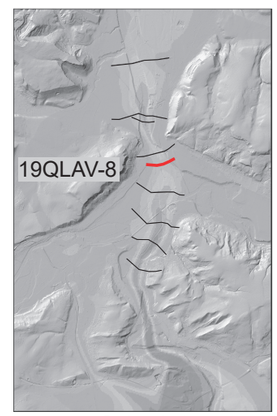
B: Equivalent shear wave velocities $v_{s,E}$

Equivalent shear wave velocity value of overburden $v_{s,E}$ used to convert fundamental frequency f_0 into depth of bedrock. The velocities are derived from active point (red) measurements performed at several positions along the seismic line.



C: Bedrock topography in depth

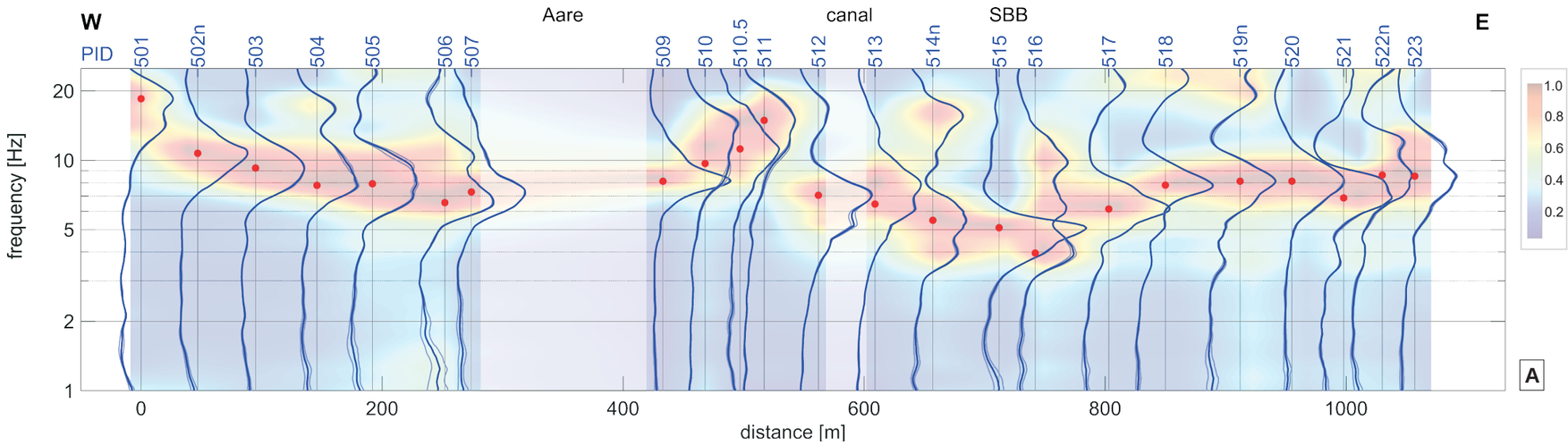
Seismic measurements indicate a shallow bedrock surface. No borehole information is available close to this line. Malm limestone outcrops are found at the western Aare river bank, which is consistent with the high fundamental frequencies and shallow bedrock surface from seismic measurements at PID 801 and 802.



Seismic basemap

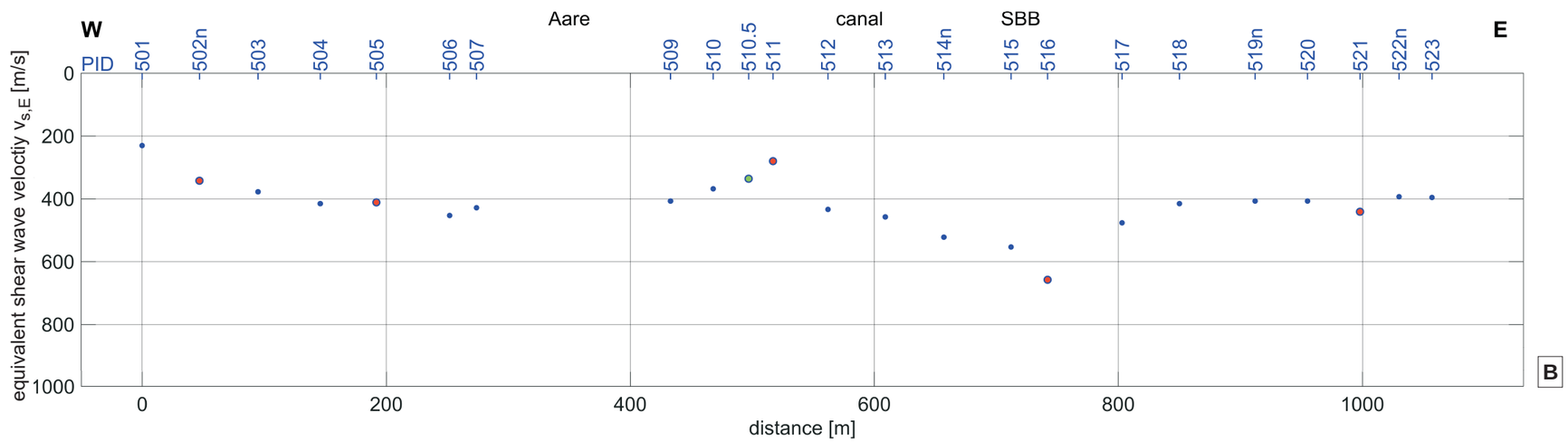
nagra	NAB 21-18
Seismic surface wave line 19QLAV-8 HVSR section, velocities and depth section	
Lower Aare Valley	DAT.: Sep. 2021 **Enclosure 5-5**

Seismic line 19QLAV-5



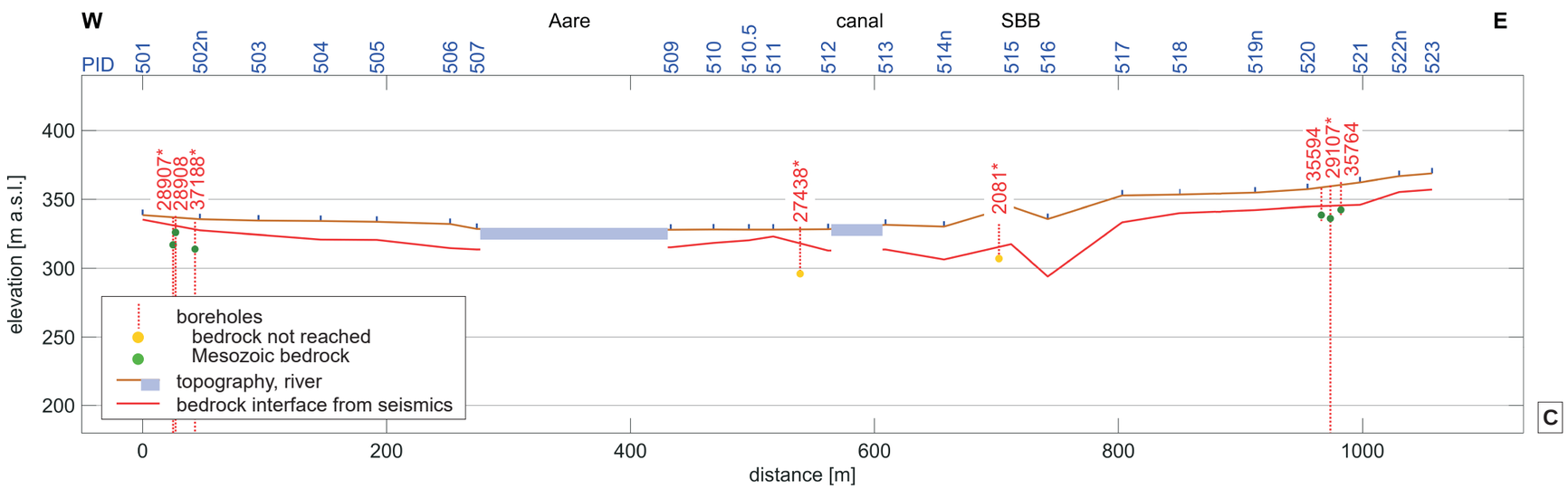
A: Raw HVSR section

The HVSR curves (thick blue lines) ± (thin blue lines) are drawn with amplitude of 1 at position of measurement along the transect.
Red dots represent peak frequencies interpreted as Base Quaternary.
Background colours denote normalised HVSR amplitudes.



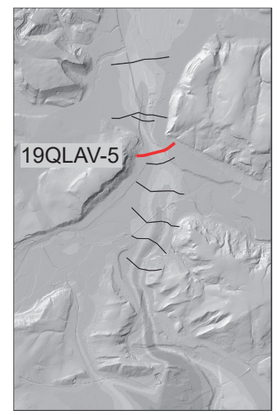
B: Equivalent shear wave velocities $v_{s,E}$

Equivalent shear wave velocity value of overburden $v_{s,E}$ used to convert fundamental frequency f_0 into depth of bedrock. The velocities are derived from active point (red) or passive array (green) measurements performed at several positions along the seismic line.



C: Bedrock topography in depth

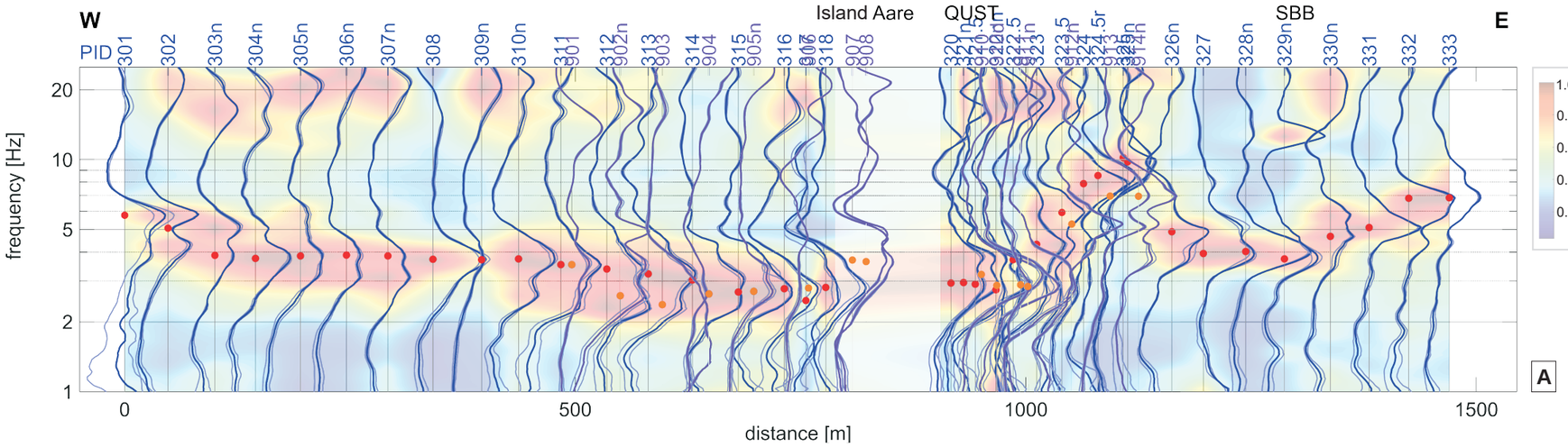
Boreholes marked with * have a lateral offset of >50 m from the line and are projected ~parallel to the strike of the bedrock surface from BQu model (Jordan & Pietsch 2014).
No data could be acquired in Aare River, resulting in a 150 m wide data gap.



Seismic basemap

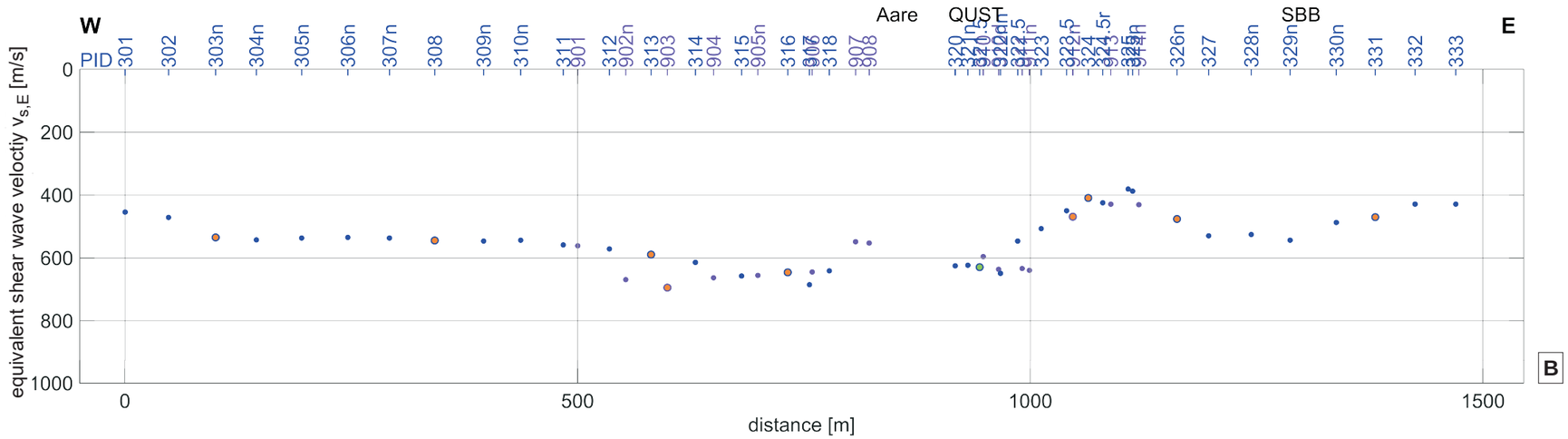
nagra	NAB 21-18	
Seismic surface wave line 19QLAV-5 HVSR section, velocities and depth section		
Lower Aare Valley	DAT.: Sep. 2021	**Enclosure 5-6**

Seismic line 19QLAV-3 & 19QLAV-9



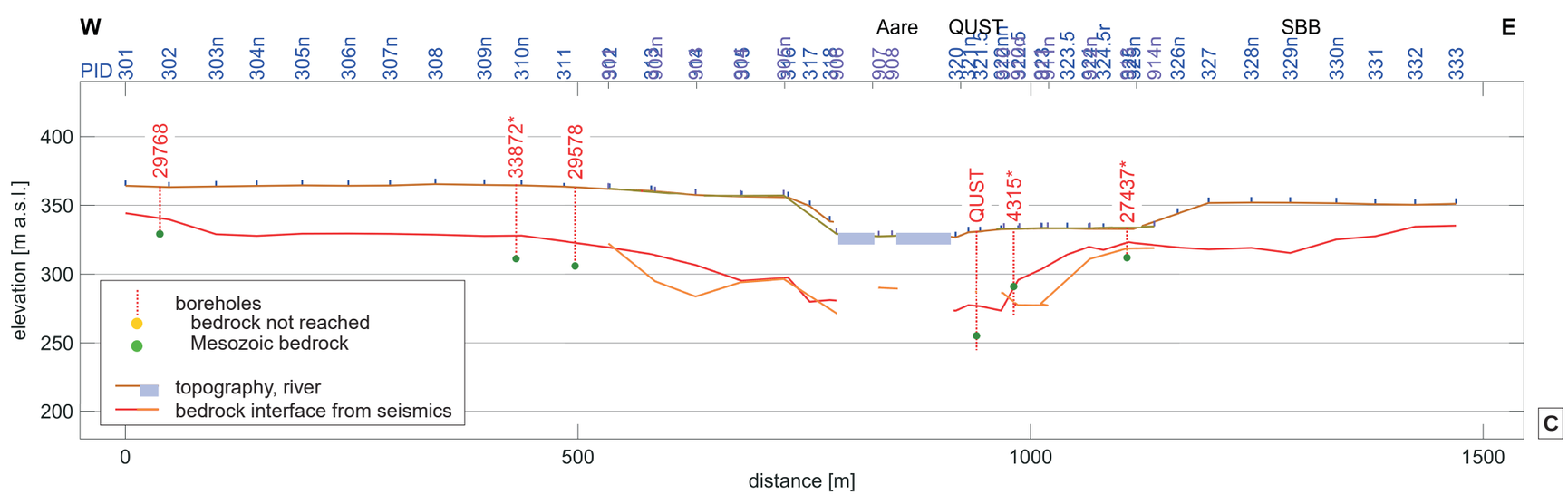
A: Raw HVSR section

The HVSR curves (thick blue lines) ± (thin blue lines) are drawn with amplitude of 1 at position of measurement along the transect.
The HVSR curves in magenta gives the data from line 19QLAV-9.
Red (line 19QALV-3) and light magenta (line 19QLAV-9) dots represent peak frequencies interpreted as Base Quaternary.
Background colours denote normalised HVSR amplitudes from line 19QLAV-3.



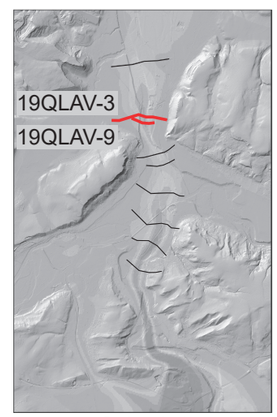
B: Equivalent shear wave velocities $v_{s,E}$

Equivalent shear wave velocity value of overburden $v_{s,E}$ used to convert fundamental frequency f_0 into depth of bedrock. The velocities are derived from active point (red) or passive array (green) measurements performed at several positions along the seismic lines. Blue markers represent measurements on line 19QLAV-3, magenta those on line 19QALV-9.



C: Bedrock topography in depth

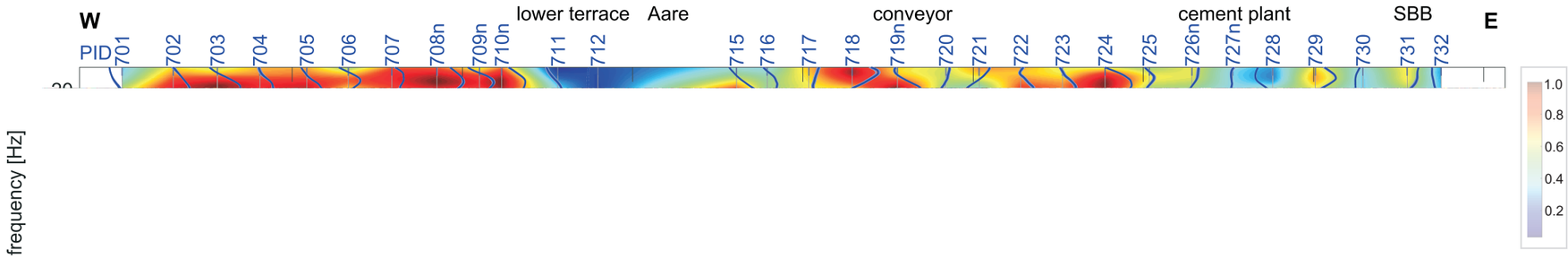
Bedrock depth model derived from both parallel lines 19QLAV-3 (red line) and 19QLAV-9 (orange). Boreholes marked with * have a lateral offset of >50 m from the line. These boreholes and PIDs from line 19QLAV-9 are projected onto transect 19QLAV-3 ~parallel to the strike of the bedrock surface from BQu model (Jordan & Pietsch 2014). The data is fairly consistent.



Seismic basemap

nagra	NAB 21-18
Seismic surface wave line 19QLAV-3 & 19QLAV-9 HVSR section, velocities and depth section	
Lower Aare Valley	DAT.: Sep. 2021 **Enclosure 5-7**

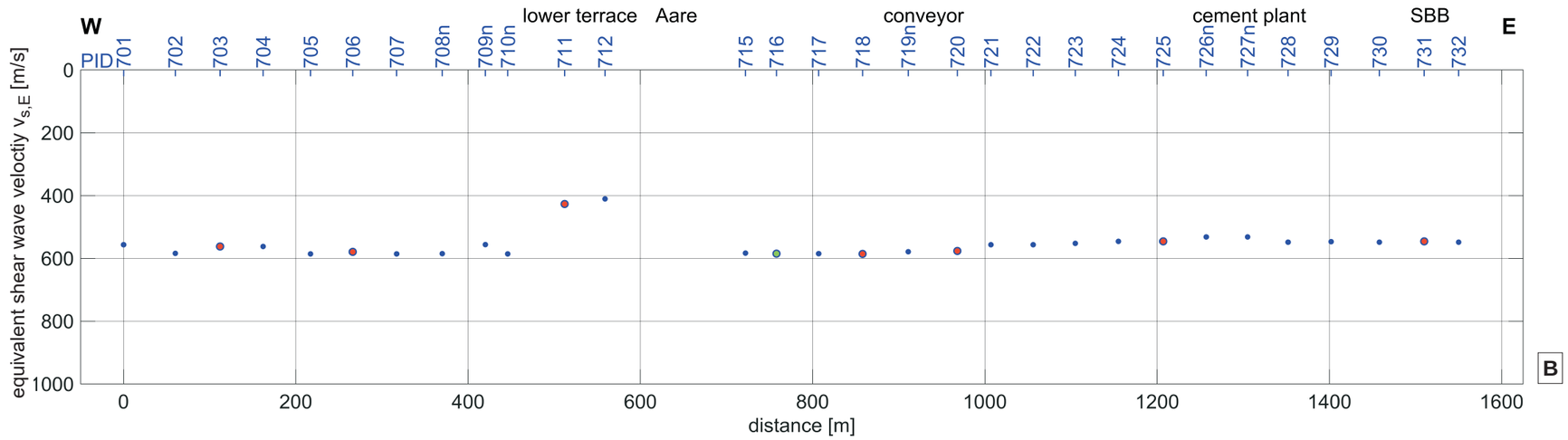
Seismic line 19QLAV-7



A

A: Raw HVSR section

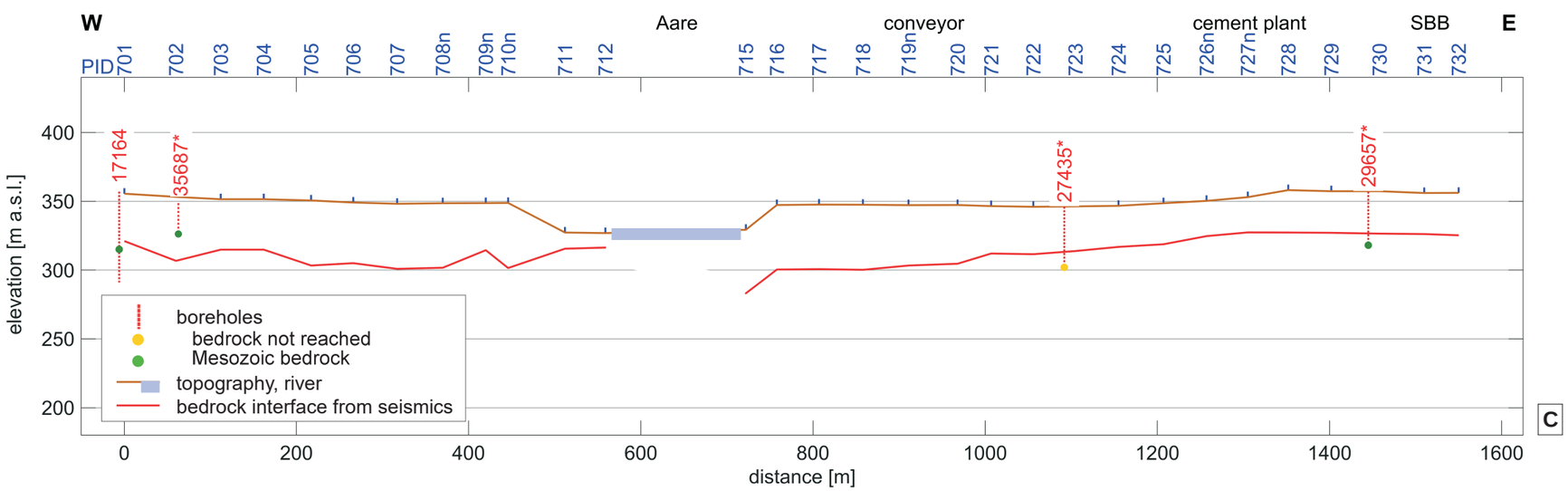
The HVSR curves (thick blue lines) ± (thin blue lines) are drawn with amplitude of 1 at position of measurement along the transect.
Red dots represent peak frequencies interpreted as Base Quaternary.
Background colours denote normalised HVSR amplitudes.



B

B: Equivalent shear wave velocities $v_{s,E}$

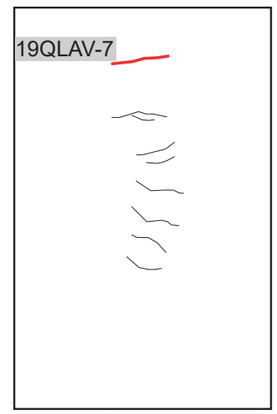
Equivalent shear wave velocity value of overburden $v_{s,E}$ used to convert fundamental frequency f_0 into depth of bedrock. The velocities are derived from active point (red) or passive array (green) measurements performed at several positions along the seismic line.



C

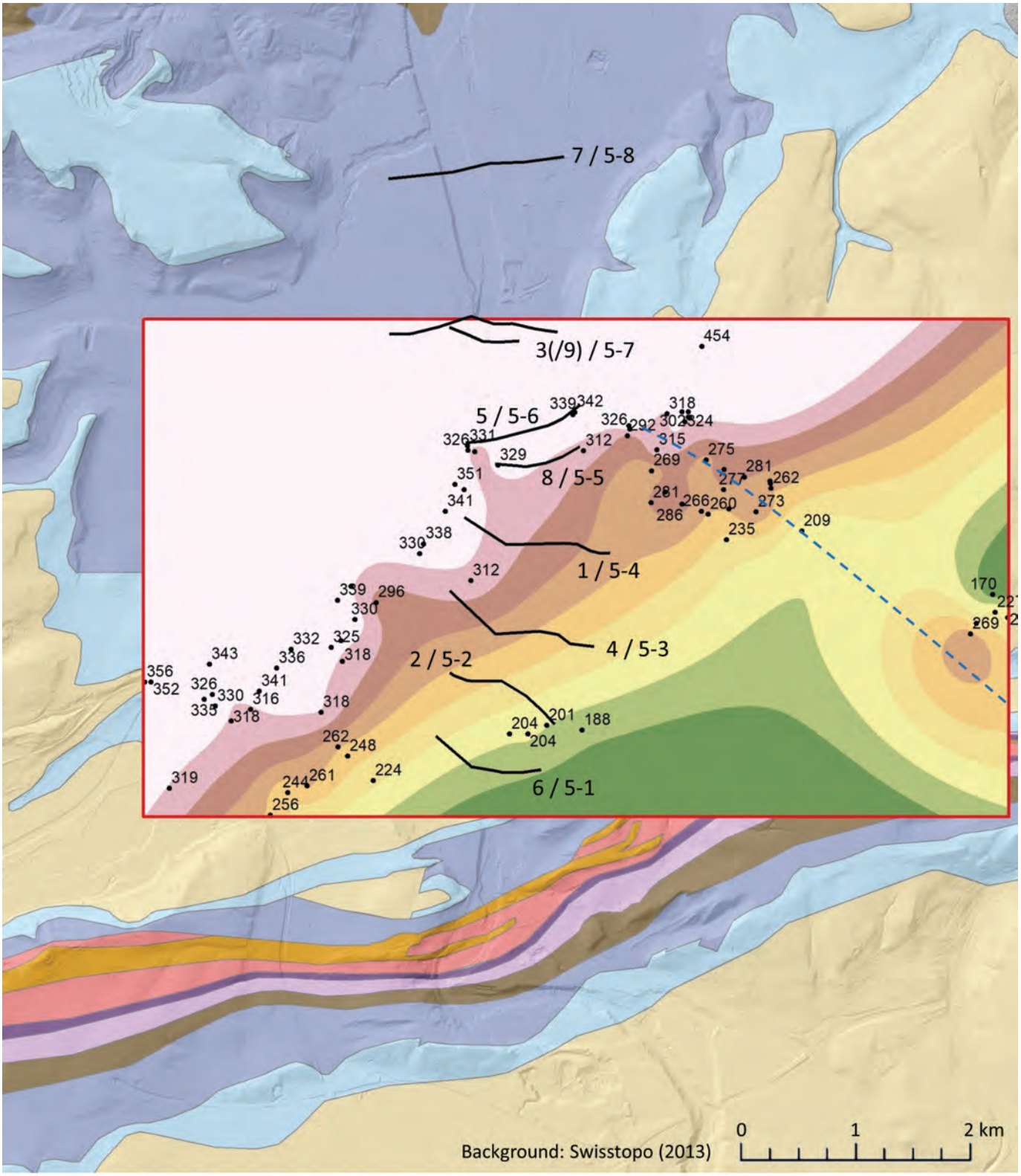
C: Bedrock topography in depth

Three boreholes reached Mesozoic bedrock (green dots) and confirm the seismic measurements near the profile extremities.



Seismic basemap

nagra	NAB 21-18	
Seismic surface wave line 19QLAV-7 HVSR section, velocities and depth section		
Lower Aare Valley	DAT.: Sep. 2021	**Enclosure 5-8**



Base Quaternar subcrop stratigraphy (see Encl. 2-1)

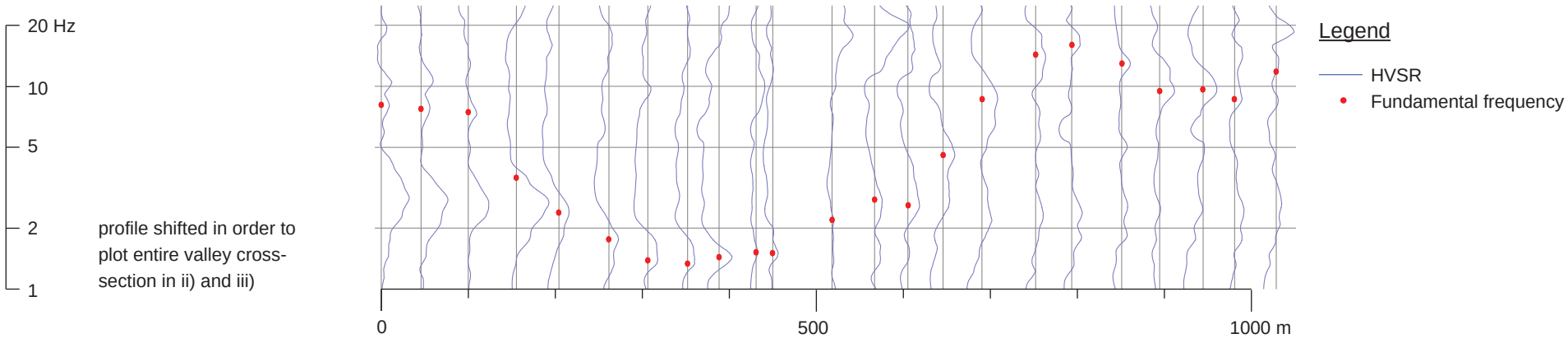
- Molasse, undifferentiated
- Villigen/Burghorn Fm.
- Wildegg Fm.
- PKI
- Opalinus Clay
- Staffelegg Fm.
- Klettgau/Bänkerjoch Fm.
- Schinznach Fm.
- Top Malm model
- Seismic line
- Fault?
- Elevation of Top Malm in borehole (Nagra borehole database)
  - < 180 m a.s.l.
  - 180 – 200 m
  - 200 – 220 m
  - 220 – 240 m
  - 240 – 260 m
  - 260 – 280 m
  - 280 – 300 m
  - 300 – 320 m
  - > 320 m

nagra	NAB 21-18	
Base Quaternary subcrop map with Top Malm overlay		
Lower Aare Valley	DAT.: Sep. 2021	**Enclosure 7-1**

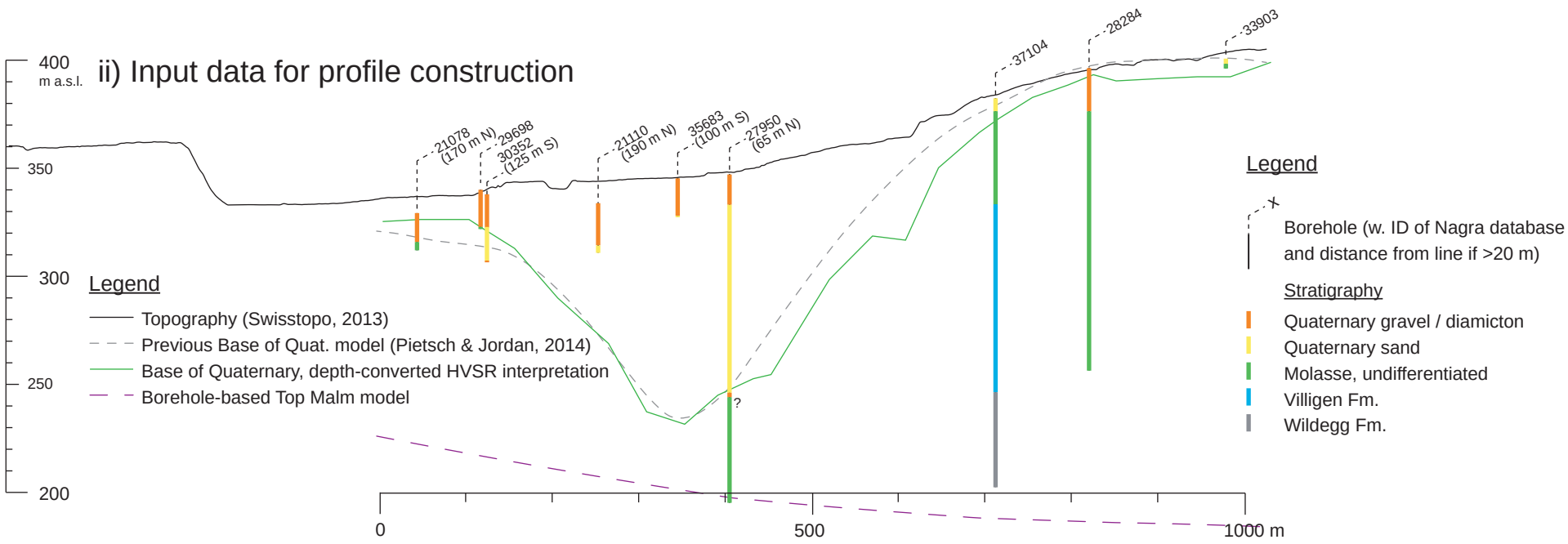
W

i) HVSR data with interpretation

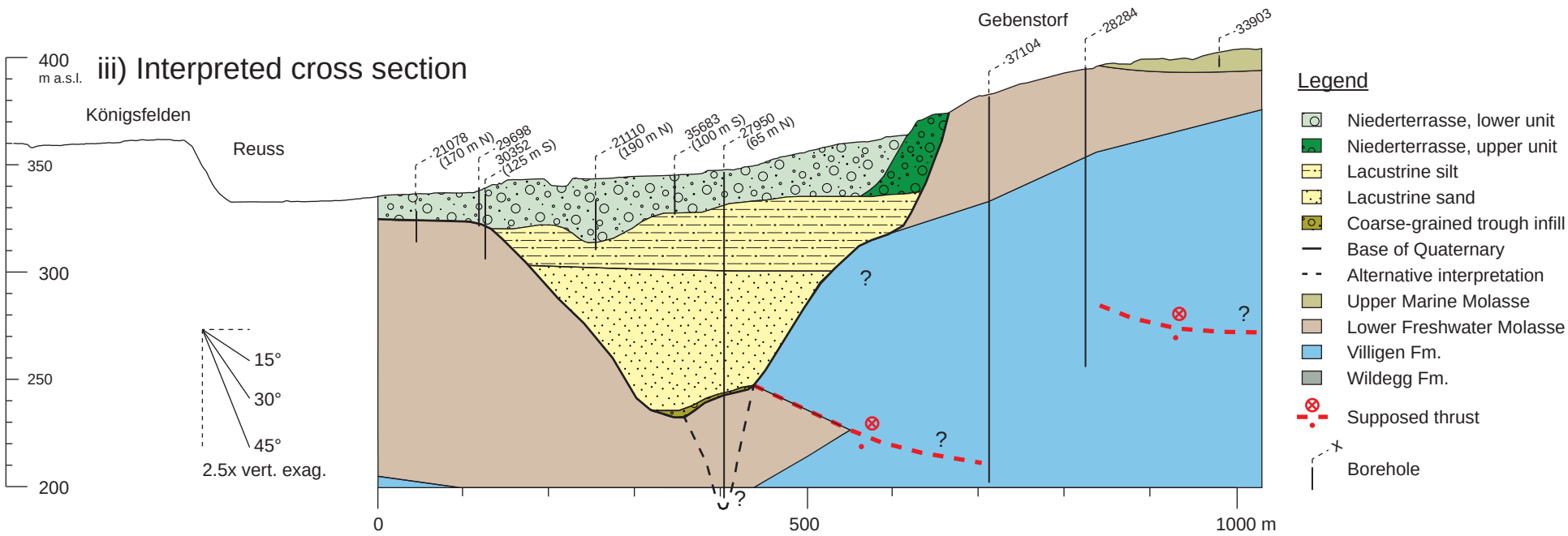
E



ii) Input data for profile construction



iii) Interpreted cross section



Trough shape

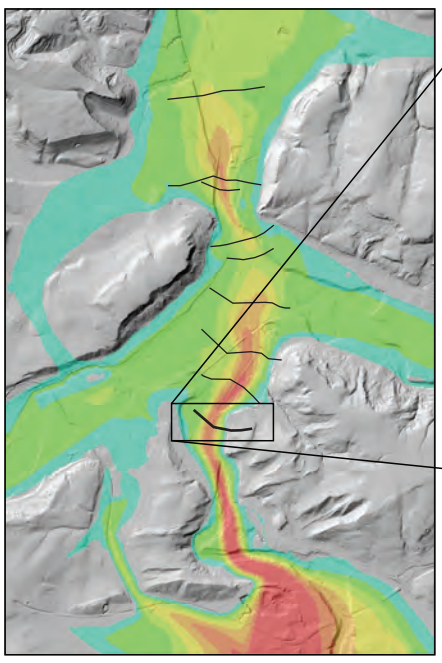
- width ~350 m at 300 m a.s.l.
- deepest point ~235 m a.s.l., possibly deeper
- V-shaped (VI = 0.21)
- gently sloped western flank
- stepped (?) eastern flank

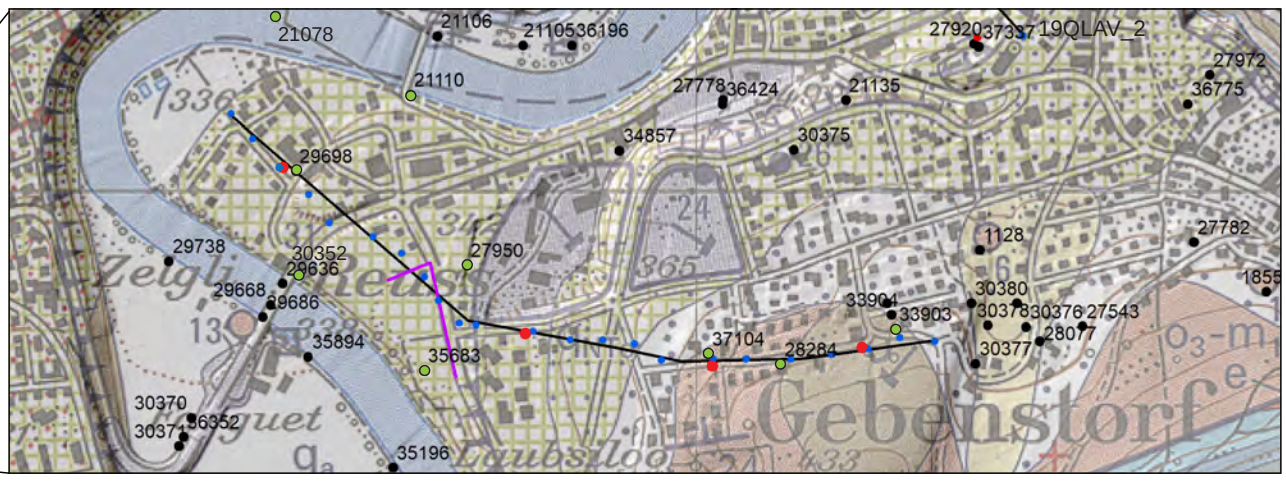
Trough infill

- Niederterrasse with irregular base: incised channel
- infill predominantly sand, fining upwards into silt
- borehole 27950: coarse-grained sediment at 246-244 m a.s.l. - basal gravel / till with misinterpreted Molasse below?

Uncertainties

- full dataset: average error of base of Quaternary at boreholes is -7/+10 m
- destructive boreholes (incl. boreholes further east, e.g. 28077, 27782) recorded conflicting depths to Top Malm: inferred complex bedrock structure (thrust wedges?)
- borehole 27950: Molasse not recognized? Or trough base <200 m?
- trough shoulder at ca. 600 m: topographical artifact ?





Legend

- Trace of seismic line
- HVSR measuring point
- MFA measuring point
- ESAC measuring array
- Borehole used for interpretation (with ID of Nagra database)
- Borehole, not used for interpretation

0 100 200 m

Background:
Graf *et al*. (2006), Swisstopo (2013)

nagra NAB 21-18

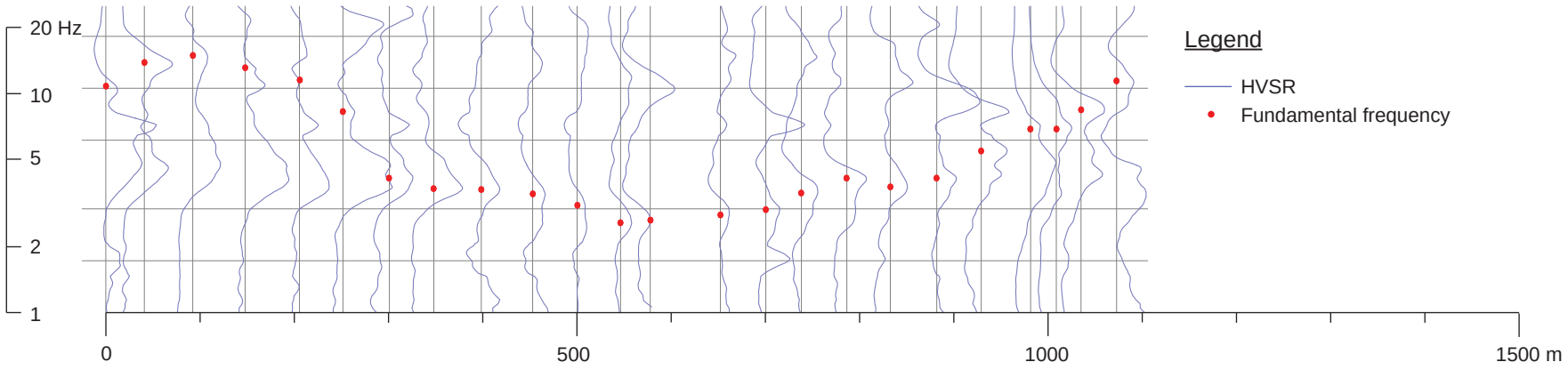
Seismic surface wave line 19QLAV-6
HVSR section, borehole data and interpretation

Lower Aare Valley | DAT.: Sep. 2021 | **Enclosure 7-2**

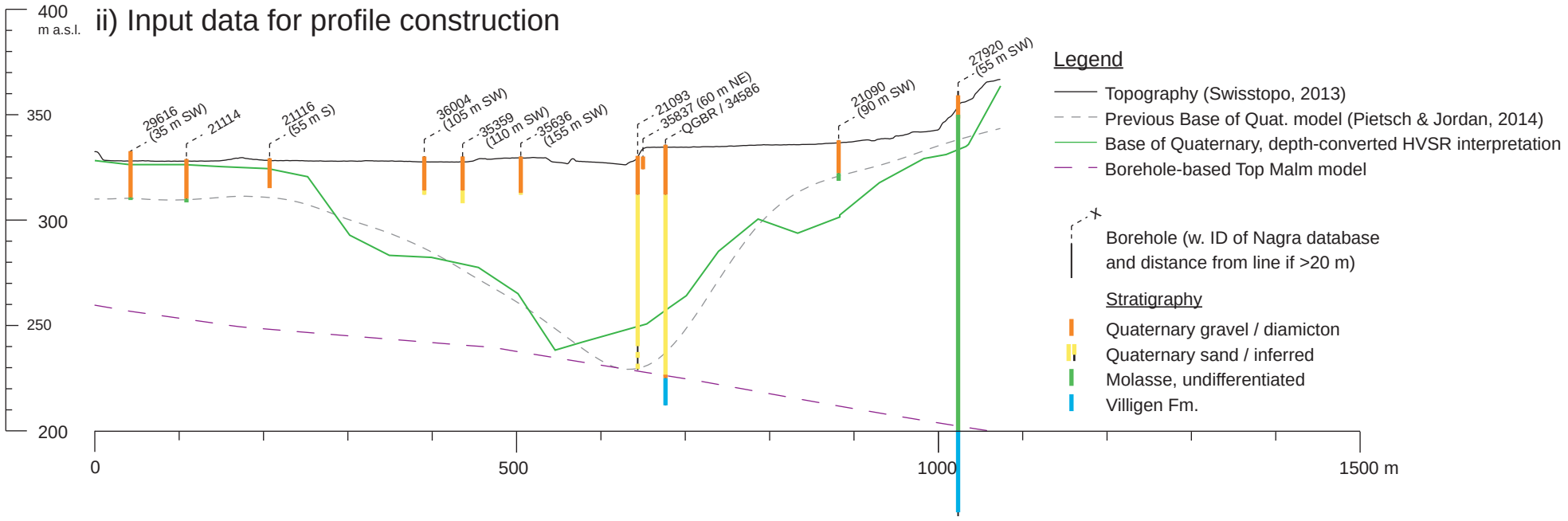
W

i) HVSR data with interpretation

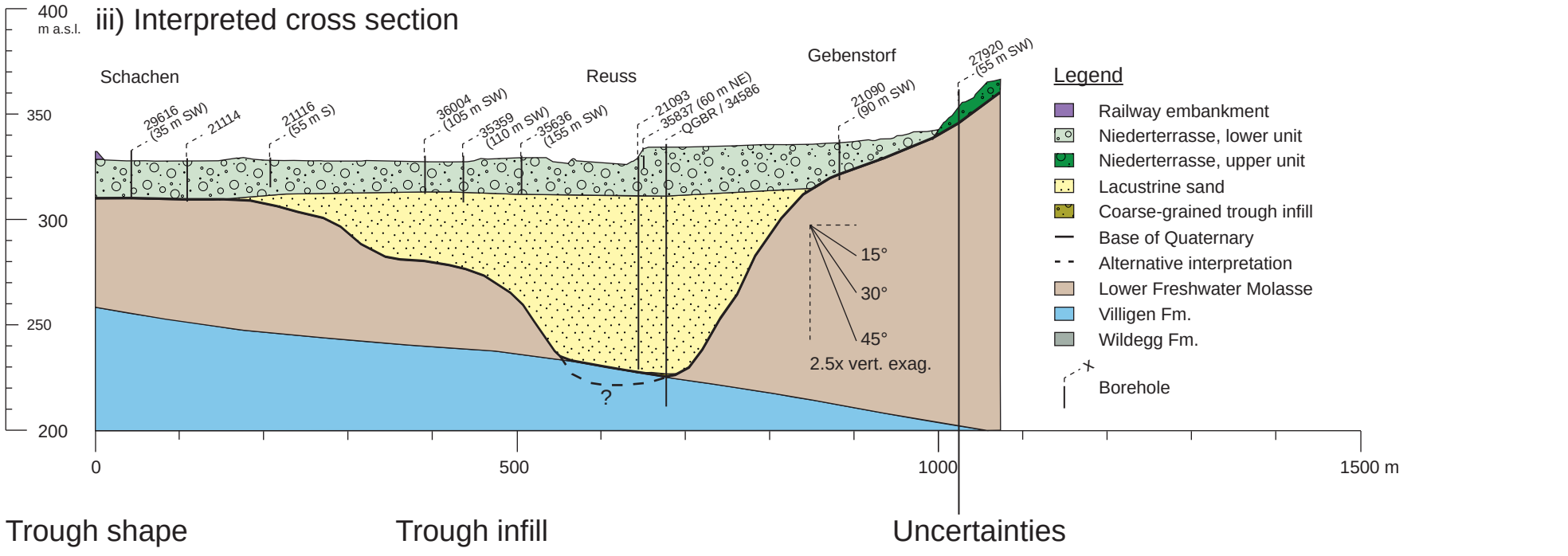
E



ii) Input data for profile construction



iii) Interpreted cross section



Trough shape

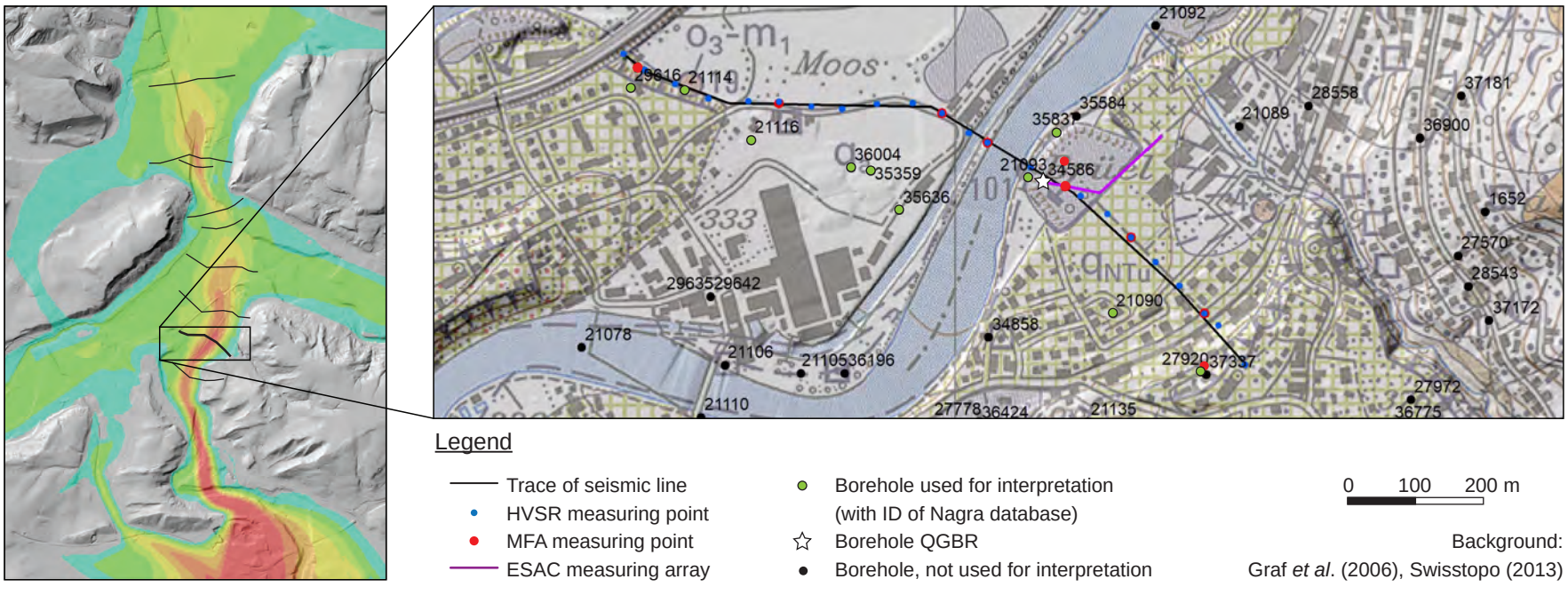
- width ~540 m at 300 m a.s.l.
- deepest point ~225 m a.s.l.
- V-shaped (VI = 0.09)
- stepped western flank
- apparently steep but poorly constrained eastern flank

Trough infill

- Niederterrasse with apparently regular base (filling two broad channels?)
- predominantly well-sorted sand
- few m of coarse-grained material at the trough base recovered in QGBR

Uncertainties

- full dataset: average error of base of Quaternary at boreholes is -7/+10 m
- depth of Base of Quaternary underestimated west, but overestimated east of the trough
- trough center not imaged by surface seismics (acquisition gap below the Reuss river), but well constrained by boreholes 21093 and QGBR



nagra NAB 21-18

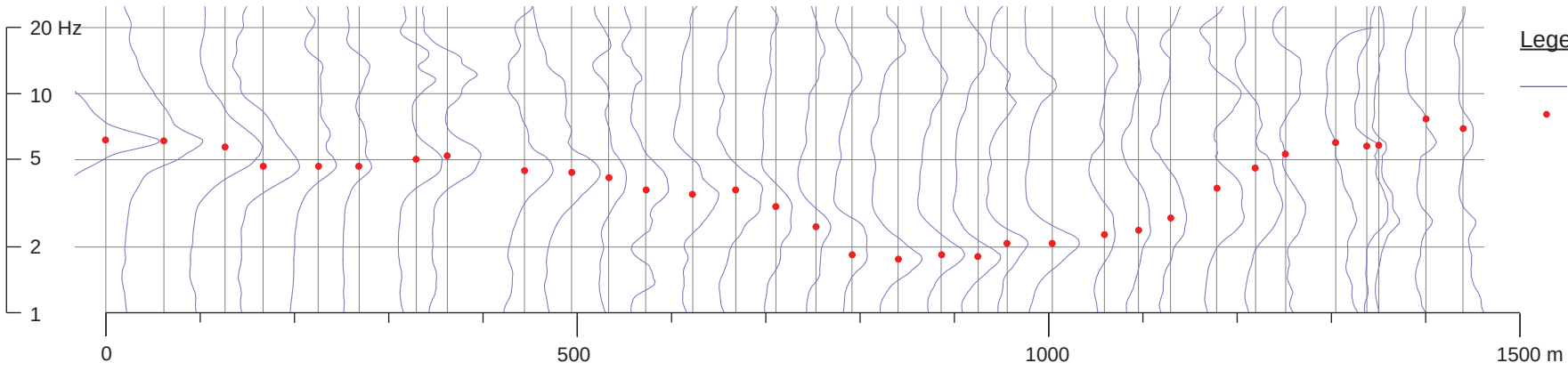
Seismic surface wave line 19QLAV-2
HVSR section, borehole data and interpretation

Lower Aare Valley | DAT.: Sep. 2021 | Enclosure 7-3

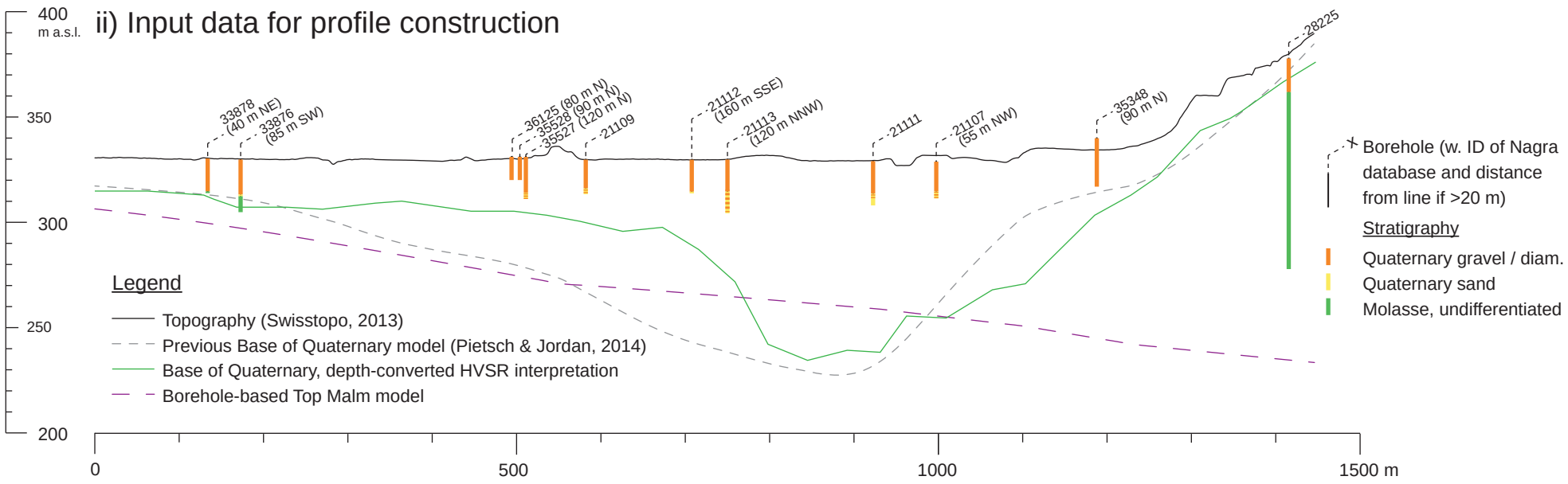
W

i) HVSR data with interpretation

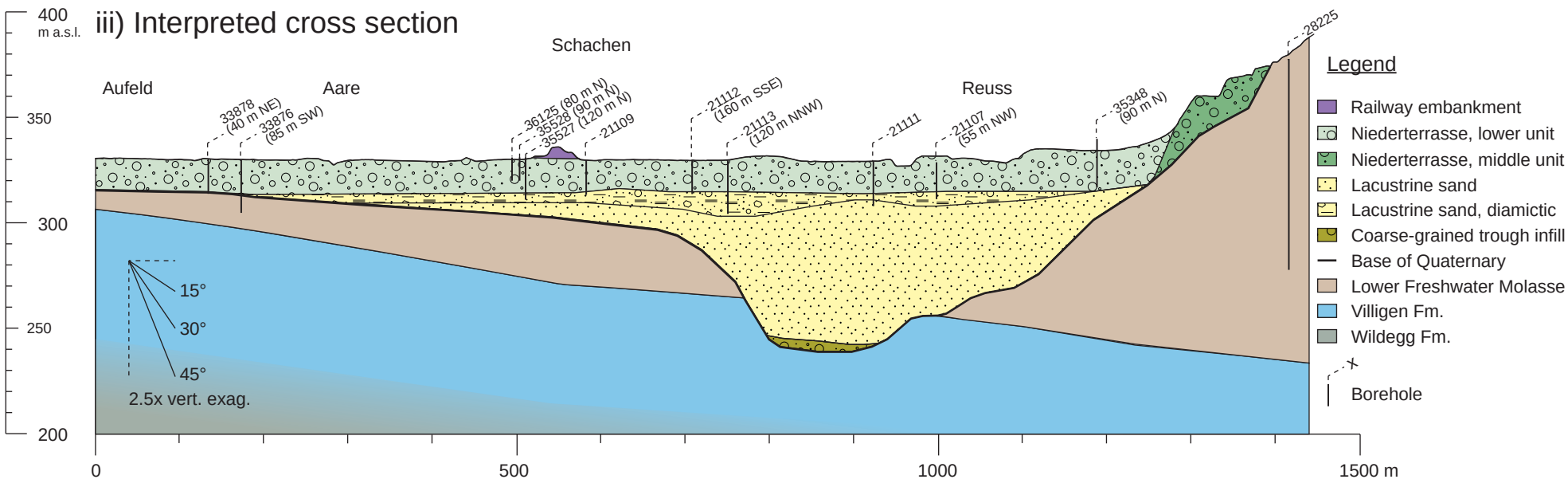
E



ii) Input data for profile construction



iii) Interpreted cross section



Trough shape

- width ~580 m at 300 m a.s.l.
- deepest point ~240 m a.s.l.
- V-shaped (VI = 0.13)
- steep western flank
- stepped eastern flank?

Trough infill

- Niederterrasse with apparently regular base (filling two broad channels?)
- predominantly well-sorted sand, diamictic at the top
- few m of coarse-grained material at the trough base suggested by south-/northward adjacent lines

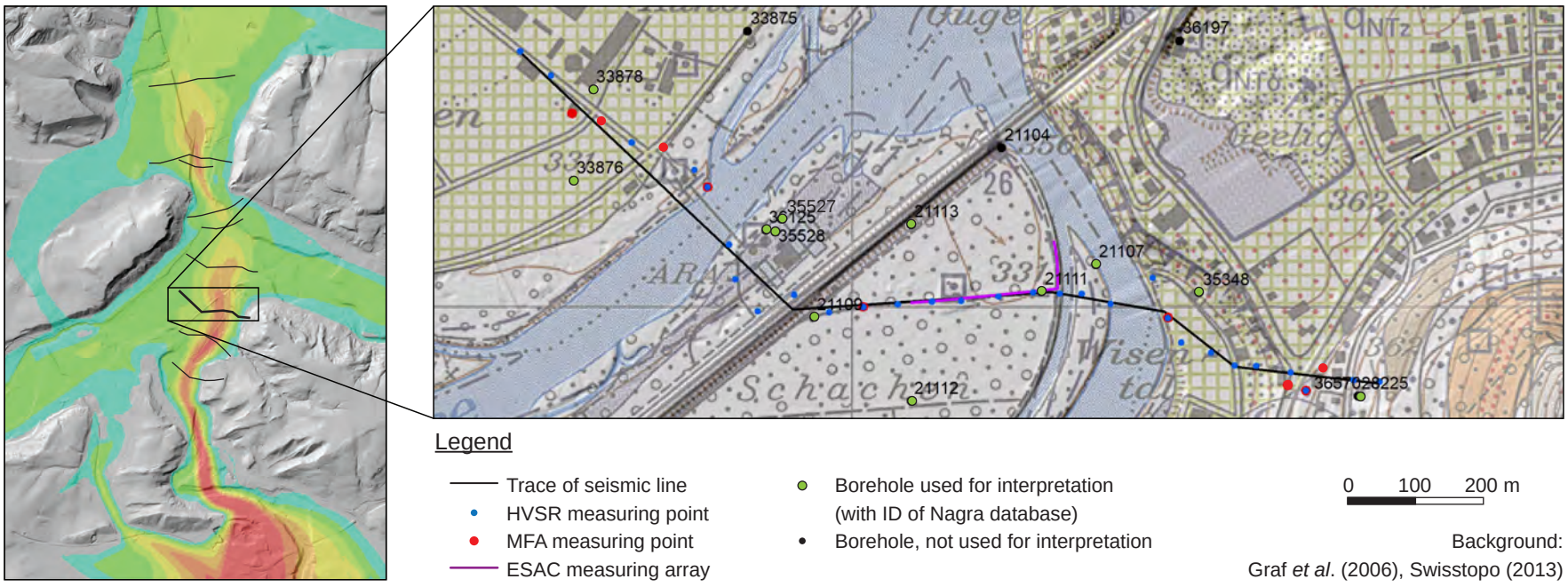
Uncertainties

- full dataset: average error of base of Quaternary at bore-holes is -7/+10 m
- only shallow part of the trough (top 20 m) is well constrained by boreholes
- steps in eastern flank: topographical artifacts?

nagra NAB 21-18

Seismic surface wave line 19QLAV-4
HVSR section, borehole data and interpretation

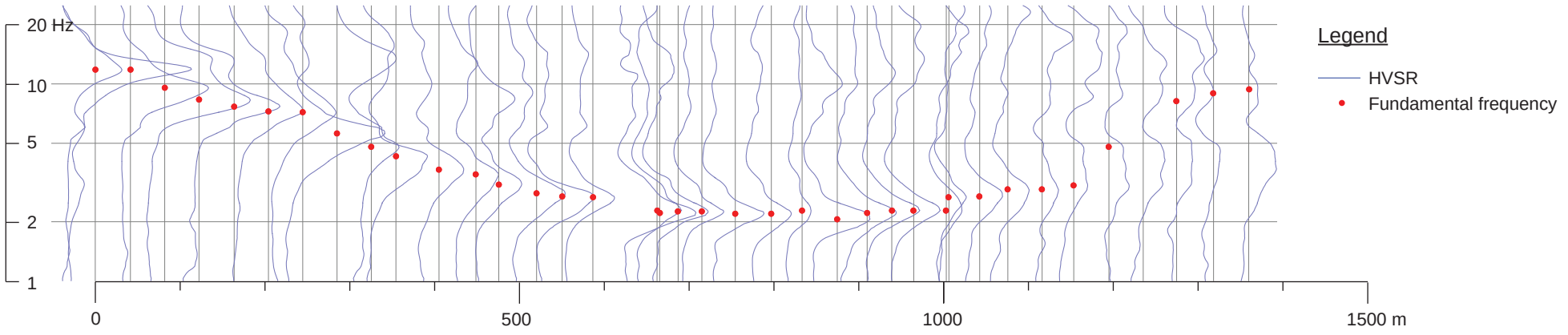
Lower Aare Valley | DAT.: Sep. 2021 | Enclosure 7-4



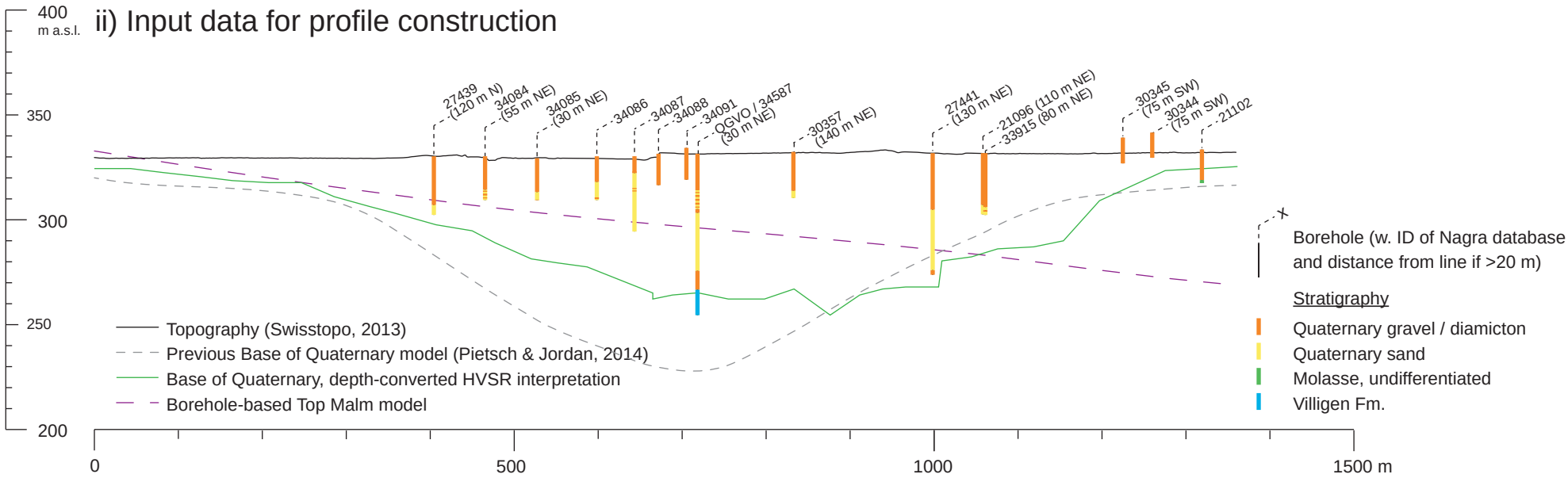
W

i) HVSR data with interpretation

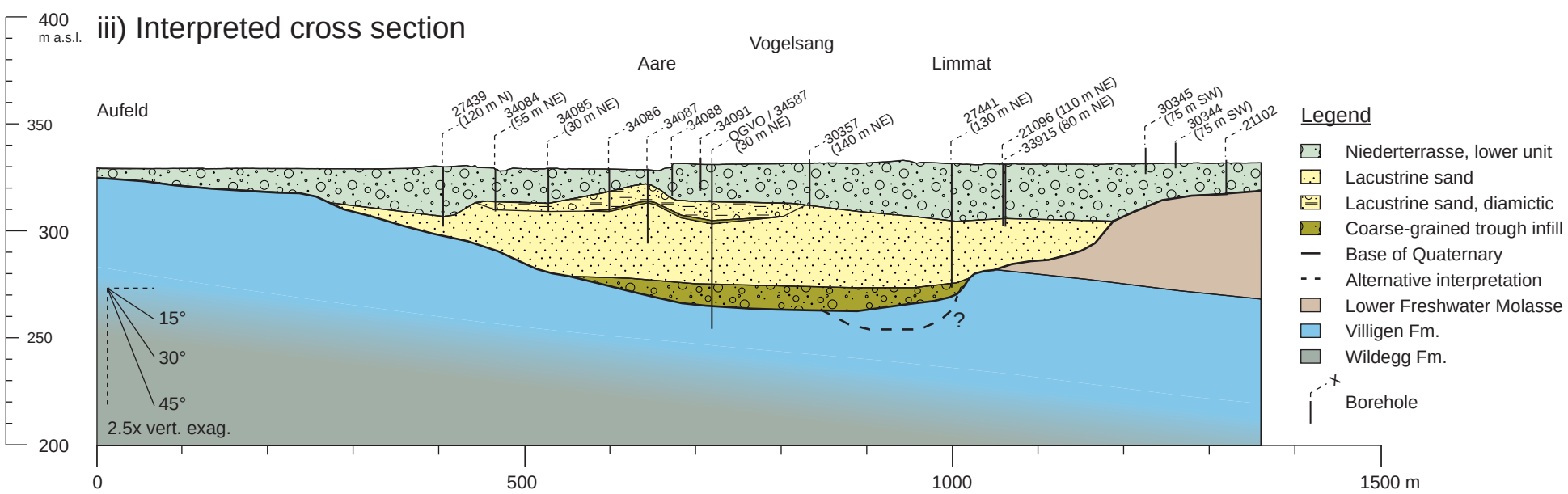
E



ii) Input data for profile construction



iii) Interpreted cross section



Trough shape

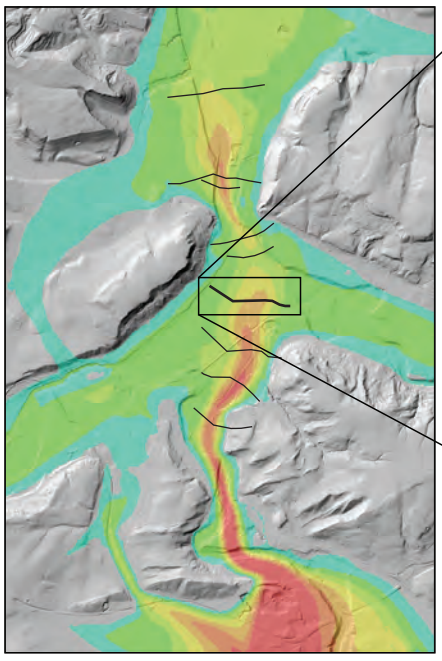
- width ~800 m at 300 m a.s.l.
- deepest point ~265 m a.s.l.
- intermediate shape (VI = 0.39)
- gently sloped western flank
- stepped eastern flank

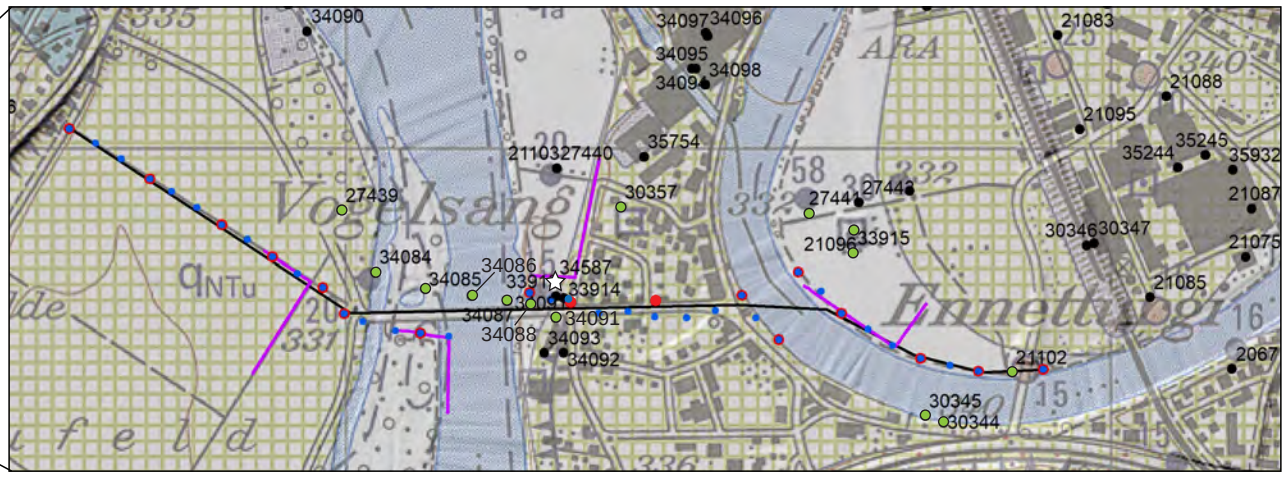
Trough infill

- Niederterrasse with irregular base: two separate, broad channels
- predominantly well-sorted sand
- gravelly interbed at ~303 m a.s.l., sand above partly diamictic
- ~10 m of gravel at the base

Uncertainties

- full dataset: average error of base of Quaternary at boreholes is -7/+10 m
- seismic data is in good agreement with boreholes





nagra

NAB 21-18

Seismic surface wave line 19QLAV-1

HVSR section, borehole data and interpretation

Lower Aare Valley

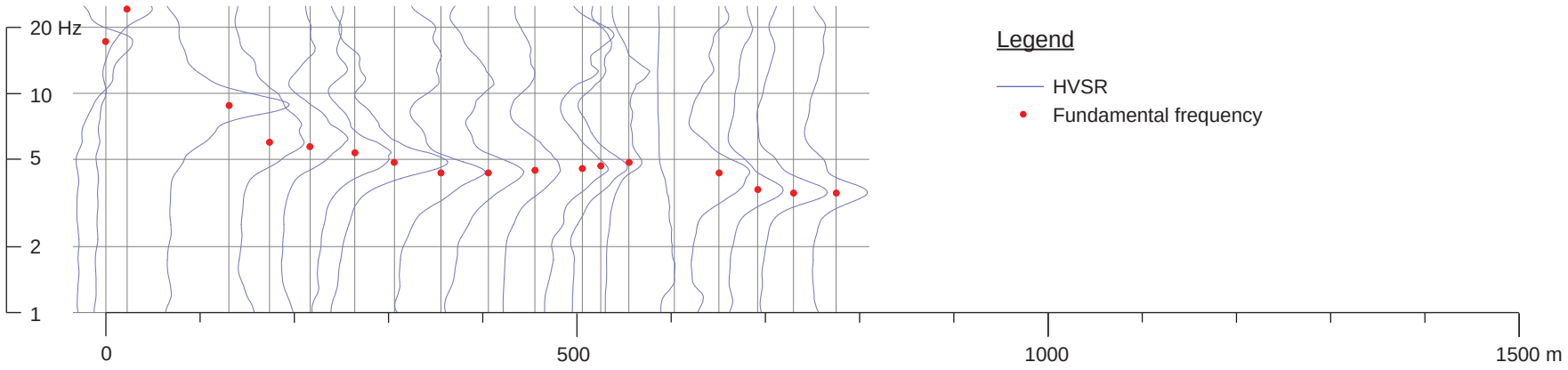
DAT.: Sep. 2021

Enclosure 7-5

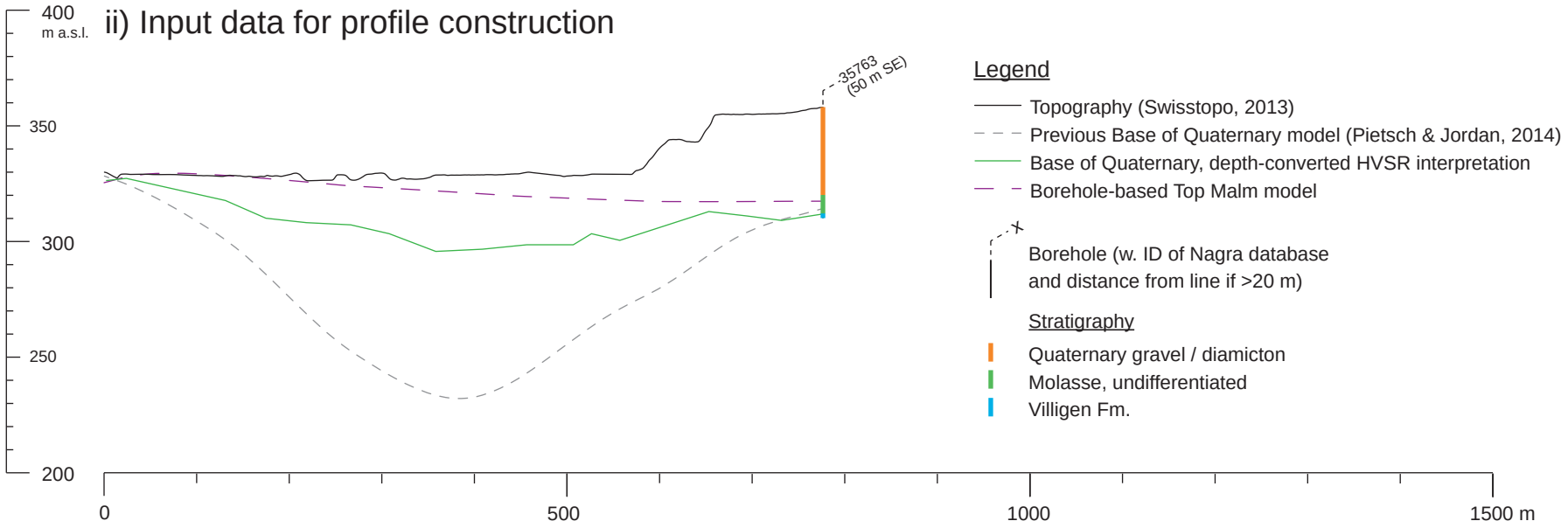
W

i) HVSR data with interpretation

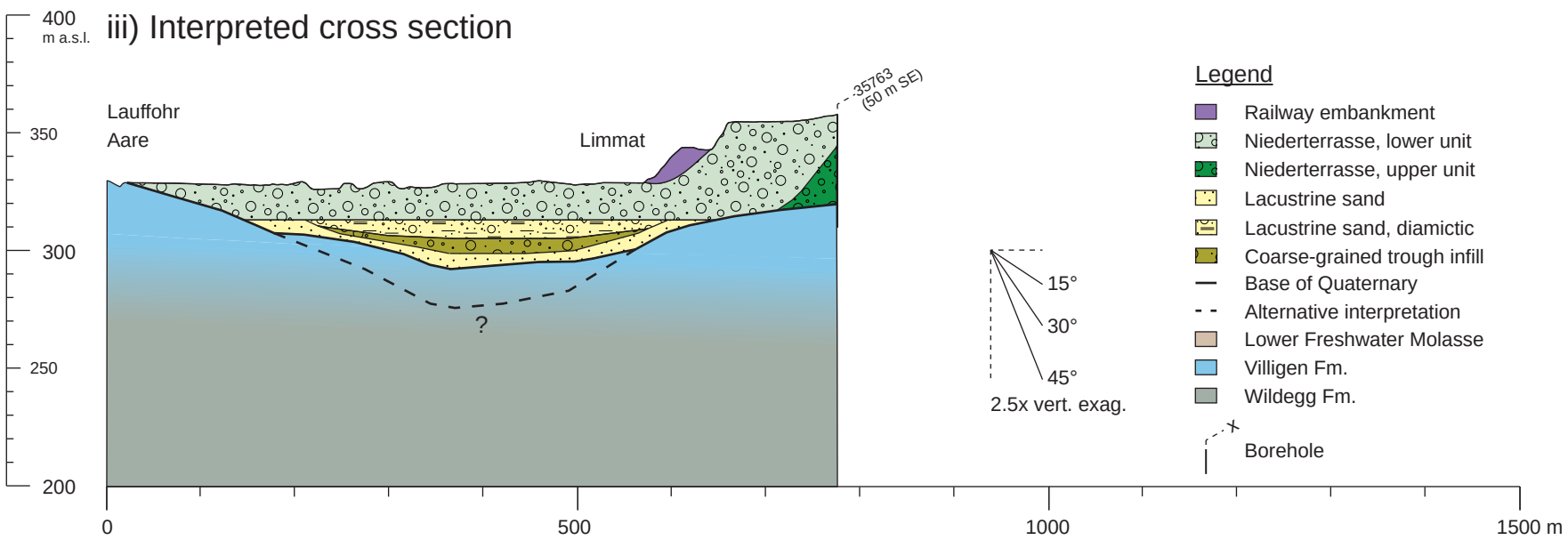
E



ii) Input data for profile construction



iii) Interpreted cross section



Trough shape

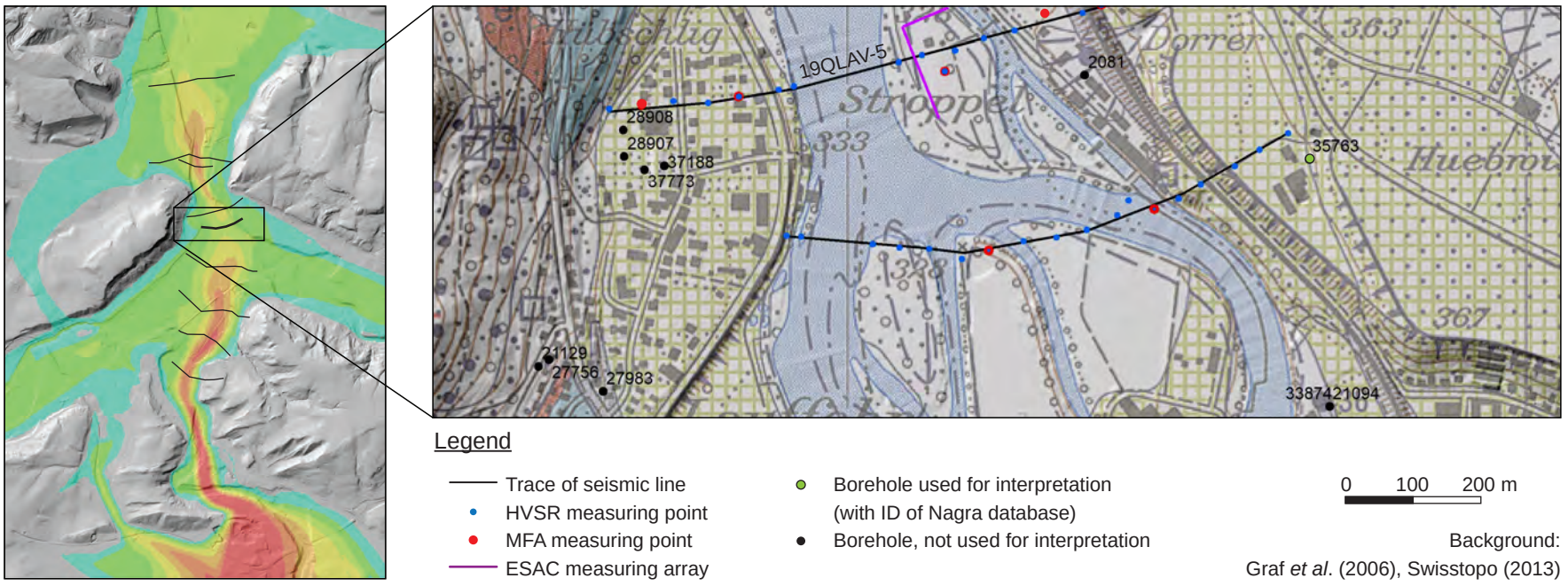
- width ~260 m at 300 m a.s.l.
- barely overdeepened:
  deepest point ~295 m a.s.l.
- U-shaped (VI = 1.04)
- slightly stepped western flank
- gently sloped eastern flank

Trough infill

- poorly constrained by boreholes at this site
- infill construction largely based on south-/northward adjacent lines

Uncertainties

- full dataset: average error of base of Quaternary at boreholes is -7/+10 m
- poorly borehole-constrained line
- trough depth possibly underestimated by surface seismics? (see northward-adjacent lines)



nagra NAB 21-18

Seismic surface wave line 19QLAV-8
HVSR section, borehole data and interpretation

Lower Aare Valley

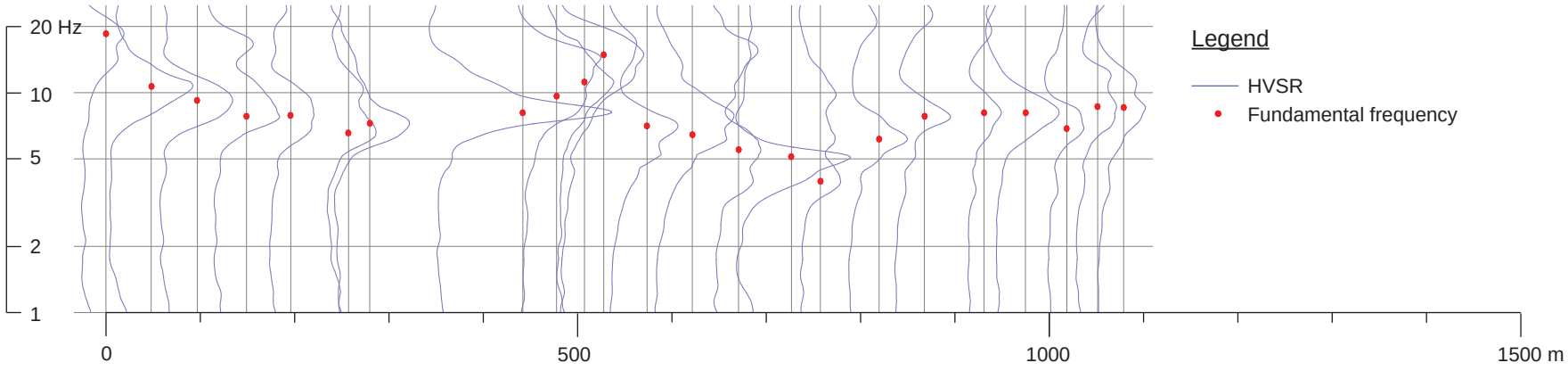
DAT.: Sep. 2021

Enclosure 7-6

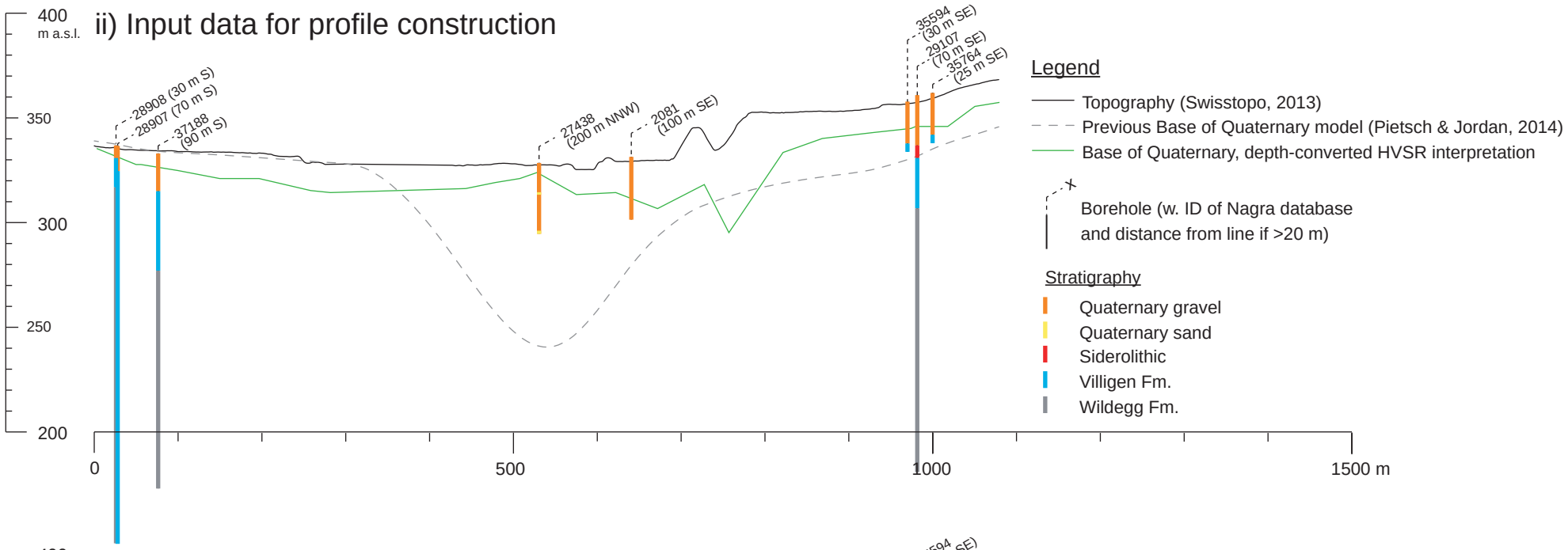
W

i) HVSR data with interpretation

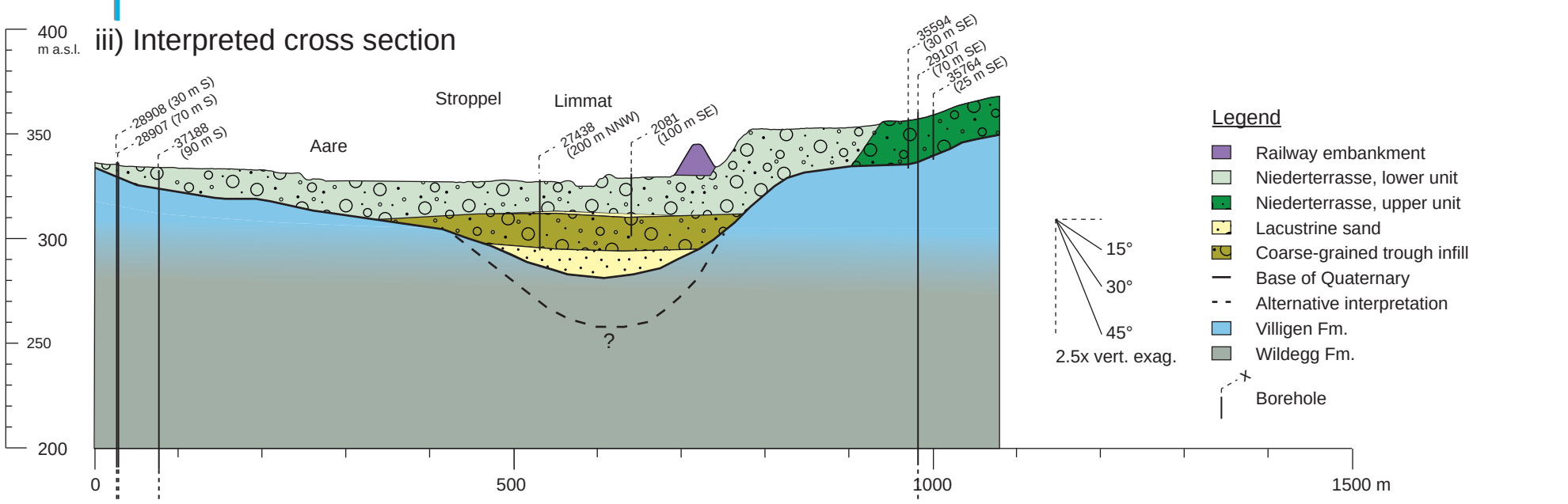
E



ii) Input data for profile construction



iii) Interpreted cross section



Trough shape

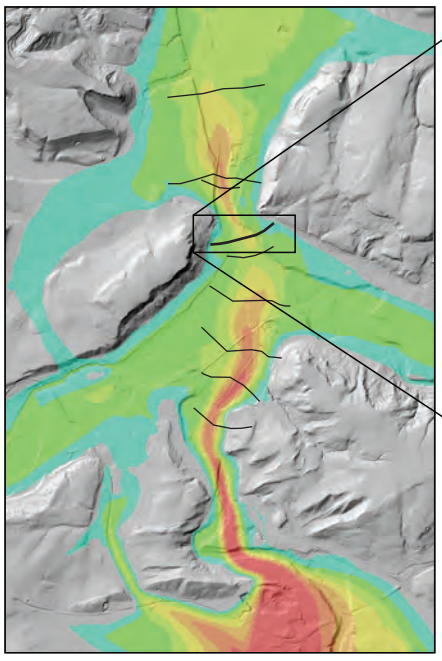
- width ~300 m at 300 m a.s.l.
- deepest point ~280 m a.s.l. (?)
- poorly constrained shape, interpretation largely based on south-/northward adjacent lines

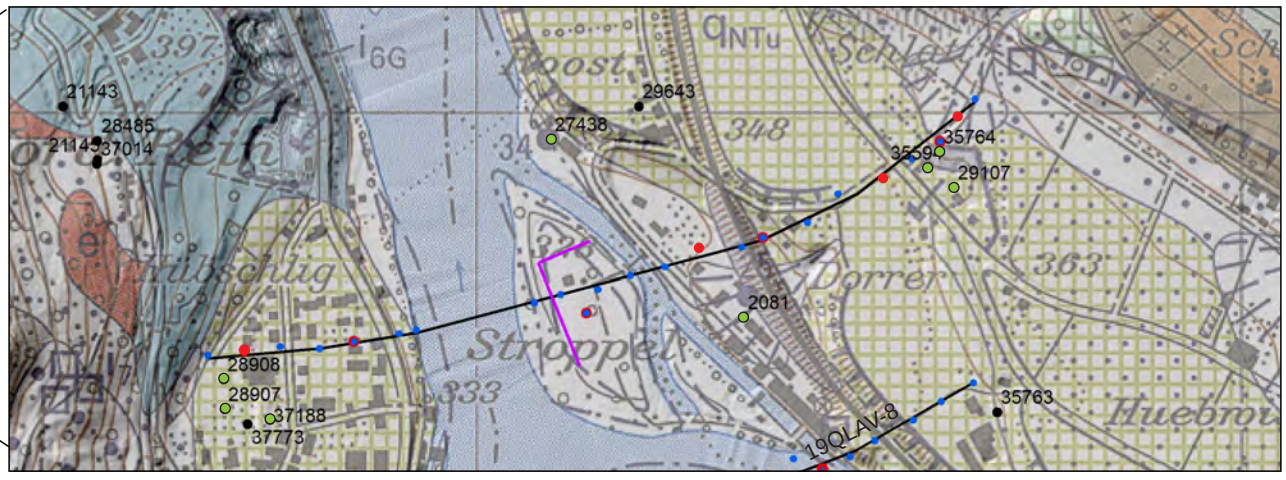
Trough infill

- boreholes suggest gravel-dominated infill
- infill construction largely based on south-/northward adjacent lines

Uncertainties

- full dataset: average error of base of Quaternary at boreholes is -7/+10 m
- depth of base of Quaternary underestimated by surface seismics
- no overdeepened trough center imaged
- data gaps below Aare and Limmat
- topographical artifacts at 700-800 m along x axis





nagra NAB 21-18

Seismic surface wave line 19QLAV-5
HVSR section, borehole data and interpretation

Lower Aare Valley

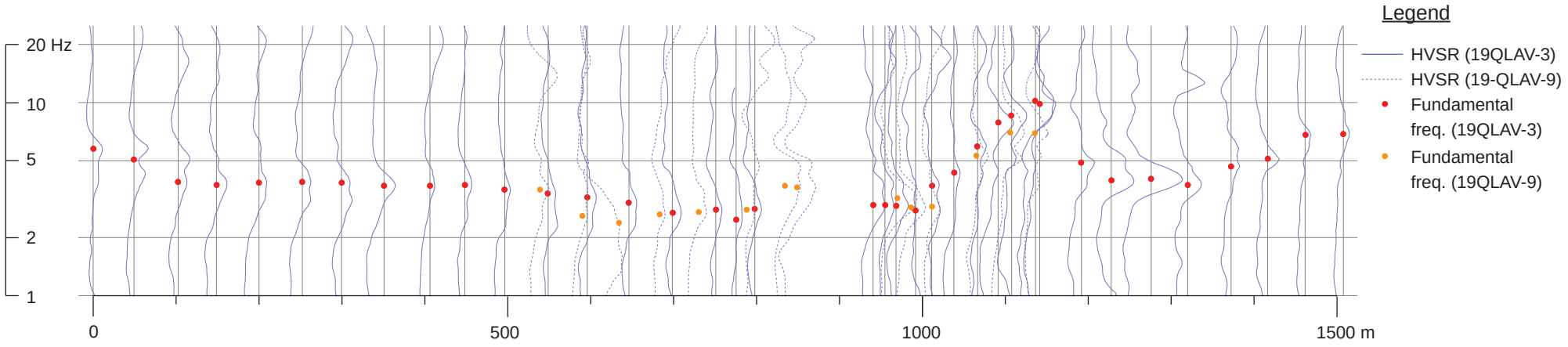
DAT.: Sep. 2021

Enclosure 7-7

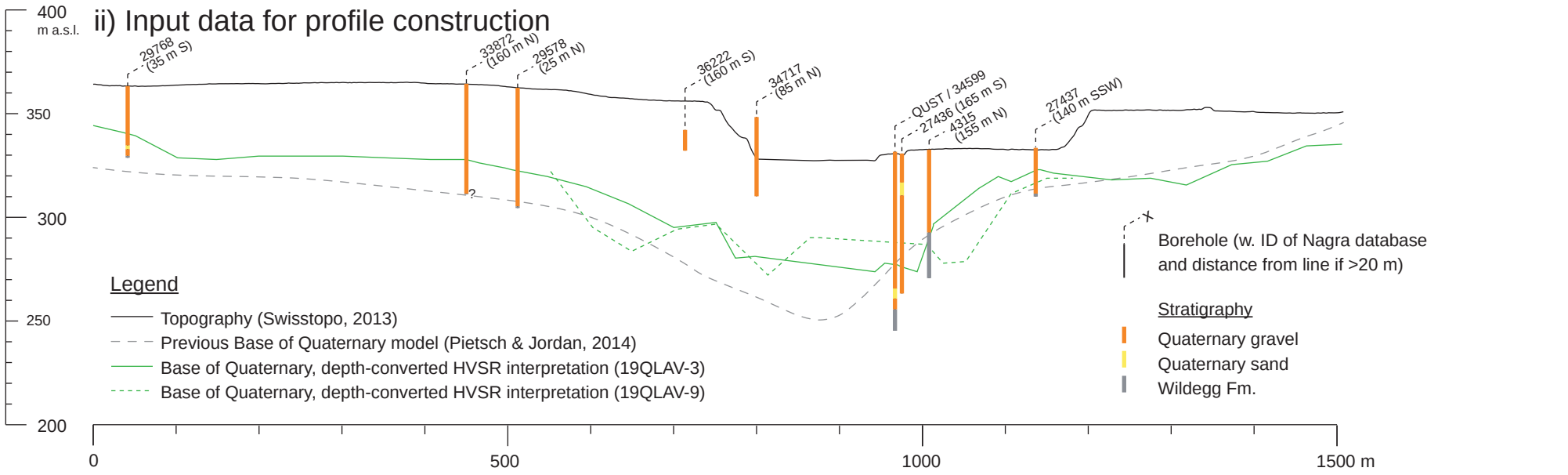
W

i) HVSR data with interpretation

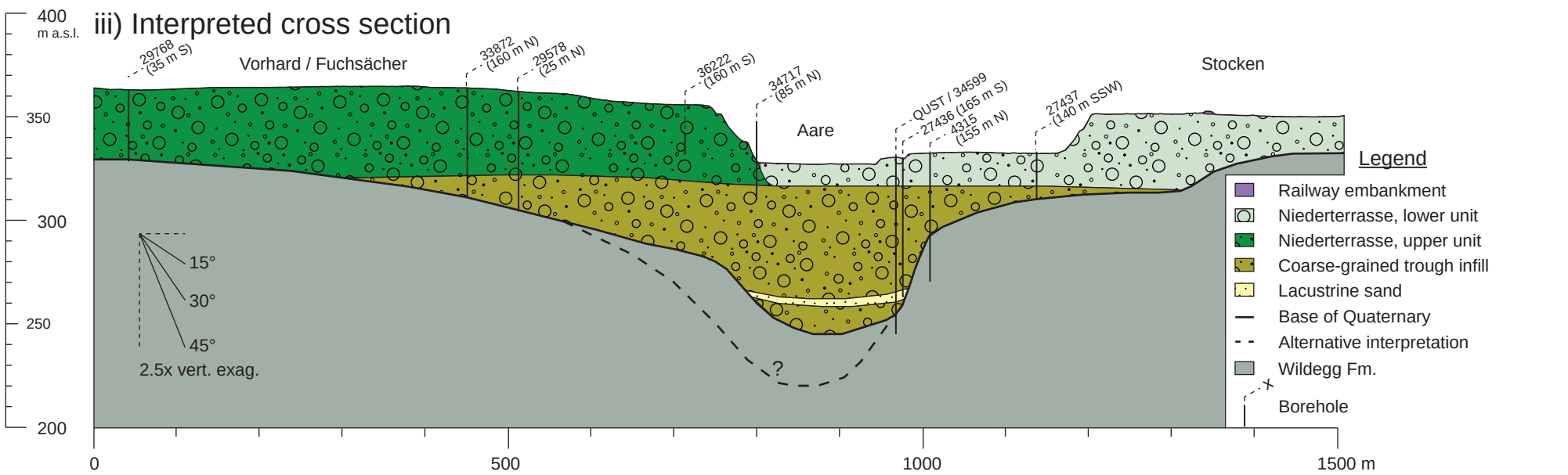
E



ii) Input data for profile construction



iii) Interpreted cross section



Trough shape

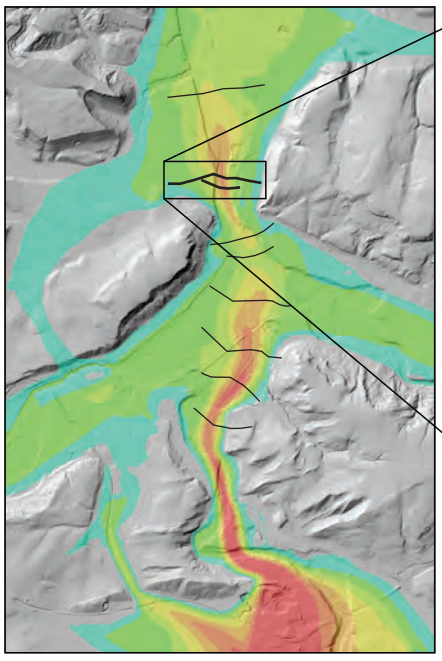
- width ~300 m at 300 m a.s.l.
- deepest point ~245 m a.s.l. (?)
- poorly constrained trough center
- steep eastern flank constrained by boreholes: U-shaped cross section (VI ≈ 0.60)?
- distinct flank shoulders (topographical artifacts?)

Trough infill

- gravel-dominated infill
- limestone block layer recorded in boreholes 29578, 34717, QUST, 27436, 27437 at ~320 m a.s.l. (base of Niederterrasse?)

Uncertainties

- full dataset: average error of base of Quaternary at boreholes is -7/+10 m
- depth of base of Quaternary underestimated
- overdeepened trough center not imaged: data gap below Aare





nagra NAB 21-18

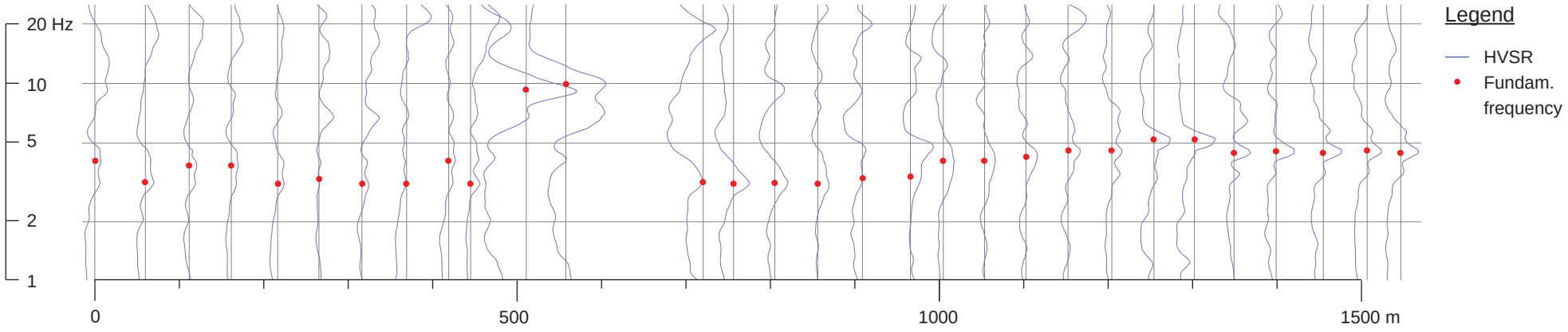
Seismic surface wave lines 19QLAV-3 & 19QLAV-9
HVSR sections, borehole data and interpretation

Lower Aare Valley | DAT.: Sep. 2021 | Enclosure 7-8

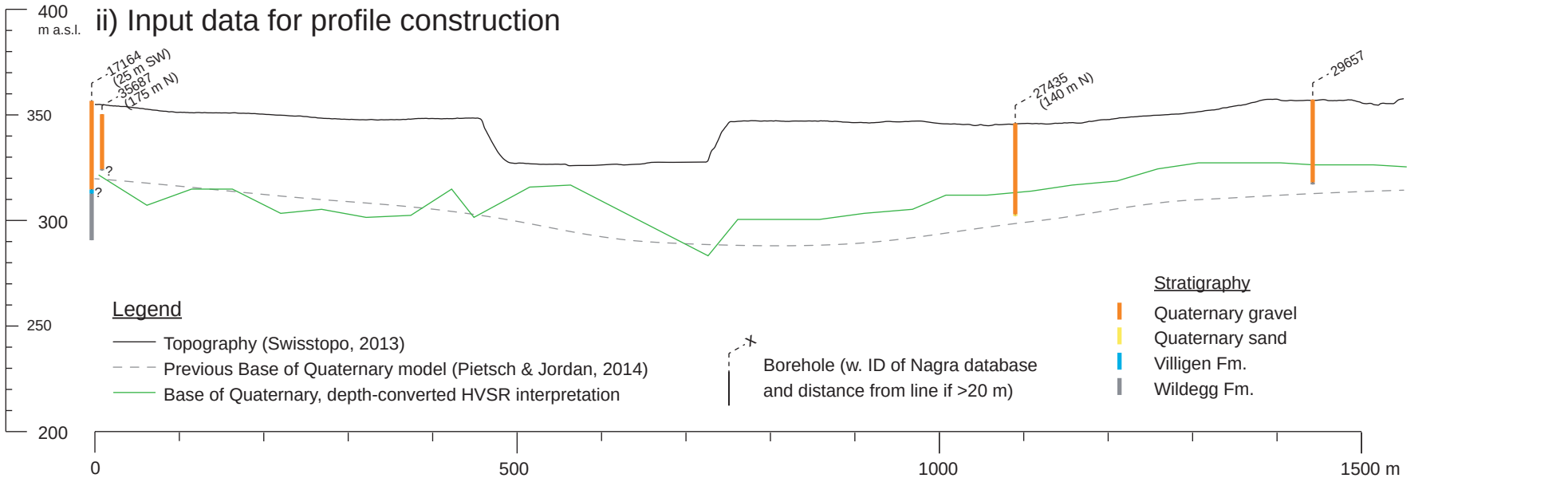
W

i) HVSR data with interpretation

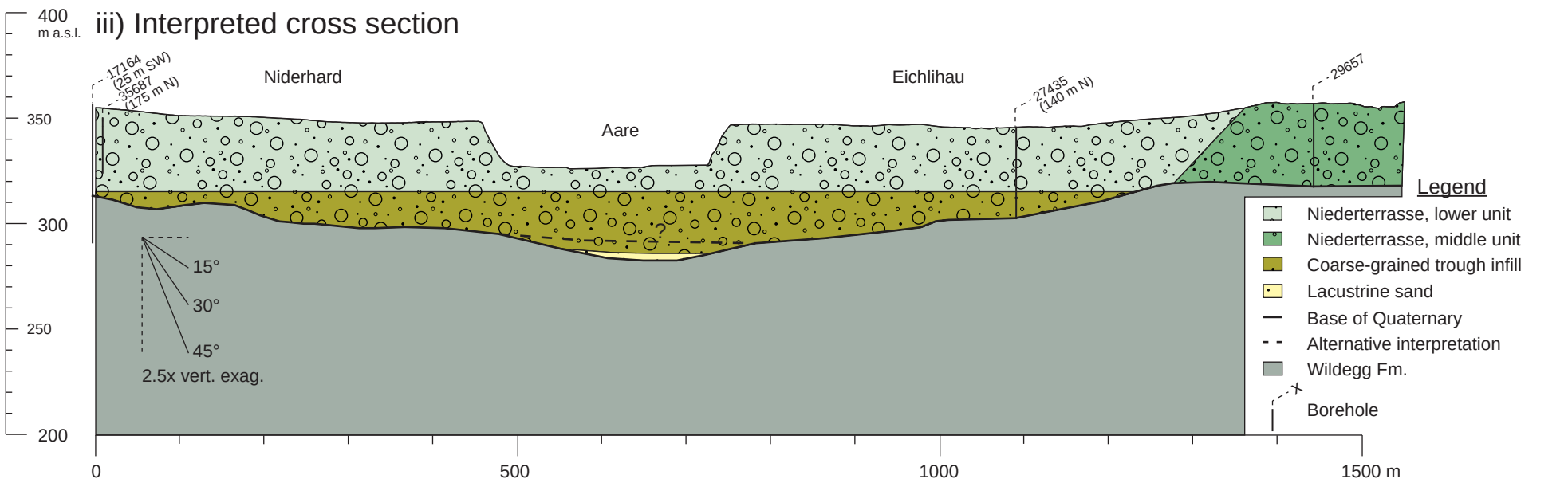
E



ii) Input data for profile construction



iii) Interpreted cross section



Trough shape

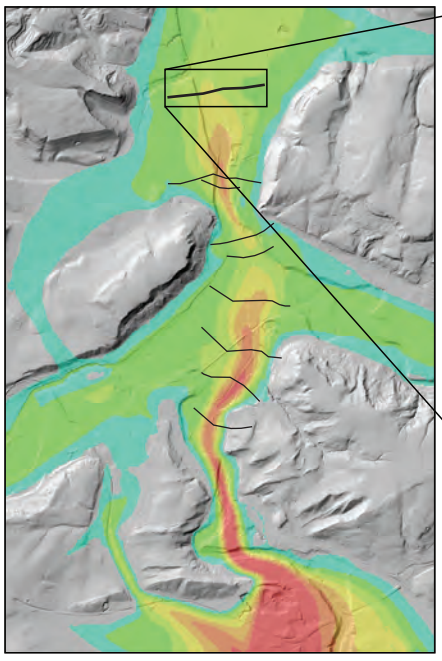
- width ~570 m at 300 m a.s.l.
- deepest point ~285 m a.s.l.
- relatively flat base, no clear trough center imaged by seismics

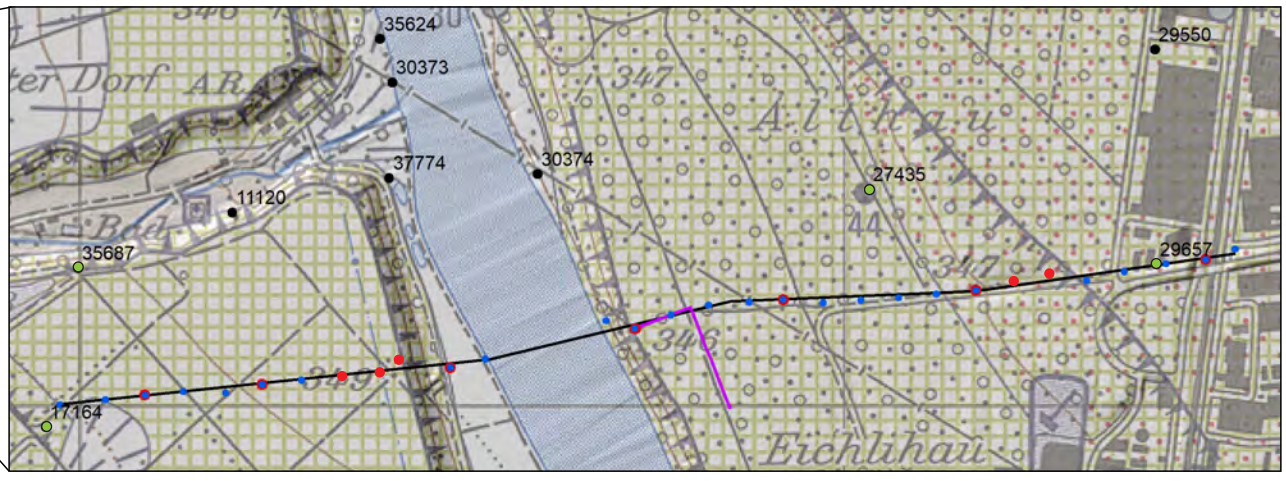
Trough infill

- gravel-dominated infill
- boreholes 37774 (250 m N) and 29531 (400 m N) suggest existence of fine-grained deposits below the gravel

Uncertainties

- full dataset: average error of base of Quaternary at boreholes is -7/+10 m
- depth of base of Quaternary underestimated
- topographical artifacts at ~500 and ~750 m?
- data gap below Aare (suspected trough center)

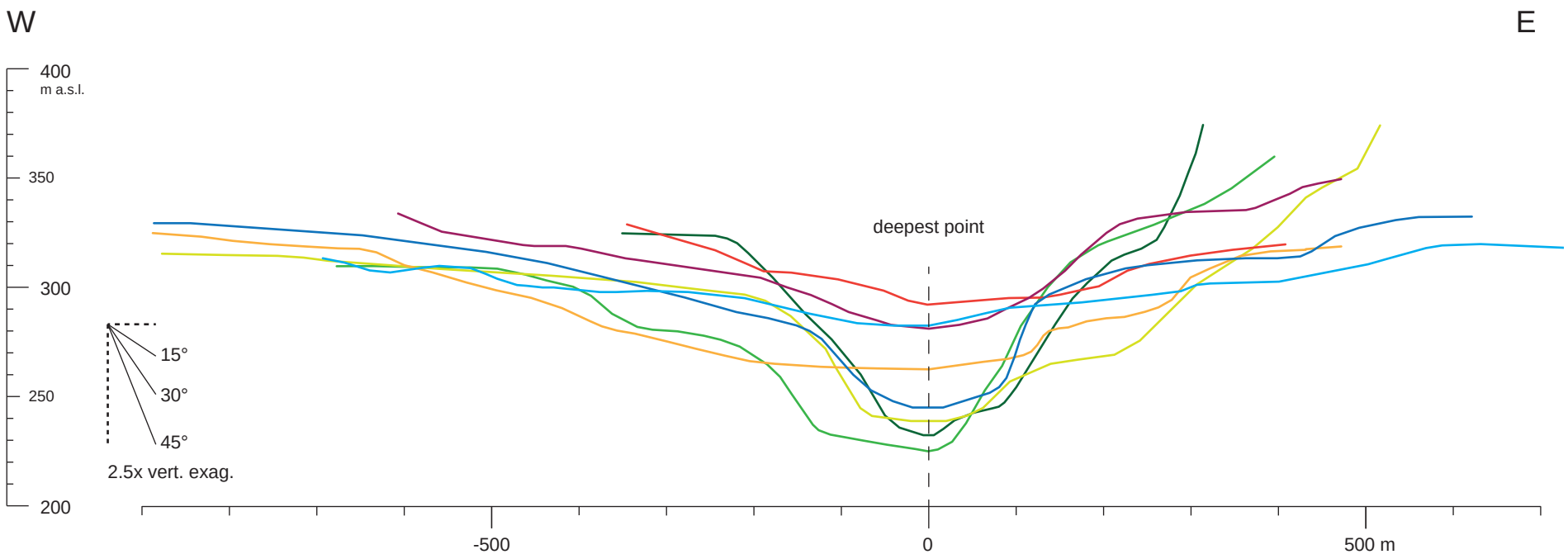




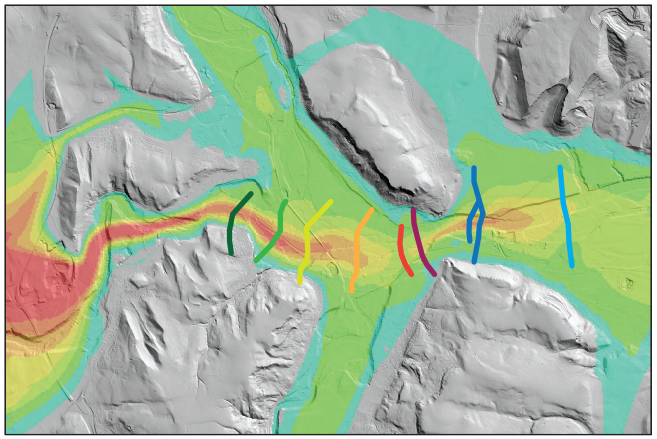
nagra NAB 21-18

Seismic surface wave line 19QLAV-7
HVSR section, borehole data and interpretation

Lower Aare Valley | DAT.: Sep. 2021 | Enclosure 7-9



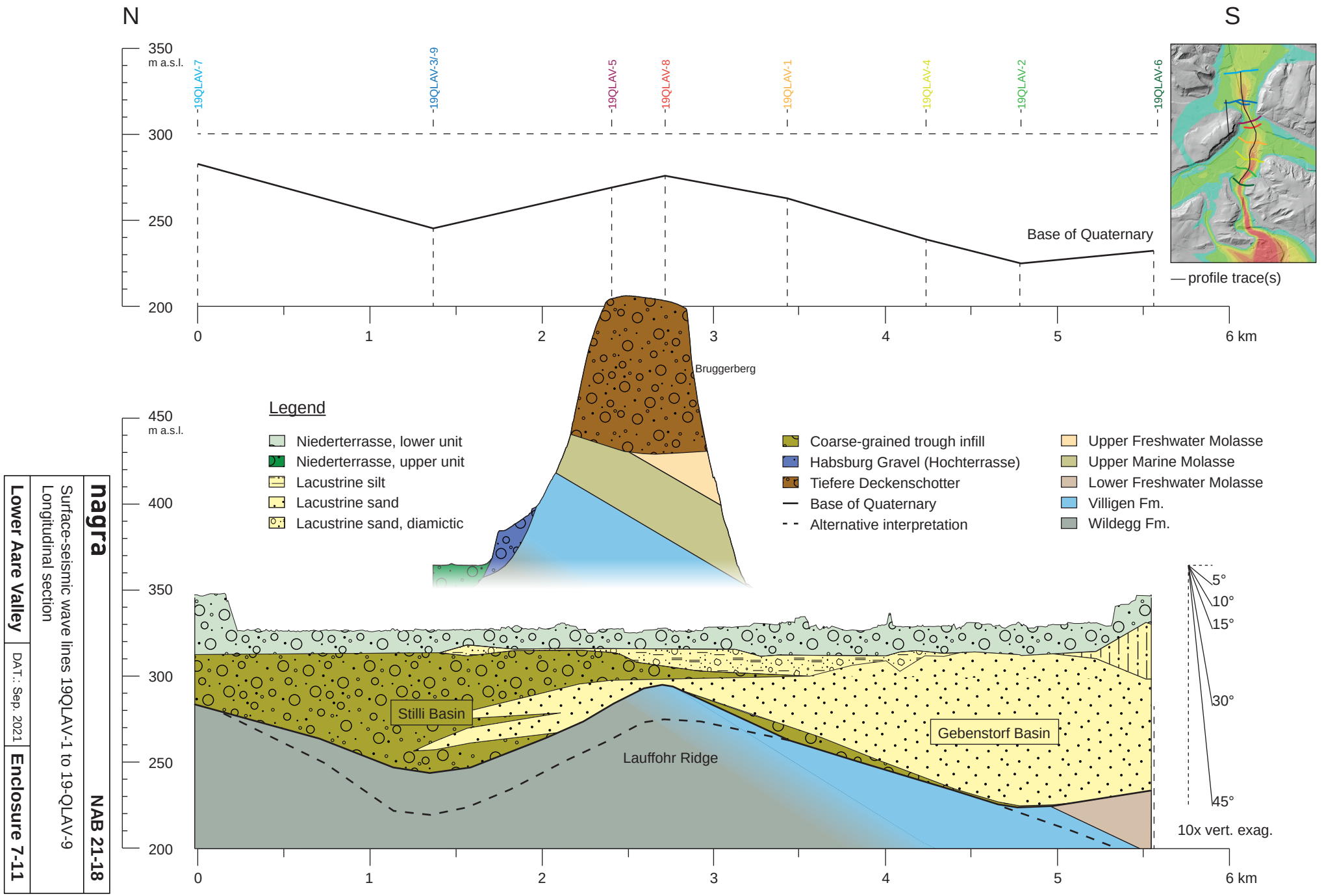
19QLAV-6
19QLAV-2
19QLAV-4
19QLAV-1
19QLAV-8
19QLAV-5
19QLAV-3/-9
19QLAV-7



nagra **NAB 21-18**

Surface-seismic wave lines 19QLAV-1 to 19-QLAV-9
Summary plot

Lower Aare Valley DAT.: Sep. 2021 **Enclosure 7-10**



nagra NAB 21-18

Surface-seismic wave lines 19QLAV-1 to 19-QLAV-9

Longitudinal section

Lower Aare Valley

DAT.: Sep. 2021

Enclosure 7-11